Title	Water Resource Assessment of Yodo River Basin Using Coupled Hydrometeorological Modeling Approach
Author(s)	Shrestha, Kundan Lal
Citation	大阪大学, 2010, 博士論文
Version Type	VoR
URL	https://hdl.handle.net/11094/565
rights	
Note	

Water Resource Assessment of Yodo River Basin Using Coupled Hydrometeorological Modeling Approach

(気象水文統合モデル手法を用いた淀川流域の水循環評価)

A Thesis
Submitted to the Graduate School of Engineering, Osaka University
in partial fulfillment of the requirements for the degree of
Doctor of Philosophy in Engineering

Kundan Lal Shrestha

(クンダン　ラル　セレスタ)

January 2010

Division of Sustainable Energy and Environmental Engineering,
Graduate School of Engineering, Osaka University, Japan

CONTENTS

LIST OF FIGURES

LIST OF TABLES

INTRODUCTION

1.1 BACKGROUND

Water cycle

Freshwater, so essential for the survival of all the living beings and ecosystems in the world, is a renewable and changeable, but limited natural resource. In nature, while only 3% of the water on Earth is freshwater, only 0.3% is in the form of surface water. The freshwater in nature gets renewed only through the process of the water cycle.

Water cycle or hydrological cycle is a circulatory system in earth that includes the movement of water by means of precipitation, evaporation, storage in reservoirs, infiltration, surface runoff, snow melting, and water distribution processes (Fig. 1). Water cycle can be visualized at global, regional as well as basin scales. The basin-scale water cycle is significant for the utilization and management of water resources at regional and urban levels because many phenomena occurring at the basin scale, such as local downpour, flooding, surface runoff, etc. affect the water intake and supply in the basin region. Coming into the 21st century, we have witnessed many changes in the factors affecting the hydrological cycle, such as rapid urbanization of rural areas, industrial development and subsequent increase in water demand, contamination of water, and change in climate due to global warming.

Impact of climate change on water cycle

The global warming is having a profound effect on the atmospheric and hydrological environment. The impact of climate change has been felt all over the world and it has potential to affect our environment in the future as well. Climate change due to anthropogenic global warming has brought new types of environmental risks. These risks include the increase in extreme climatic
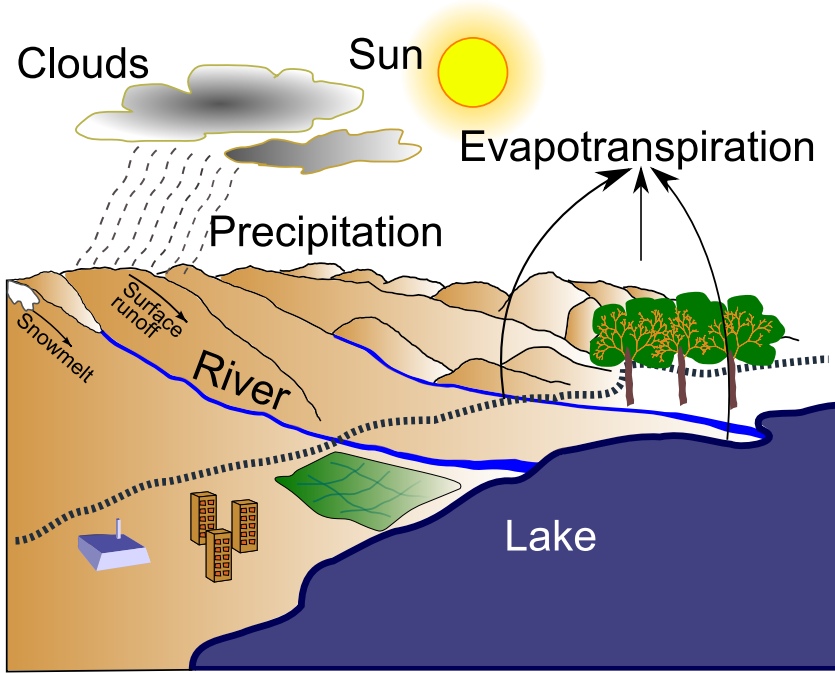
Figure 1: Simple representation of hydrological cycle.

conditions such as higher intensity of rainfall, elongation of drought periods, early periods of snow and glacier melting, increase in sea level, increase in the effect of urban heat island, and so on. These risks pose many water resource problems such as deterioration of water quality and decline in the water supply function.

IPCC (2007a) has projected a substantial impact of human-induced climate change on the water resources at global and regional scales. The effect of climate change on water resource is not uniform throughout the world. Several places will witness an increase in river flow rates and water availability and some places may witness water shortage problems when drought periods increase. Two important phenomena affecting the water resources are: (i) change in precipitation pattern, and (ii) increase in air temperature. Both of these phenomena have potential to influence water cycle in river basins.

In Japan, Ministry of Land, Infrastructure, Transport and Tourism (2008b) has reported that snow cover in upstream of major rivers will decrease and consequently the water reservoir levels will decrease. Floods are also projected to increase due to higher intensities of precipitation. For example, in a future

environmental scenario, yearly average maximum daily rainfall is predicted to increase by 11% under the A1B scenario (2080-2099 compared with 1979-1998) in Tokyo and surrounding region.

Issues related to water resources in Japan

Water use and water shortage

In Japan, annual use of water is about 83.5 billion m^3, out of which approximately 16.2 billion m^3 is for domestic use, 12.1 billion m^3 is for industrial use, and 55.2 billion m^3 is for agricultural use (Ministry of Land, Infrastructure, Transport and Tourism, 2008a). Nearly 88% of the total used water is obtained from rivers, lakes and reservoirs, and the remaining amount is obtained from groundwater. During the period of 1965 and 2004, domestic and industrial water use increased by more than three times due to increase in population, rapid urbanization and industrialization, and economic growth. But presently, the water use trend has more or less stabilized.

Water shortage is a global problem created by increase in population, and industrial and economic advances. It affects domestic water, food supply, and public health. Several water shortages occurred in Japan in the past: for example, 1939 in Lake Biwa, 1964 during Tokyo Olympics, 1967 in Nagasaki, 1973 in Takamatsu, 1978 in Fukuoka, etc. Presently, Japan has nearly 789 multi-purpose dams and 1,878 single-purpose dams for agricultural, domestic and industrial water supply, and they have contributed nearly 11.9 billion m^3 of water resource to tap water and 5.9 billion m^3 of water to industrial water. So, today's water shortage problem is not frequent as before, though nation-wide water shortage have occurred, just like in 1994 when nearly 16 million people were affected by water shortage and nearly 140 billion yen worth of agricultural products were lost.

Japan has nearly 70% of the land covered with mountains and slopes. The rivers have steep slope and their lengths are comparatively shorter than major rivers in rest of the world (Yodo River Office, 2004). The river flow rates fluctuate and water levels keep changing with time. Considering that the water demand in domestic and industrial sectors is mostly stable, a sustainable water supply system is necessary.

Nearly 13% of the total water used in Japan comes from groundwater (12.4 billion m^3). In the past, problems like land subsidence and groundwater salinization occurred in Japan due to rapid economic and industrial development. Now, these problems are tackled by placing restrictions on river water intake and other preventive measures. Even then, these problems may resurface when emergency water intake from groundwater occurs during acute water shortage events.

Changing pattern of precipitation in Japan

Generally, precipitation in Japan is nearly 1718 mm or 650 billion m^3 in volume (average of 1971-2000 period), and it is more than two times the world average. As 230 billion m^3 of this precipitation gets lost due to evapotranspiration, the available water resource is approximately 420 billion m^3 but water resource per capita of Japan is only around 3300 m^3, which is less than half of the entire world. During the years having very low rainfall, the available water resource can get reduced as low as 280 billion m^3. Since 1970, several low precipitation years like 1973, 1978, 1984, 1994 and 1996 had less than average rainfall. It created water shortage and environmental damages.

Looking at the annual precipitation trend in Japan in the 20th century, a slightly decreasing long-term trend can be seen with approximately 90 mm of decrease in this period (Fig. 2). But today, a rainfall trend has been fluctuating from the low extreme to high extreme. During the low precipitation years, rainfall has decreased by roughly 300 mm in the 20th century. This kind of fluctuating trend of precipitation in Japan points toward a high possibility of extreme climate in the coming years that may include high-intensity precipitation, longer dry periods and low precipitation, less snowfall and early snow melt.

The spatial distribution of precipitation in the 20th century in Japan shows decreasing in most of the areas except Hokkaido region. There is seasonal variation with many places having increasing trend of precipitation in spring and summer. In autumn and winter, most of the places have decreasing trend of precipitation except Hokkaido (Fig. 3).

In Japan, many multi-purpose dams were constructed to improve water allocation and secure a stable water supply. But recently, low precipitation periods have caused the river water levels to fall and the water supply has
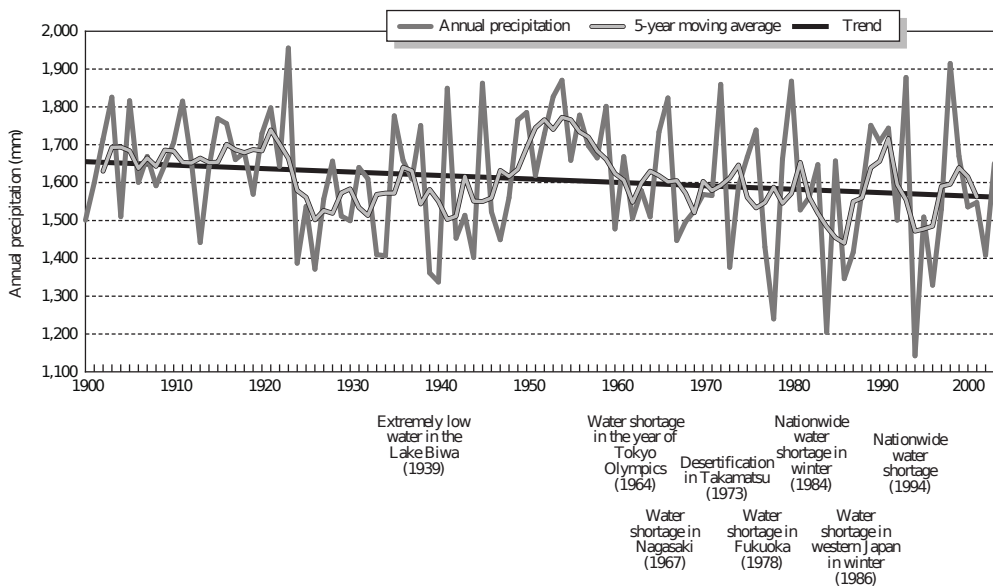
Notes: 1. The value represents the arithmetic mean of values observed at 51 points across the country.
2. Trend is based on the regression line.
3. Observation points for each year may be less than 51 due to missing observation.

Source: Data presented by Japan Meteorological Agency

Figure 2: Long-term changes in annual precipitation in Japan from 1900 to 2003.
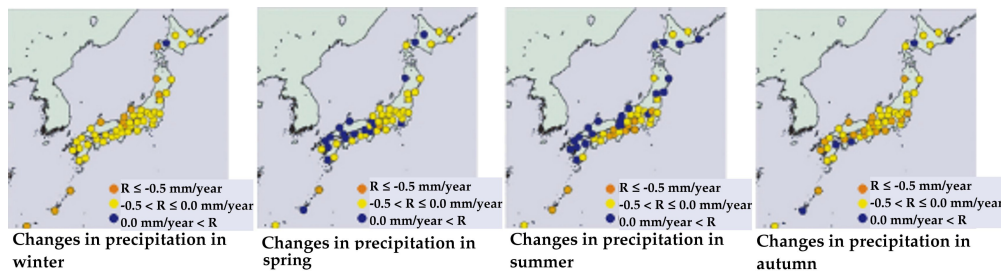
Figure 3: Change in seasonal precipitation in Japan. Note: With respect to the precipitation by season at 51 spots for the period between 1900 and 2006, annual increase or decrease was calculated from the inclination of the trend (by regression line) for each spot. Winter: December (of the preceding year) to February; spring: March to May; summer: June to August; autumn: September to November. (Source: Ministry of Land, Infrastructure, Transport and Tourism (2008a))

often been unstable. It is also difficult to construct new dams and reservoirs to create more water resources because of many natural, environmental, public and economic limitations. While considering that these problems may persist or may even aggravate in the future, effective water resource management is undeniably important to adapt to such scenarios.

Rising air temperature: from global warming and urbanization

During the 20th century, global average air temperature increased by approximately 0.74 °C and the Japanese air temperature rose by nearly 1.06 °C (Fig. 4). Intergovernmental Panel on Climate Change (IPCC) has predicted that it may rise by $1.1 - 6.4$ °C in the 21st century. This type of increase in temperature is a consequence of global warming due to increase in greenhouse gases. With the increase in air and water temperature, the rate and occurrence of natural processes like evapotranspiration, precipitation and snow melting also change. Consequently, intensity and magnitude of precipitation and typhoons may increase, frequency of downpours and droughts may increase, snow may melt earlier than expected, and so on. Such increase in extreme climatic features will create many risks to water resources, such as the increase in river flow rate, increase in frequency and magnitude of floods, higher probability of dry periods, and an overall imbalance in the water supply and demand in river basins.

In river basins affecting the urban population, the effects of climate change can be more pronounced, considering that urban regions have high density of population and a limited supply of water. Thus, along with the urban development scenarios, the urban living environment may get deteriorated by environmental risks created by climate change. In other words, urban development is directly linked with river basin development in order to mitigate the effects of human-induced global warming. Moreover, adaptation goals in river basins need to be redefined along with the process of urban development.

In a basin-scale climate, the anthropogenic warming from urban system is important to be considered while predicting the effect of climate change on the water resources. The comparatively higher temperature in the cities and suburbs than the rural areas creates urban heat islands. The effect of
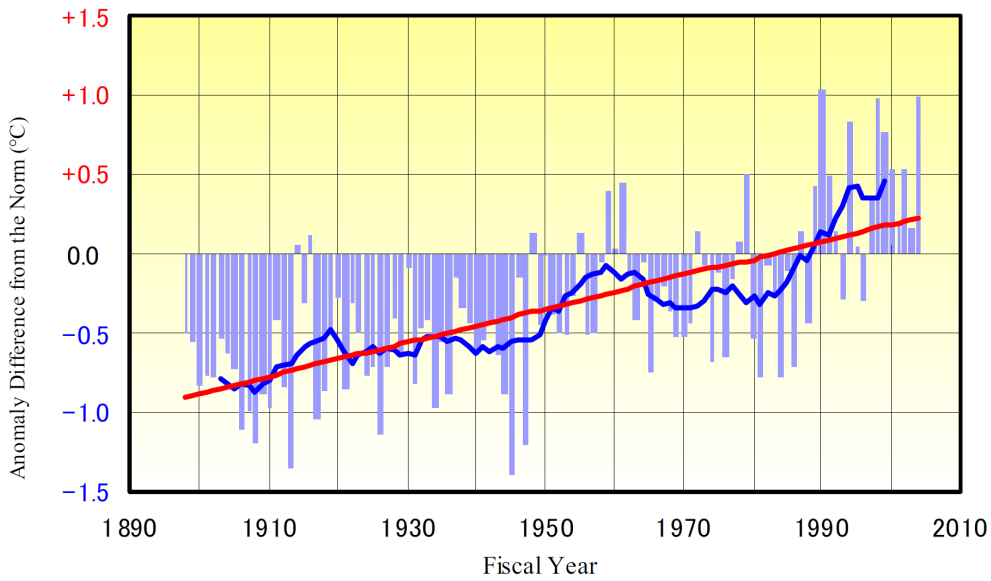
Figure 4: Change in the anomaly difference from the norm of annual mean surface temperature in Japan from 1898-2004. Light blue bars are yearly values. The mean temperature is calculated as the average of 30 years (1971-2000). (Source: Government of Japan (2006))

urban heat island can potentially induce changes in evapotranspiration and precipitation patterns in the river basins.

River basins: adapting to climate change

Integrated water resources management is an effective method of taking adaptive measures against the adverse effects of climate change on the water cycle and water resources. To develop a concrete national policy regarding such measures, Ministry of Land, Infrastructure, Transport and Tourism, Japan (2008) has proposed the following principle and purpose of integrated water resource management:

Principle: *Establishment of a lasting water-using society and a healthy water circulation system.*

Basic Purpose: *All the people can enjoy safe, untroubled, and rich water blessings.*

To apply the integrated approach of integrated water resource management, Water Resources Development Promotion Law, Ministry of Land, Infrastructure and Transport has termed river systems needing water supply measures due to urban and industrial development as "river systems for water resources development." Seven such river systems have been identified: Tone River, Arakawa River, Toyokawa River, Kiso River, Yodogawa River, Yoshino River and Chikugo River. Each of these river systems has "Water Resources Development Basic Plan" for water resource development. Out of these river systems, Yodogawa or Yodo River system (Fig. 35) lies in the Kinki region of Japan, which is situated in the southern central region of Honshu, and has a densely populated urban region. The Kinki region includes many big cities like Osaka, Kyoto and Nara. Yodo River originates from Lake Biwa (670.4 km^2), which is the biggest freshwater lake in Japan. Yodo River is nearly 75 km long and the Yodo River basin covers an area of 8240 km^2.

There are several important factors significantly affecting the water resources of Yodo River basin. The Yodo River basin receives many seasonal typhoons and heavy rainfall. Besides rainfall and typhoons, the river discharge in Yodo River basin is also affected by snow melting. Yodo River basin has also witnessed several cases of water supply shortage. Water demand has also increased due to urbanization and regional development. Kinki region is located mostly below the river water levels of the major rivers like Yodo River flowing through the region. So, the risk of embankment collapse and flood is substantial, and nearly 95% of the highly urbanized region of Osaka City has risk of flooding. In river basins, a more regional and local approach is necessary for study the effects of climate change on water resources.

The major problems and issues in Yodo River basin are:

- Integrated water resource management in Yodo River basin.

- Potential risk to water resources from climate change.

1.2 PURPOSE OF RESEARCH

1.2.1 *Major objectives*

To develop effective prediction tools for regional water resource management in Yodo River basin, the following objectives are considered:

- Develop a hydrometeorological prediction system to simulate water cycle of Yodo River basin by coupled modeling approach.

- Apply the hydrometeorological prediction system to study the impacts of future climate change on water resources of Yodo River basin.

1.2.2 *Importance of the study*

Japan is facing several water related problems due to the impacts of climate change (see subsection 1.1), and preventive measures are required to tackle them. So, integrated water resource management as an adaptation measure is essential to cope with adverse effects of climate change. In water resource management, integrated approach of predicting hydrological cycle is required to define risks associated with the effect of climate change on environment such as flooding, drought and depletion of water resources. Since the basin-scale water cycle can fluctuate along with the supply and demand of water in the future, prediction of the effect of climate change on water cycle is also crucial for stable water supply.

The interaction between air and landmass, including water, plays an important role in water cycle of a river basin. At river basins, the local impacts of meteorological forcings on the water cycle are difficult to be estimated using only climate models at global scale. The spatial resolutions of such models are very coarse and the fine spatial variability of river basins cannot be represented in such models. To regionalize the modeling approach, higher-resolution regional models are needed to reproduce more local effects of climate change on the river basins. The regional models can better represent the complex orographic features and land-use distribution of a river basin. Moreover, regional and local atmospheric phenomena like sea breeze, storm and mesoscale flows can be represented in such models.

Yodo River basin provides water resource to the highly populated areas of Kinki, Japan and Yodo River basin is vulnerable to negative impacts of climate change. Hence, integrated regional hydrometeorological modeling approach is necessary for integrated water resource management in Yodo River basin. Since the highly accurate prediction of extreme events is essential for assessing the impact of climate change, integrated monitoring and prediction system can be developed using the hydrometeorological system to track the magnitude

and frequency of extreme weather and climate. Water managers can also assess impact of changing climate variability on Yodo River basin.

Various urban development plans are implemented in the Yodo River basin to accommodate the urbanized and industrial sectors. The urban development also brings about several water related problems in the basin area. The effect of urban heat island and increase in water demand during dry periods will prove to be detrimental to the quantity and quality of water resources in Yodo River basin. The hydrometeorological prediction system can be synergistically applied in urban development implementations to adapt to the human-induced climate change.

1.3 METHODOLOGY

To achieve the objective of developing a high-resolution hydrometeorological prediction system for the Yodo River basin, the following approach was followed (Fig. 5).

- Validation and analysis of meteorological model

  Mesoscale meteorological models are used to simulate long-term mesoscale precipitation and other hydrometeorological variables in the Yodo River basin.

- Validation and analysis of urban canopy model

  The urban canopy model, coupled with the mesoscale meteorological model, is used to demonstrate the contribution of urban heat island effect on the water resources of urban region. The anthropogenic heat flux in urban region and the effect of urban canopy are included in the meteorological model to improve the representation of the effect of urban heat island on hydrometeorological variables.

- Validation and analysis of hydrological model

  Distributed hydrological model based on a rainfall-runoff model with a suitable evapotranspiration model and dam reservoir model is used to simulate the response of Yodo River to precipitation.

- Hydrological simulation of Yodo River basin by coupled hydrometeorological model

Hydrometeorological modeling of Yodo River basin is implemented using one-way coupled modeling approach. The meteorological forcings like air temperature and precipitation are converted into inputs for the hydrological model. The high-resolution modeling of meteorology and hydrology of Yodo River basin are carried out with mesoscale meteorological models and distributed hydrological model respectively.

- Effect of future climate change on hydrometeorology of Yodo River basin

  Response of the Yodo River basin to climate change is projected using an integrated hydrometeorological modeling approach consisting of regional basin-scale modeling of atmosphere and hydrology. The future trends of water resources in Yodo River basin are assessed by using the coupled hydrometeorological model.

1.4 CHAPTER ORGANIZATION

The chapters in the thesis are organized in the following manner (Fig. 5):

Chapter 1 introduces and discusses the issues and problems related to water resources in Japan. The importance of a high-resolution hydrometeorological prediction system for Yodo River basin is also described. Chapter 2 surveys the past research work related to water resource assessment in Japan, and different atmospheric and hydrological modeling approach taken by previous researchers. The need for further research work in water resource assessment in Yodo River basin is highlighted. Chapter 3 describes the meteorological models, urban canopy model and hydrological model used for developing a coupled hydrometeorological modeling system to study the water resources of Yodo River basin. Chapter 4 validates the use of MM5 and WRF mesoscale meteorological models to simulate the hydrometeorological variables like precipitation, air temperature, wind and solar radiation in Yodo River basin. Meteorological variables are validated against observed data. For example, precipitation output from WRF mesoscale model is compared with observation station data and radar precipitation results. In chapter 5, WRF mesoscale meteorological model is coupled with a single-layer urban canopy model to demonstrate the effect of urban heat island phenomenon on basin-scale air temperature and precipitation. The effect of urban heat on nocturnal temperature is highlighted and the change in precipitation events due to anthropogenic

heat flux and urban geometry is also indicated. In chapter 6, the use of distributed hydrological model containing runoff model, evapotranspiration model and simple reservoir model is shown to be able to simulate the water resource of Yodo River basin with some validation of reservoir outflows and river discharge against observed station data. Chapter 7 describes the coupling of WRF mesoscale meteorological model and distributed hydrological model to simulate the response of Yodo River basin to atmospheric forcings. Atmospheric forcings like air temperature and precipitation from WRF mesoscale model are applied as input to hydrological model in one-way coupling mode. The distributed hydrological model is shown to be capable of simulating the basin hydrology of Yodo River basin by replacing the atmospheric forcings from observation station data with the high-resolution gridded hydrometeorological variables from WRF mesoscale meteorological model. Chapter 8 discusses the effect of climate change on the water resources of Yodo River basin using the coupled hydrometeorological modeling approach described in chapter 7. Finally, chapter 9 summarizes some important conclusions of the work studied in this thesis. The limitations of the presented results and recommendations for future research are also presented in the summary.

Water Resource Assessment of Yodo River Basin Using Coupled Hydrometeorological Modeling Approach

Predicting the impact of climate change on water cycle of Yodo River basin

Integrated hydrometeorological modeling approach for air-water interaction in hydrological cycle

Precipitation and evapotranspiration processes

Soil storage, infiltration, river runoff processes, dam reservoir operations

Ch. 1: Introduction   Ch. 2: Literature review

Using mesoscale meteorological model

Using urban canopy model coupled with mesoscale model

Using distributed hydrological model

Ch. 3: Model descriptions   one-way coupling

Ch. 4: Meteorological modeling

Ch. 5: Urban canopy modeling

Ch. 6: Hydrological modeling

Precipitation from mesoscale meteorological modeling of Yodo River basin

Effect of urban heat and geometry on precipitation process in Yodo River basin

Rainfall-runoff modeling to predict response of Yodo River basin to precipitation

Coupled hydrometeorological modeling to predict hydrologic response of Yodo River basin to precipitation

Using one-way coupling of mesoscale meteorological model and distributed hydrological model

Ch. 7: Coupled hydrometeorological modeling

Response of Yodo River basin to climate change

Using future climate change scenario

Ch. 8: Effect of climate change

Conclusion

Ch. 9: Summary

Figure 5: Methodology and chapter organization.

LITERATURE REVIEW

The investigation on the impact of climate change on hydrology of a river basin and subsequently on its water resources is invariably based on regional climate modeling and distributed high-resolution hydrological modeling. In this chapter, earlier works conducted on these fields in general and those related to Yodo River in particular are briefly reviewed.

2.1 MESOCALE METEOROLOGICAL MODELING APPROACH

Global climate system and its future scenarios are generally studied by means of Atmosphere-Ocean General Circulation Models (AOGCMs). AOGCMs can produce some consistent regional responses to climate change, but due to the sheer complexity and length of simulation periods, AOGCMs used by IPCC have typical horizontal resolution from 400 to 125 km (IPCC, 2007a). To study regional climate changes, downscaling of AOGCM output is done using mainly dynamical and statistical approaches. Statistical downscaling approach is computationally cheap and it uses observational data to develop empirical relationship between multiple scales found in climate. But statistical downscaling can lack the ability to represent physical perturbations in the climate and it can also neglect regional feedbacks. Physically-based regional and mesoscale high-resolution atmospheric models can generate boundary conditions by dynamically downscaling the observed and AOGCM output data to simulate the atmospheric climate at mesoscale levels. But regional climate models can be computationally demanding and physical parameterizations may be imperfect for simulation at high-resolution spatial scales (IPCC, 2007a). With the increase in computing power and resources, the high-resolution regional and mesoscale atmospheric modeling efforts have gained momentum. For example, to increase the spatial resolution of GCMs, the Japan Meteorological Agency developed a global circulation model with 20-km resolution (http://www.kakushin21.jp/kyousei/k041open/) to provide

very high resolution required in regional climate studies (Water Resources Department, Ministry of Land, Infrastructure, Transport and Tourism, 2008). This high-resolution global climate data is being used by regional climate researchers to study the regional climate changes in the future.

IPCC (2007b) has extensively reviewed the current regional climate research and modeling efforts. IPCC (2007b) explains that Regional Climate Models (RCMs) can be used for regional climate modeling if large-scale atmospheric variables are available as lateral boundary conditions and SST as lower boundary condition. One-way and two-way coupling of RCM with GCM have also been used to study regional climates. RCM grids vary from nearly 50 km to very high resolution of 15-20 km and even to 5-km grids for short periods. In regional climate studies, the RCMs are increasingly being coupled with other regional counterparts such as regional ocean model, regional hydrological model, regional vegetation model, and so on. Long-term regional simulations are becoming the norm and regional ensemble simulations are also gaining attention. In fact RCMs have been shown to have capabilities to reproduce large-scale variabilities in air temperature and precipitations.

IPCC (2007b) also highlights some of the problems with RCMs such as the problems with lateral boundary conditions. Lateral boundary conditions could affect the RCM internal solutions at different levels depending on the size, season and location of the modeling domain. To overcome such problems, lateral boundary conditions from GCMs and Analyses data with high temporal resolution are used in RCMs. Biases in GCM can adversely affect the RCM simulations but RCMs are able to produce structures with higher resolution than GCMs. The current generations of AOGCMs have improved considerably and they can provide more accurate lateral boundary conditions for regional climate models. Even if these boundary conditions from GCMs do not contain small-scale phenomena, RCMs are capable of producing such fine-scale phenomena.

Hong and Lee (2009) used Weather Research and Forecasting (WRF) model to study flash flooding inducing heavy rainfall event in South Korea. They used nested domains with the smallest domain having 3-km horizontal resolution. They found that thunderstorms, squall line, convective band and precipitation were reasonably reproduced. The orographic effect was also simulated over the Korean peninsula.

Qian et al. (2009) used two dynamical downscaling techniques, known as subgrid parameterization and regional climate modeling, to investigate mountain hydrology. They downscaled NCAR Community Atmosphere Model (CAM3) GCM data at 1 degree x 1.25 degree horizontal resolution. They used subgrid orographic precipitation scheme for subgrid parameterization and WRF mesoscale meteorological model for regional climate modeling. Subgrid orographic precipitation scheme divides model grid cells into subgrid cells using high-resolution terrain data and then calculates the vertical motion of air parcels in subgrids based on the difference in terrain height of subgrid and the main grid. In regional climate modeling, WRF was used at 15-km horizontal resolution in Western U.S. region. Both downscaling methods produced similar spatial distribution of precipitation and snow cover but WRF produced better spatial representation of precipitation and snow cover in mountains because WRF could reproduce rain-shadow effects in the mountainous region.

Caldwell et al. (2009) used WRF mesoscale meteorological model to downscale Community Climate System Model (CCSM3) from 1 degree x 1.25 degree horizontal resolution to 12 km resolution in California. They found that spatial distribution of precipitation and surface temperature was improved by using dynamic downscaling. Prediction of extreme precipitation was also improved by WRF simulation. Dynamic downscaling also helped to better predict snowfall and snow cover. CCSM results for snowfall and snowmelt were nearly 4 times low than observed values but WRF results were nearer to the observation data due to better topographical representation and more snowfall at high terrains. But they also found some overprediction in wintertime precipitation, especially in mountainous region. This wintertime overprediction was not coming from CCSM and it may have been caused by WRF itself. They also reported that coastal sea surface temperature (SST) was overpredicted by both CCSM and WRF.

Takayabu et al. (2007) nested two regional climate models, known as Central Research Institute of Electric Power Industry RegCM3 (CRIEPI - RegCM3) and Meteorological Research Institute Regional Climate Model (MRI - RCM), into Meteorological Research Institute atmosphere-ocean coupled general circulation model (MRI CGCM2.2) to investigate the effect of global warming on regional climate. The two regional climate models at 60 km horizontal resolutions were used to project the past climate at the end of the 20th century and future A2 SRES climate scenario in 2050s in Asian monsoon region. They

found that regional near-surface air temperature was simulated satisfactorily. Precipitation in higher latitudes was better simulated than the lower latitude regions and change in precipitation was statistically insignificant in future scenario. They also showed that precipitation tended to converge at places having low model bias, thus suggesting the significance of regional climate modeling approach.

Considering that the computational resources are getting more and more accessible, and the mesoscale and regional climate models are being improved to increase accuracy and reliability, the use of dynamic downscaling of GCM and Reanalysis data to provide initial and boundary conditions for regional climate modeling of basin hydroclimate opens up a bright prospect of improving the assessment of water resources in river basins.

Precipitation from atmospheric models

Trenberth (1999) has proposed an explanation for increasing precipitation with climate change due to global warming. The increase in greenhouse gases increases global surfacing heating, and subsequently, air temperature and evaporation also increases. Then moisture content increases and the overall precipitation rate increases, thus increasing the risk of flooding and peak discharge.

But O'Gorman and Schneider (2009) have argued that the simulated future climate change scenarios do not show consistent change in extreme precipitations. They showed that precipitation extremes can also change with the changing climate and that they are related to moist-adiabatic temperature lapse rate, upward velocity and temperature during such extreme events. They have also explained that tropical precipitation extremes may not be accurately simulated by current climate models due to inaccuracies in upward velocities.

Shin and Hong (2009) used Weather Research and Forecasting (WRF) mesoscale meteorological model to reproduce heavy rainfall events. They carried out several quantitative experiments by changing different parameters and options. WRF was able to fairly simulate heavy rainfall but initial structure of typhoon was needed to correctly represent synoptic forcings. They found that one-way and two-way nesting and change in physics options did not improve the WRF simulation of extreme rainfall event. Cumulus

parameterization and planetary boundary layer scheme were recommended for improvement in order to better simulate the extreme precipitations. They also reported that WRF grid size of 3-km or less is required for accurate precipitation simulation.

Zwiers and Kharin (1998) used Canadian Center for Climate Modelling and Analysis GCM to study extreme climate changes in CO2 doubling scenario. They found that temperature extremes were fairly simulated by the model. The extreme temperatures might have been affected by changing albedo due to snow cover reduction and decrease in soil moisture. In the case of extreme precipitation, the increase was seen in several places in the world. They found the largest increase in extreme precipitation in northwest India due to increasing intensity of summer monsoon.

Sasaki and Kurihara (2008) used Nonhydrostatic Regional Climate Model (NHRCM) to relate precipitation with terrain elevation in Japan. They obtained increase in precipitation with elevation in all places of domain but with low correlation. The correlation between precipitation and elevation was improved by detailed classification of observation points into river systems. They concluded that the regional climate model could reasonably reproduce the precipitation-elevation relationship.

All in all, precipitation is one of the most important hydrometeorological forcing data to be used in the study of hydroclimate of a river basin. The model performance of climate models in simulating accurate spatio-temporal distribution of precipitation is not predictable as in the case of air temperature. So a comprehensive validation of precipitation results from atmospheric models is necessary to examine if further processing or improvement in precipitation is required.

2.2 EFFECT OF URBAN HEAT ISLAND ON BASIN HYDROCLIMATE

Heat island effect changes the local weather pattern, increases energy costs to offset this effect, and increases demand for cooling. While considering urban heat island, local effects due to waste heat from vehicles, as well as from building and commercial energy consumption should be taken into consideration.

The effect of urbanization on the regional and local scale climate is well-known, and urban warming, or urban heat island effect, is one of the major consequences of urban development. Urban warming in a regional setting with complex land-use including green space and suburban vegetation is caused by a blend of different physical factors such as the so-called urban canopies, surface materials and their characteristics, moisture characteristics, anthropogenic heat flux, and air pollution. Urban warming increases demand for air conditioning, and consequently, more air conditioners generate more heat and adversely affect the local scale climate including human comfort and demand for cooling (Grimmond, 2007). The world population is expanding and urbanization will double in next two decades leaving nearly 80% of world population in urban areas (Crutzen, 2004). Thus the understanding of the causes of urban heat island effect is crucial in developing and implementing mitigation strategies for urban warming.

Many physically based urban energy budget models (Masson, 2000; Masson et al., 2002; Grimmond, 1992; Arnfield and Grimmond, 1998) and urban canopy models (Ashie et al., 1999; Kondo et al., 2008; Kusaka et al., 2001; Kusaka and Kimura, 2004a; Bonacquisti et al., 2006)have been developed for the study of urban heat island. Thousand of literatures are available on the topic of urban heat island. Some reviews of research on urban heat island can be found in Rizwan et al. (2008) and Taha (1997), and review of Japanese urban heat study can be found in Ooka (2007). Similarly, numerous studies on urban heat island are available for cities around the world (Kim and Baik, 2002, 2004, 2005; Tong et al., 2005; Sailor and Dietsch, 2007; Saitoh et al., 1996; Sang et al., 2000; Oke, 1982, 1988; Ooka et al., 2004; Giridharan et al., 2004, 2005; Jauregui, 1997; Magee et al., 1999; Kolokotroni et al., 2006).

Effect of Urbanization on Precipitation

Lowry (1998) reviewed the urban precipitation climatology and proposed some research methods to study the urban effects on local and regional climate.

Shepherd (2005) reviewed the effect of urbanization on precipitation. Several impact mechanisms to describe urban-induced precipitation were listed, such as: higher convergence due to higher urban surface roughness, thermal perturbations of boundary layer and convective clouds created by urban heat

island effect, increase in urban aerosols for cloud condensation nuclei sources, diversion of precipitating system by urban canopy, and moisture urban source for convective flow.

Shepherd (2006) studied 108-year of precipitation data to search for rainfall anomalies in two arid urban areas of Phoenix in Arizona and Riyadh in Saudi Arabia. The comparison between pre-urban (1895 -1949) and post-urban (1950 - 2003) periods showed reasonable increase in mean precipitation by nearly 12 to 14% in monsoon season. Shepherd (2006) has also proposed to test the hypothesis that urban structure and irrigation change precipitation in arid regions.

There has been very few studies on urban-induced precipitation when compared to study on air temperature changes due to urban heat island effect. The urban-induced precipitation may have significant effect on the basin-scale water resources and the precipitation change due to urbanization should be investigated by using the mesoscale models coupled with urban canopy model.

Nocturnal heat island

The use of urban canopy model in idealized experiments with two-dimensional atmospheric model has shown the importance of using urban canopy models for the nocturnal heat island (Kusaka and Kimura, 2004a,b). Nocturnal heat island is caused by the larger heat storage in urban canopies compared to the surrounding rural areas, and the subsequent release of the stored heat as sensible heat at nighttime in urban canopies (Kusaka and Kimura, 2004b). Sensitivity experiments in idealized conditions have revealed that anthropogenic heating has a greater impact on the nocturnal temperature than other urban canopy parameters like heat capacity of wall, sky view factor and albedo (Kusaka and Kimura, 2004a). Compared to the idealized experiments, the use of real meteorological conditions in a mesoscale model can improve the accuracy and authenticity of the simulation results.

Though experiments related to urban heat island have been generally carried out for the Tokyo region in Japan (Kondo et al., 2008; Ichinose et al., 1999; Ooka et al., 2004; Ashie et al., 1999; Mochida et al., 1997), very few experiments are available for Osaka (Narumi et al., 2002), which is one of the metropolitan cities of Japan.

Lin et al. (2008) used Weather Research and Forecasting (WRF) mesoscale model coupled with Noah land surface model and urban canopy model to investigate the effect of urbanization in Taiwan. They used finest domain with horizontal resolution of 1 km size and they assumed anthropogenic heat of 200 W/m^2. They reported an improvement in the simulation of urban heat island effect, boundary layer development and land sea breeze. They found a significant effect of anthropogenic heat on nocturnal urban heat island intensity and boundary layer development.

Bonacquisti et al. (2006) developed an urban canopy layer model using energy balance equations and used the model to investigate urban heat island episodes in Rome. They confirmed the presence of nocturnal urban heat island in both summer and winter but they did not find major contribution from anthropogenic heat. They found the urban structure and thermal properties of materials to be the main causes of nocturnal urban heat island.

As mentioned above, urban heat island effect can significantly affect the meteorological as well as hydrological environment in urban regions. The use of urban canopy models with mesoscale meteorological models is bound to be effective in improving the atmospheric forcings applied on hydrological cycle of river basins that are influenced by urban effects.

2.3   HYDROLOGICAL MODELING FOR RIVER BASINS

In river basin, several modeling techniques have been employed to simulate the hydrological cycle and water balance for many purposes like flood forecasting, river discharge forecasting, reservoir operational management, rainfall-runoff relationship, effect of climate change on water resources and ecosystem, groundwater flows, water quality, orographic effect on basin discharge, urban drainage flow, and so on. Recent modeling techniques include stochastic models utilizing statistical relationships such as regressional and transfer functions between precipitation and runoff, and more complex physically-based distributed hydrological modeling that typically involve several sub-models such as evapotranspiration, surface runoff, subsurface water flow, groundwater flow, soil moisture flow, snow accumulation, snow and glacier melting, river channel routing, reservoir storage, lake retention, and so on.

Firstly, some hydrological modeling efforts in Japan are discussed with main emphasis on distributed hydrological modeling in river basins like Yodo River basin, which is also being used as the study domain in this thesis. Since many river basins in Japan are inherently linked with urbanized regions, the studies focusing on urban treatment of hydrological processes are also discussed. Then some other relevant examples of hydrological modeling of river basins in other parts of the world are briefly discussed.

Sayama et al. (2005) developed hydrological prediction system using Object-oriented Hydrologic Modeling System (OHyMoS) to simulate flood attenuation processes involved in dam reservoir operations in river basins. The hydrological prediction system consists of a river element model with kinematic wave model to represent channel flow, a sub-catchment element model to represent both the surface and sub-surface runoff at sub-catchments, and a lake element model to represent lake water flow. They also formulated dam operation rules to simulate the real dam operations by predicting the water level and discharge of dams based on precipitation and existing conditions of reservoir network. The dam model simulates by classifying complex dam operations into six categories of ordinary operation, operation under flood warning, preliminary release operation, peak attenuation operation, flood release operation and post-flood operation. Using the dam model, they assessed the dam effect in Yodo River basin and found that the construction of several dams in the basin caused peak attenuation, with specific result at Hirakata, where the flood discharge caused by 100-year return period of rainfall was corresponding to the allowable maximum flood discharge in 2000. In comparison, 30-year return period of rainfall was corresponding to the allowable maximum flood discharge in 1960 in Hirakata.

Tachikawa et al. (2007) built a "real-time distributed runoff forecasting system" for the Yodo River basin. The modeling system consists of a one dimensional slope flow simulation by a physically-based distributed hydrological model that uses a kinematic wave model. The modeling system also contains dam reservoir model. Real-time rainfall data from Japan Weather Association with 6-hr ahead forecast at 2.5 km horizontal resolution is used to drive the prediction system in order to predict river discharge at 3-km resolution in Yodo River basin. Dam inflow, outflow and operational stages are also predicted for eight dams in the basin.

Shrestha et al. (2005) used multiplicative random cascade method based on beta log normal model, multiplicative random cascade HSA method, and space-time rainfall modeling to disaggregate rainfall field from a coarse domain having 48-km and 100-min resolution to fine domain having 3-km and 10-min resolution in order to run hydrological simulation of Yodo River sub-basins. They tried to improve the hydrological simulation of Yodo River basin in Japan by using distributed hydrological modeling containing 250-m resolution DEM at each of the sub-basins of Yodo River basin. They also included dam and reservoir operation models. The distributed hydrological model also used OHyMoS model and surface-subsurface flow models. They found the disaggregated rainfall from space-time rainfall modeling to be nearer to the observed radar data.

Kojiri et al. (2008) used Hydrological River Basin Environment Assessment Model (HydroBEAM, Kojiri et al. (2002)) to investigate the impacts of global warming on the water resources and ecosystem of Nagara River basin in Japan. HydroBEAM runoff model consists of gridded mesh structure in a basin with digital elevation data for each mesh and four soil layers called A, B, C and D to represent the surface layer and sub-surface layers and to facilitate the vertical water movement. D layer represents the bottommost layer of the soil and does not contribute to the lateral water flow from the soil to the river channel of the corresponding mesh. Thus water has lateral movement in every single mesh of the basin from soil layers A, B, and C into the river channel. The river channel flow direction is set for all the mesh of the river basin. In HydroBEAM model, water intake and supply from various processes like domestic water supply, irrigation water supply, paddy field water storage and reservoir water storage systems are included. Several important hydrological processes including evapotranspiration, snow cover, snow melt, surface runoff, groundwater flow, channel routing, water intake and release, and paddy field runoff are included in the HydroBEAM modeling system.

Nawahda et al. (2005) calibrated the HydroBEAM runoff model for different initial conditions and parameters in Yasu River basin, Japan, and investigated the interaction between the surface and groundwater flows. They used kinematic wave model to represent surface runoff, Richard's equation to represent unsaturated soil and sub-surface flow, and unconfined groundwater flow model to represent groundwater levels. They also considered interception of rainfall, depression water storage processes, and reservoir operations. They

found the HydroBEAM runoff model, combined with a groundwater flow model, could generally reproduce the observed river flows and groundwater flows.

Ikebuchi et al. (2006) used a river basin environment assessment model (HydroBEAM) to study the variation and transport of water quantity and water quality. They used a long-term simulation of Nagara River basin using distributed mesh-type Hydro-BEAM rainfall-runoff model with multi-layered soil representation. They used digital elevation map to produce single river channel flow directions for each grid mesh of the basin.

Jia et al. (2001, 2002) used Water and Energy transfer Processes (WEP) distributed hydrological to simulate river discharges and groundwater levels in Ebi river watershed. They used a grid size of 50 m with a time step of 1 hour and they compared the present scenario (year 1993) and future scenario (2035) of water cycle after simulating the spatial distribution of water and energy in the watershed. The WEP model was found be suitable for catchments having complex distribution of land-use. They found a notable effect of urbanization on the hydrological cycle at watershed scales. From a 5-year study of the basin, they found that the use of infiltration trench in urban area can improve the water cycle by infiltrating storm water. They also compared the water balance of 1993 with that of 2035 and found infiltration will decrease and surface runoff will increase in the future due to the effect of urbanization.

Jia et al. (2007) used Water and Energy transfer Processes in Large river basins (WEP-L) to study hydrology and water quality in Yellow River basin, China. They improved the previous WEP hydrological model by adding a new criterion to accommodate the contributions of large as well as small river channels. They found that water quality had deteriorated more than the previously estimated values in the Yellow River basin by using the improved hydrological model. They could improve the simulation of water quantity and quality in the large basin areas, and thus, it produced better water information for better management and development of water resources in basin.

Smith et al. (2002) investigated the regional hydrological response of Charlotte metropolitan region in North Carolina, U.S. to the rapid urban growth in the region. They observed that many large floods occurred after urban growth in the region. They examined several hypotheses to link urbanization with increase in flood peaks. They studied spatio-temporal distribution of precipitation, soil moisture, increase in impervious surfaces, and changes in

urban drainage for five extreme flooding events since 1995 by using various observational data like radar data, rain gauge network data and stream gauge data.

Vaes et al. (2005) utilized areal rainfall correction coefficients to generate spatial variability of rainfall for simulation of urban drainage system. They used two types of areal correction coefficients used for model calibration and design applications. Using a spatial rainfall generator for hydrological modeling of urban drainage system in Flanders, Belgium, they found that the areal correction coefficients were dependent on the size of basin, scale of rainfall aggregation and rainfall intensity.

Daly et al. (1994) have used a statistical-topographic analytical model called Precipitation-elevation Regressions on Independent Slopes Model (PRISM) to prepare gridded precipitation in mountainous region of Willamette River basin, Oregan and entire western regions of the U.S. PRISM analyzes orographic precipitation using DEM and windowing method of grouping stations into common "topographic facets." Then PRISM calculates gridded precipitation using regressional relationship between terrain elevation and precipitation at each of the topographic facets. They found the localized precipitation−elevation relationship used in PRISM to have less bias and absolute error than other methods such as kriging, detrended kriging and co-kriging.

2.4   COUPLED HYDROMETEOROLOGICAL MODELING APPROACH

One of the main phenomena governing land-air interaction is the movement of water between atmosphere, lithosphere, hydrosphere and biosphere. Precipitation and evapotranspiration are two important processes in this hydrological cycle. In global as well as regional settings, global warming and climate change are intricately related with change in precipitation (Ramanathan and Feng, 2009). Basin-level regional modeling requires the consideration of climate change and high spatial resolution in precipitation to accurately simulate or forecast the regional hydroclimate (Dolph et al., 1992). The accurate representations of precipitation rate and the spatial distribution of precipitation are challenging and complex models are being used to improve the simulation of gridded high-resolution precipitation. Recently, mesoscale meteorological models have been widely used to predict and forecast high-resolution

mesoscale precipitation needed for heavy precipitation events and flood events (Mölders and Raabe, 1997; Lin et al., 2006; Verbunt et al., 2006; Seuffert et al., 2002; Hong and Lee, 2009). But only episode simulation and few long-term results on basin scale are available.

One-way coupling of meteorological and hydrological models is mostly used to drive hydrological models by the hydrometeorological variables like air temperature and precipitation generated by meteorological models (Mölders, 2005). Recently, the feedback from hydrological models to the atmospheric models are also being studied with special attention given to atmosphere−land surface interactions related mostly to changes in precipitation and soil moisture fields. Several researchers have investigated the method of solving the problem of spatial and temporal scale difference between atmospheric and hydrological models. They have come up with different downscaling and upscaling techniques as discussed below. Most researcher have focused on how to effectively use atmospheric forcing like precipitation in high spatial resolution settings of hydrological models. Several cases discussed below also highlight the importance of precipitation on hydrological processes and the effect of climate, orography and feedback from soil on precipitation formation. Due to high resolution of spatial and temporal scales needed for coupling atmospheric and hydrological model, many computational problems arise during such integrated hydrometeorological studies. These computational limitations are also being overcome with the use of more powerful computing resources and better atmosphere-hydrology coupling techniques such as some methods discussed below.

Yoshitani et al. (2001) developed two-way coupled Integrated Regional Scale Hydrologic/Atmospheric Model (IRSHAM) using areally averaged conservation equations in a regional atmospheric model for simulating long-term atmospheric and hydroclimate in Japan. The mesoscale atmospheric model employed in the integrated model consisted of 12 vertical layers and the atmospheric model was two-way coupled with the soil moisture flow model at the boundary layer. They used land surface model having vegetation model for interception of water by vegetation, evapotranspiration model and soil moisture flow model. They used the integrated model to simulate the climate of 1989 in Japan using a domain of 20 by 20 km^2 horizontal resolution nested inside a bigger domain having 60 x 60 km^2 resolution, and found that the

results reliably matched with the corresponding observed data in Tsukuba station, Japan.

Chino and Nagai (2003) developed a regional environmental assessment tool called "System for Prediction of Environmental Emergency Dose Information Multi-model Package" (SPEEDI-MP) to study pollutant flow across different media like atmosphere, land and ocean in the Asian environment. They used MM5 mesoscale meteorological model as the atmospheric model, Princeton Ocean Model (POM) as the oceanic model, and SOLVEG atmosphere - soil - vegetation model as the land surface model. All the sub-models in SPEEDI-MP were coupled to exchange heat, wind stress, precipitation and so on. The coupling was done using the vectorized and parallelized model programs for parallel simulation. Recently they have also been involved in the use of WRF mesoscale meteorological model at a very grid resolution of 1 x 1 km^2 to couple the atmospheric part of the model with the hydrological part containing the transfer of precipitation and evapotranspiration from the mesoscale model to hydrological model.

Yoshikane et al. (2005) coupled WRF mesoscale model with a hydrological model to simulate regional climate of Yellow River basin, China. They used WRF at 20 km horizontal resolution and simulated precipitation in the Yellow River basin. They found that orographic precipitation was more or less overestimated by WRF and they commented that it could adversely affect river discharge prediction by hydrological model, which would be driven by the WRF-generated precipitation results.

Verbunt et al. (2006) coupled numerical weather prediction models called hydrostatic Swiss Model (SM) and non-hydrostatic Alpine Model (aLMo) with Precipitation Runoff EVApotranspiration Hydrotope (PREVAH) distributed hydrological model in a one-way manner and validated the system at Rhine basin, Europe for flood predictions. The PREVAH hydrological model had spatial resolution of 500 x 500 m^2 and 1-hr time step. PREVAH model uses aggregation of gridded spatial information into hydrologic response units, HRUs, and it also contains evapotranspiration, snow and glacier melt, and soil moisture models. To couple the atmospheric and hydrological models, precipitation forecasts from weather prediction model were bilinearly interpolated from the atmospheric coarse grid of around 14 to 5 km resolution to 500 m grids of PREVAH hydrological model. Elevation correction was used to interpolate the air temperature data from atmospheric to hydrological model

and no bias correction was applied for precipitation and air temperature data. They also used lake retention function to model the retarding and flattening effect of Lake Constance by implementing linear reservoirs with translation function to simulate the routing and retention in the lake. They found that the coupled model could adequately predict extreme runoff peaks in the basin.

Lin et al. (2006) coupled Canadian atmospheric Mesoscale Compressible Community Model (MC2) with the Chinese Xinanjiang hydrological model to simulate heavy precipitation and flood events in Huaihe River basin, China. They used the hydrological model to predict flood and peak discharges using rain gauge precipitation and then MC2 precipitation. Though MC2 overpredicted the total basin precipitation, the use of precipitation data from the MC2 mesoscale model was found to be usable in flood simulations at basin-scale.

Yu (2000) developed an integrated Hydrologic Model System (HMS) and implemented subgrid-scale spatial variability in precipitation and hydraulic conductivity to improve the streamflow prediction. HMS basically connects the climate and atmospheric forcings between air, land surface and water bodies present at land surface and sub-surfaces. HMS can use the traditional observational meteorological data as atmospheric forcing or it can couple a mesoscale meteorological model with the hydrological model to use the meteorological variables simulated by mesoscale models as atmospheric forcing for the hydrological model. Yu (2000) used precipitation from coupled MM5 model in HMS to drive the hydrological model but found some serious underpredictions in streamflow, which was improved upon by applying subgrid-scale spatial variability in precipitation and hydraulic conductivity. Important parameters in hydrological model were improved by introducing subgrid-scale variability calculated by means of remotely observed digital data. HMS can be run at different time scales ranging from a few minutes to a few days of time step so that mesoscale models can be easily coupled with hydrological model. Yu (2000) applied HMS in a sub-basin of Susquehanna River basin in Pennsylvania, U.S., and found that the coupling of MM5 model with the hydrological model and use of spatial variability in precipitation and hydraulic conductivity produced good streamflow predictions when compared with the observed streamflows.

Yu et al. (2002) coupled Hydrologic Model System (HMS) with Regional Climate Model (RCM) to model the effect of multiple storm events in Susquehanna River basin on its soil, land and groundwater. HMS was calibrated

using observed soil and streamflow data and subgrid-scale variability in precipitation and hydraulic conductivity was also included. RCM can also obtain boundary conditions from a global climate model. RCM was used to simulate six storms by nesting 12-km gridded domain inside 36-km and 108-km domains. The 12-km domain precipitation results from RCM were downscaled to 1-km hydrological grid structure to simulate streamflows that compared quite realistically with the observed streamflows. But they also found some spatio-temporal difference between the RCM precipitation and the observed precipitation.

Westrick and Mass (2001) coupled MM5 mesoscale meteorological model and Distributed Hydrology Soil Vegetation Model (DHSVM) to simulate flood events in Snoqualmie River basin in Washington, U.S. They used MM5 with nested domains of 36, 12 and 4 km horizontal resolutions and hydrological model with 100 m horizontal resolution. They found that using only the observational precipitation data in DHSVM hydrological model produced underpredicted flows when compared with the observed data. They downscaled MM5 temperature, humidity, wind speed, shortwave and longwave radiation, and surface pressure to DHSVM grid by biparabolic interpolation, and also downscaled precipitation using Cressman method. Elevation correction was also applied to air temperature field and the feedback from hydrological model to the atmospheric model was neglected due to small scale of the basin. They found that the use of MM5 meteorological fields including some adjustments according to observation data could capture nearly 90% of the total the water flow.

He et al. (2009) coupled MM5 mesoscale meteorological model and "Soil and Water Assessment Tool" (SWAT) hydrological model to study the effect of orography on hydrological climate change in Qinling Mountains area in China. They found that climate change and orography of the region had significant effect on the hydroclimate in the surrounding region. They also reported that precipitation reduced appreciably due to increase in average air temperature. They used 5 x 5 km^2 horizontal resolution in the finest grid of MM5 to produce precipitation data for 44 sub-basins used in SWAT hydrological model. They have suggested that topographical and macro-scale effects may dominate the mesoscale meteorology at river basins.

Kunstmann and Stadler (2005) coupled MM5 mesoscale meteorological model with distributed Water Simulation Model (WaSiM) in a one-way mode

for high-resolution hydrometeorological simulation of alpine and orographically complex basin of Mangfall River in Germany. They calibrated WaSiM with station data from 18 gauges using 150 by 150 m^2 horizontal grid structure. To confirm the possibility of using MM5 meteorological output to drive the hydrological model, they downscaled global reanalysis data from 100 by 100 km^2 grid resolution to 2 by 2 km^{2}resolution. They found that the coupled hydrometeorological model could reasonably predict the observed runoff in the basin though it produced 21% less annual precipitation than station-based simulation. Some limitations of the coupled hydrometeorological model were some terrain bias in the modeled precipitation and difficulty in predicting snow accumulation and snow melting in the basin.

Wagner et al. (2009) compared three methods of producing meteorological forcings to drive distributed hydrological models for sustainable water management in regions with limited available meteorological data. The three methods applied in White Volta catchment in West Africa consisted of MM5 mesoscale meteorological model to produce the meteorological data, TRMM satellite data, and station data respectively. They found that TRMM data did not produce significant improvement in hydrological simulation. They found that MM5 generated meteorological gridded data was suitable for running the distributed hydrological model.

Kunstmann and Jung (2003) studied the feedback between land surface and atmosphere using MM5 mesoscale model in order to find the effect of evapotranspiration on rainfall in West Africa. They found both positive and negative feedback between initial soil moisture and precipitation. They also investigated the effect of change in land use on rainfall by changing the land use between various types and obtained spatially varying change in precipitation.

Kumar et al. (2008) coupled a high-resolution land data assimilation system called NASA's Land Information System (LIS) with Weather Research and Forecasting (WRF) mesoscale model to improve the interaction and feedback between the atmosphere and land surface. LIS contains several land surface models, high-resolution satellite and observation data, and data assimilation tools. The coupled modeling system can be used with different high-resolution land surface models. They found that the coupled LIS−WRF improved the prediction of clouds and precipitation by virtue of the better simulation of interaction between land surface and atmosphere.

Mölders et al. (1996) used two methods of subgrid scaling the hydrometeorological variables from a mesoscale meteorological model called GESIMA. They used mosaic approach considering land-use categories within a grid cell that interact independently with the mean atmospheric variables in the grid. Another approach was explicit subgrid strategy in which finer subgrid structure is developed inside the grid and the interaction between land and atmosphere is simulated for all the subgrids within the grid.

Mölders and Raabe (1997) coupled GESIMA mesoscale meteorological model with NASMO hydrological runoff model in a two-way manner. The hydrological model is driven by the evapotranspiration and precipitation from the mesoscale meteorological model and the effect of hydrological processes such as lateral movement of water is fed back to the meteorological model. GESIMA meteorological model was run at 5 x 5 km^2 horizontal resolution and NASMO runoff model was run at 1 x 1 km^2 horizontal resolution. Explicit subgrid scheme (Mölders et al., 1996) was used to downscale the meteorological variables to the hydrological model domain. Precipitation field was downscaled by using a relationship between grid elevation and precipitation. A one-day simulation using the two-way coupled model showed that hydrological processes such as lateral flow of water in hydrological model affected soil moisture and soil temperature, and thus it affected the formation of cloud and precipitation too.

Mölders and Rühaak (2002) added hydro-thermodynamic soil-vegetation scheme (HTSVS) in the GESIMA mesoscale meteorological model for integrated coupling between the meteorological model and a physically-based hydrological model. The meteorological fields from the mesoscale model were downscaled from 5 x 5 km^2 to 1 x 1 km^{2}grid structures and hydrological fields were upscaled in the opposite direction from hydrological model to the mesoscale model. They found that the effect of change in land-use was more pronounced when surface runoff was considered by using the coupled hydrometeorological model.

Seuffert et al. (2002) coupled Lokal Modell (LM) mesoscale weather prediction model with TOPMODEL-based Land Surface−Atmosphere Transfer Scheme (TOPLATS) in a two-way manner to find the effect of land surface hydrological model on the local weather. They found that the coupled model could improve the prediction of energy fluxes and precipitation. They used same grid structures for both models so that downscaling and upscaling was

not used but such downscaling and upscaling would be necessary in other cases when the two grids differ. They found that the two-way coupling could produce better soil moisture compared to just using soil moisture to initialize the meteorological model.

Zhan et al. (2008) used integrated hydrological−meteorological modeling approach to predict actual evapotranspiration at large spatio-temporal scales in China. They found that soil moisture was important for accurately predicting evapotranspiration. The integrated hydrometeorological model can be important in the study of impacts of climate change, land cover change and soil moisture on evapotranspiration.

2.5 IMPACT OF CLIMATE CHANGE ON WATER CYCLE

In Japan, the assessment of the impact of climate change on water cycle and water resources is being emphasized by the government and researchers. To provide a strong computational platform for distribution, use and sharing of various simulation models and model data, a common integrating platform called CommonMP (http://framework.nilim.go.jp/eng/index.html) is being developed in Japan (Water Resources Department, Ministry of Land, Infrastructure, Transport and Tourism, 2008). It contains several models like OHyMoS hydrological models and hydraulic models. Thus, CommonMP provides a common research tool for integrated assessment of water resources.

Today, the need of regional climate studies has increased due to increased risks associated with the impact of climate change on limited water resources. and basin-scale prediction of water resources are being sought after for gaining insight into the regional and local effect of climate change in the future scenarios. On this premise, several global and regional studies of hydroclimate and water resources are being carried out. Some of them are discussed below.

Barnett et al. (2004) used National Center for Atmospheric Research Parallel Climate Model (PCM) to assess the effect of climate change on water resources of western U.S. They argue that since the PCM is very conservative regarding climate sensitivity, the predicted rise in air temperature from PCM for global warming scenario is comparatively lower than most of the other GCMs. In spite of such conservative approach, the simulation results suggest that water resource problems will arise in the future due to increasing water demand.

Yoshitani et al. (2001) used coupled Integrated Regional Scale Hydrologic/Atmospheric Model (IRSHAM) to simulate the climate change scenario of atmospheric 1 x CO_2 and 2 x CO_2 concentration in Japan using initial and boundary conditions interpolated from Meteorological Research Institute GCM (MRI) output. They found that entire main island of Japan would experience an increase of nearly 2 °C increase in air temperature in doubled CO_2 climate change scenario. They also reported that annual precipitation would decrease over entire Japan with major decrease in central mountainous region of Japan.

Kojiri et al. (2008); Ikebuchi et al. (2006) used HydroBEAM to study the impacts of global warming on the water resources and ecology of Nagara basin, Japan. They validated the hydrological model for 1979 - 2000 period by using AMeDAS observation precipitation data from Japan Meteorological Bureau, and simulated the IPCC A2 SRES future scenario of the basin for 2079-2100. They used statistically downscaled GCM data from regional climate model called Meteorological Research Institute of Japan Meteorological Bureau RCM20 having 20 km resolution, which re-simulates the Coupled Global Circulation Model (CGCM2) for Japan. They reported that the effect of global warming will be evident at basin-scale with increase in summertime precipitation and river discharge, increase in air and water temperature, decrease in snow cover and increase in evapotranspiration. They are hopeful that better models to represent the effects of global warming can even more elaborate on the existing knowledge of the effect of global warming on basin hydrology.

Kim et al. (2008) studied the effect of climate change on Tone Rive basin and Yodo River basin using a distributed hydrological model called OHyMoS. They obtained hydrological input data from the output of 20-km super high-resolution global atmospheric general circulation model (AGCM20). AGCM20 run in the parallel-vector supercomputer system of Japan Meteorological Agency (JMA) called Earth Simulator. AGCM20 has nearly 20 km of horizontal resolution and 60 vertical layers. AGCM20 uses observed monthly mean sea surface temperature (SST) as the boundary conditions for the past time periods. For future projections, SST from Atmosphere-Ocean GCM (AOGCM) outputs used in IPCC Fourth Assessment Report. In the study of Yodo River basin, they used 18 grids of AGCM20 covering Yodo River basin to obtain the precipitation and evapotranspiration data for Yodo River basin. For Yodo River basin, they found that annual precipitation increases in the future by a

small amount, snowmelt decreases and evapotranspiration increases in the future. Even though the present snow amount in Yodo River is only about 95 mm per annum, it may decrease up to around 15 mm in future. They have projected the water resource of Yodo River basin to be uniformly distributed in the future with decrease in the seasonal variation of precipitation and river discharge. They also indicated that the present-day peak runoff might also diminish in the future with a longer rainy season.

Min et al. (2006) performed ensemble simulation of IPCC A2 and B2 climate change scenarios for East Asia using ECHO-G coupled climate model. ECHO-G uses ECHAM4 as the atmospheric model and HOPE-G as oceanic model. They found that near-surface air temperature and precipitation in East Asia were projected by all the simulations to increase in the 21st century more than the global mean values. The increase in total precipitation in JJA (June, July and August) was attributed to increase in convective precipitation and large-scale precipitations affected precipitation in DJF (December, January and February). They also found that GHG mitigation efforts would have not much impact on the contribution of convective and large-scale precipitation to total precipitation.

IPCC (2007a) has provided the results of several regional climate modeling efforts in the world. In East Asia, IPCC A1B model projected an increase in precipitation throughout the year. Several regional climate modeling are being used to study the precipitation amount, precipitation intensity, drought intensity, and other climatic variables that are affected by climate change. In Japan, regional climate models have been developed with very high-resolutions and several studies based on regional climate are available (Kanada et al., 2005; Yoshizaki et al., 2005; Yasunaga et al., 2006).

Yasunaga et al. (2006) used super high-resolution 5-km regional climate model called NHM to study precipitation during Baiu season in the future climate scenario. They found an increase in July precipitation following the increase in intensity of precipitation.

Kanada et al. (2005) also used NHM regional climate model to study mesoscale convective system during late Baiu season in global warming scenario. They found extreme heavy precipitation over Kyushu Island of Japan in July. Kitoh et al. (2005) reported that the frequencies of heavy precipitation days would increase but number of wet days would decrease in the future climate change scenario in Japan.

2.6   INTEGRATED APPROACH FOR WATER RESOURCE ASSESSMENT OF YODO RIVER BASIN

There have thus been various studies on the impact of climate change on water resources and hydrological cycle including those in Yodo River basin. Meanwhile, from the above reviews, it can be inferred that in spite of all the past and ongoing research efforts, there is still scope for improvement in the climate change studies related to the hydrological future of Yodo River basin. One such improvement can be realized by dynamically downscaling present and future global climate data by using coupled mesoscale hydrometeorological modeling approach to simulate the local and regional climatic effect on water resources of the basin, that is so vital for integrated use of water resources.

MODEL DESCRIPTIONS

3.1 METEOROLOGICAL MODELS

To investigate the hydrometeorological variables like near-surface air temperature and precipitation in a river basin, high-resolution mesoscale meteorological models can be used to resolve the spatial and temporal scales of the basin. Mesoscale models can be used to study atmospheric phenomena, such as land and sea breezes, squall lines, mountain waves, heat island circulations, thunderstorms and other mesoscale phenomena that have horizontal scale in the typical range of 2 to 2000 km (Lin, 2007). Mesoscale meteorological models are numerical models in a grid system that simulate geophysical fluid systems over the terrain. Mesoscale models are limited to a finite region, and hence, initial and boundary conditions are required to run these kinds of models. In real world applications, some physical processes like boundary layer processes, moist processes and radiative transfer processes are represented as sub-models or parameterized (Fig. 6). The interactions between the atmospheric, land surface and hydrological processes are represented in land surface models by simulating the exchange of surface moisture and energy fluxes.

Mesoscale models are computationally demanding and require a lot of computational power to run them at basin-wide scales. With the advent of parallel codes to simultaneously run the model codes in multiple computer processors, we have been able to run the mesoscale models at very high resolutions in the order of 1 km. To model the hydrometeorological variables in the Yodo River basin, the following system of software and hardware were used:

Software systems

- Mesoscale model: MM5-MPP version 3.7.0

- Mesoscale model: WRF Version 3.0
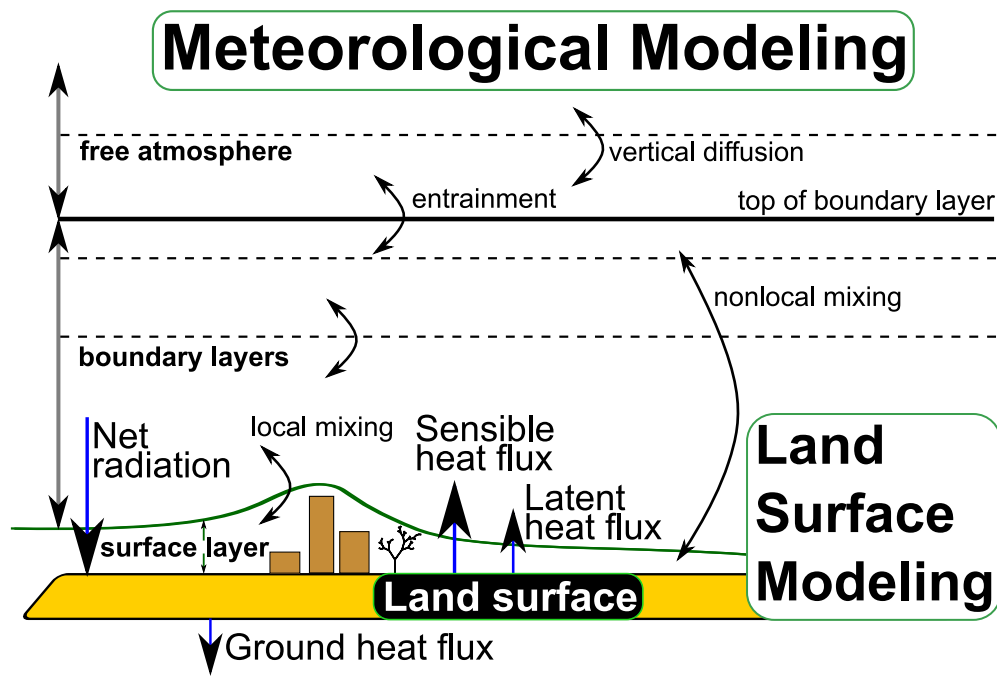
Figure 6: Processes involved in meteorological modeling.

- MPICH version 1.2.5.2 for parallel implementation of mesoscale models

- 32-bit PGI Workstation for Linux version 6.0 to run the models

- SuSe Linux Professional version 9.1 as the operating system

- RIP4, Vis5D+, NCL for data post-processing

- Python programs for data processing

Hardware systems

- Dell PowerEdge 750 and 850 (1.75 inch) (single Intel Pentium 4 processor (3.4 GHz), 1 GB RAM, Dual embedded Gigabit NICs) 17 racked boxes with hostnames: master, slave01, ..., slave17.

- Raritan Master Console II MCC 16 KVM Switch

The MPICH software was configured for the modeling system to run the program codes parallely in the available 27 CPU processors.

3.1.1 *MM5 mesoscale model*

The Pennsylvania State University (PSU)/National Center for Atmospheric Research (NCAR) Mesoscale Modeling System (MM5) is a limited-area, non-hydrostatic, terrain-following sigma-coordinate model designed to simulate or predict mesoscale and regional-scale atmospheric circulation (Dudhia et al., 2005; Grell et al., 1994). The meteorological fields like wind fields, temperature, water vapor mixing ratio, etc. can be generated by MM5 model. The final version (3.7) of MM5 was used without any four-dimensional data assimilation (FDDA). In order to initialize this model, we need input meteorological data that can be obtained from various global analyses and reanalyses data. In this study, NCEP final reanalysis data and the national mesoscale grid point value data (MSM GPV) provided by Japan Meteorological Agency were used to initialize the model. The details of this data, including its validation, are presented in subsection 4.3.2. Some pre-processing programs are available to convert the input meteorological, terrain, and land use data into the data format required by MM5.

United States Geological Survey (USGS) vegetation/land-use data having 25 categories and global coverage with the resolution of 1-degree, 30-, 10-, 5-, 2-minutes and 30-seconds was used in this study.

3.1.2 *WRF mesoscale model*

When MM5 code was frozen after version 3.7, community model development shifted to Weather Research and Forecasting (WRF) mesoscale model, which contained most of the physics and land surface models in MM5, and were re-written in a modular fashion for better code integration and more accurate numerics. So, WRF model was also adapted for meteorological modeling of Yodo River basin. WRF model is a numerical weather prediction and atmospheric simulation system with a flexible, modular and portable code design, and it is also regarded as a successor to the widely used MM5 model (Skamarock et al., 2005). WRF is a fully compressible and nonhydrostatic mesoscale meteorological model that utilizes terrain-following hydrostatic pressure coordinate. WRF is widely used at local scales to global scales. Different physics options are available for cumulus parameterization, microphysics,

longwave and shortwave radiation, land surface model, boundary layer model, etc.

The hydrometeorology of Yodo River basin is likely to be affected by the urban heat island effect due to the surrounding urban regions like Osaka. To investigate the effect of urban heat island on the urban atmosphere of Osaka region, urban canopy model is used in the mesoscale modeling system. Urban Canopy Model (UCM) used in WRF is a single-layer canopy model for energy and momentum exchange between the urban surface and the atmosphere, which includes the influence of street canyons, shadowing from buildings and reflection of radiation, anthropogenic heating, and multi-layer heat transfer equation for roof, building wall and road surfaces (Kusaka et al., 2001; Kusaka and Kimura, 2004a). Since it includes canyon orientation and the diurnal variation of solar azimuth angle, it can represent more realistic geometry than the commonly used slab models in meteorological models. This urban canopy model is coupled with the unified Noah land surface model used in the WRF modeling system.

3.3   HYDROLOGICAL MODEL

3.3.1   *Distributed hydrological model*

River flow, surface runoff, sub-surface groundwater flow, water intake, and dam reservoir operations in Yodo River basin is modeled using a high-resolution distributed hydrological model based on a rainfall-runoff model known as Hydrological River Basin Environment Assessment Model (HydroBEAM; Kojiri et al., 2002).

In the hydrological model (Fig. 7), the basin is divided into terrain grids that act as a single unit basin having 1 km x 1 km horizontal resolution. The grids also act as river flow network (Fig. 35) in which corresponding upstream grids are allocated for each of the downstream grids. The surface runoff in each grid flows into the corresponding downstream river grid. The terrain grid is divided into five land-use categories (fields, forest, urban, paddy and
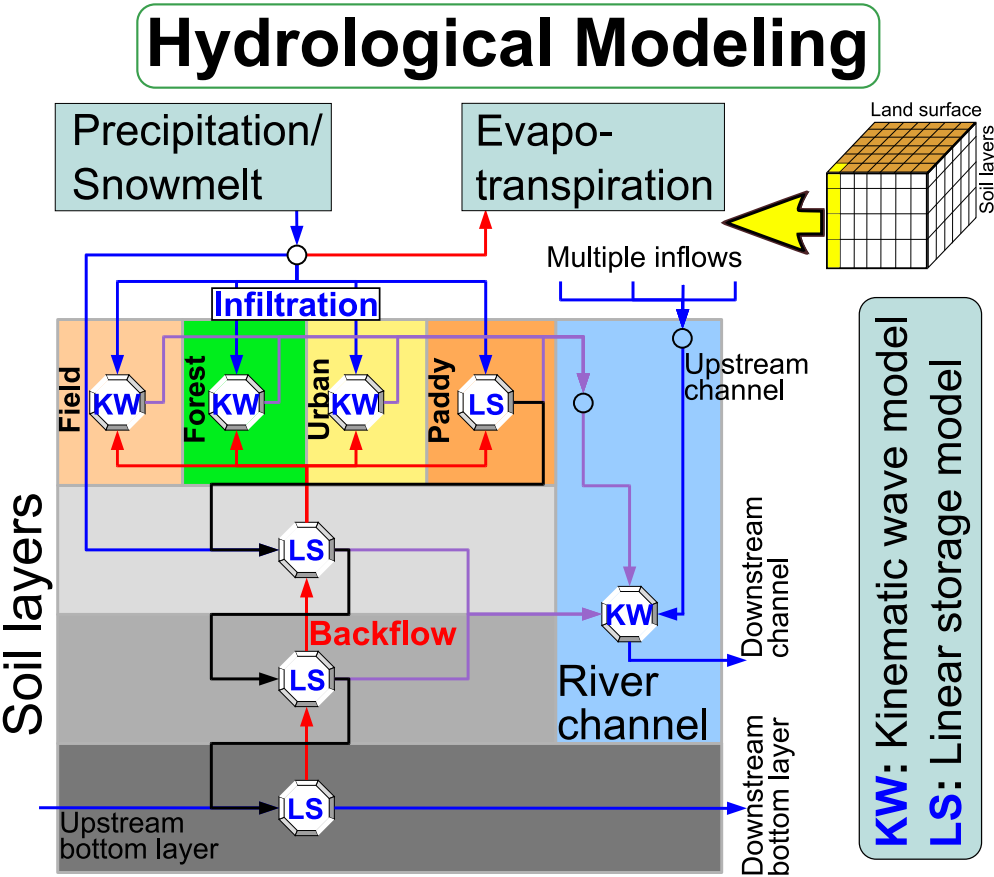
Figure 7: Rainfall-runoff hydrological model framework.

water). The basin units or the grids are vertically divided into four soil layers (A, B, C, and D from top to bottom respectively). Surface energy balance model (subsection 3.3.2) is applied at each grid to estimate rainfall, snowmelt and evapotranspiration. The surface runoff, runoff from paddy fields, ground water flow, water intake and release, and lateral water flows are simulated by HydroBEAM. The lateral movement of water in soil layers, except layer D, can flow into the river channel. The sewerage network, wastewater and irrigation canals in paddy fields are also included in the model.

3.3.2 *Surface energy balance model*

Using positive sign convention for incoming radiative fluxes and outgoing non-radiative fluxes from the surface, the surface energy balance equation for the basin grids is

$$R_N \downarrow + H_A = R_L \uparrow + H_S + H_L + H_G \tag{3.1}$$

where,

$R_N \downarrow$	Net incoming radiation
H_A	Anthropogenic heat flux
$R_L \uparrow$	Outgoing longwave radiation
H_s	Sensible heat flux
H_L	Latent heat flux
H_G	Ground heat flux

Here,

$$R_L \uparrow = \sigma T_s^4 \tag{3.2}$$

where,

σ	Stefan-Boltzmann constant
T_s	Surface temperature

$$R_N \downarrow = (1 - a) R_S \downarrow + R_L \downarrow \tag{3.3}$$

where,

$R_S \downarrow$	Incoming shortwave radiation
a	Albedo
$R_L \downarrow$	Incoming longwave radiation

Latent heat flux is given by

$$H_L = l\,E \tag{3.4}$$

where,

l	Latent heat of vaporization
E	Rate of evaporation

$$l = 2.5 \times 10^6 - 2400\,(T_a - 273.15) \tag{3.5}$$

where, T_a is near-surface air temperature.

Bulk transfer approach is used to calculate surface moisture flux. The bulk transfer equation for moisture flux is

$$E = \rho_a \beta\, C_H U\,(Q_s - Q_a) \tag{3.6}$$

where,

ρ_a	Air density
β	Evaporation efficiency
C_H	Bulk transfer coefficient
U	Near-surface wind speed
Q_s	Saturation specific humidity
Q_a	Near-surface specific humidity

Similarly, sensible heat flux is

$$H_S = c_p \rho_a\, C_H U (T_s - T_a) \tag{3.7}$$

where, c_p is specific heat of air at constant pressure.

Ground heat flux, H_G, is parameterized as having the diurnally averaged value of zero. Thus neglecting H_G,

$$(1-a)R_S \downarrow + R_L \downarrow + H_A = \sigma T_s^4 + c_p \rho_a \, C_H U(T_s - T_a) + l \, \rho_a \beta \, C_H U(Q_s - Q_a) \tag{3.8}$$

Taking all the expressions to LHS, we get the nonlinear function with respect to T_s, which is given as

$$\begin{aligned} f(T_s) = {} & (1-a)R_S \downarrow + R_L \downarrow + H_A - \sigma T_s^4 \\ & - c_p \rho_a \, C_H U(T_s - T_a) - l \, \rho_a \beta \, C_H U(Q_s - Q_a) \end{aligned} \tag{3.9}$$

Eq. 3.9 is solved by iteration method to obtain the surface temperature (T_s).

3.3.3 *HydroBEAM runoff model*

The surface discharge is calculated by kinematic wave model in all the land-use categories except paddy field. In paddy field, tank model (Fig. 8) is used. Soil layers B, C, and D are used to simulate the groundwater flow using linear storage model (Fig. 8).

Kinematic wave model for all land-use categories of A soil layer except paddy field

Kinematic wave equation for the A soil layer except paddy field is given as:

$$\frac{\partial h_{al}}{\partial t} + \frac{\partial q_{al}}{\partial x} = r \, f_{al} \tag{3.10}$$

$$q_{al} = \begin{pmatrix} \alpha(h_{al} - d_a)^{5/3} + a \, h_{al} \\ a \, h_{al} \end{pmatrix} \quad \text{when} \quad \begin{pmatrix} \geq d_a \\ < d_a \end{pmatrix}, \quad d_a = \lambda_a D_a \tag{3.11}$$

where,
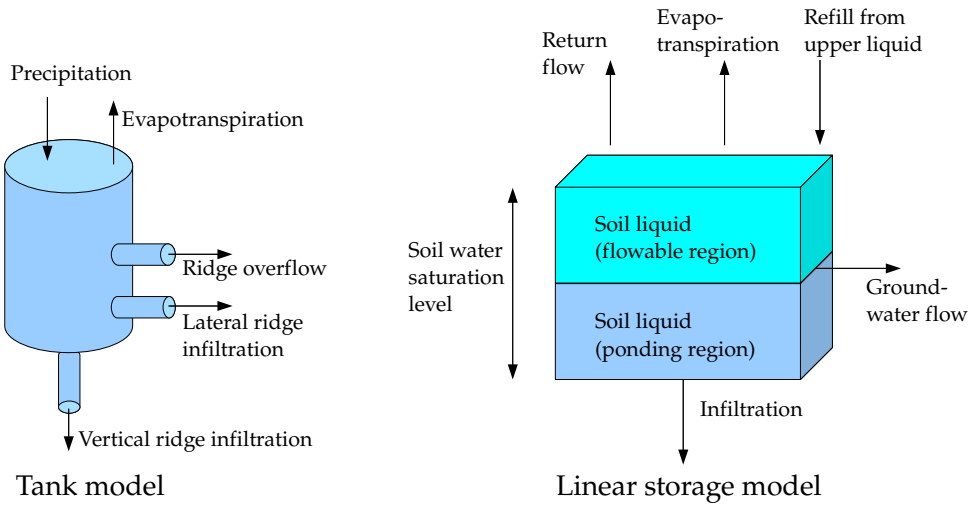
Figure 8: Sub-models used in HydroBEAM rainfall-runoff model.

h_{al}	Water depth of A soil layer for l land-use categories
q	Outflow rate per unit width
r	Rain rate
f	Direct runoff percentage
d	Saturation storage water level
α	$\frac{\sqrt{\sin\theta}}{\lambda_a}$
$\sin\theta$	Slope gradient
a	$\frac{k\sin\theta}{n}$
k	Hydraulic conductivity
n	Equivalent roughness of slope
λ_a	Porosity
D	Layer thickness
l	Land use category

Rain rate, r is calculated by deducting evapotranspiration amount from precipitation.

Tank model for paddy field

In paddy field, tank model (eq. 3.12) is used with three holes (denoted by *j*) acting as upper ridge overflow, middle lateral ridge infiltration, and lower vertical ridge infiltration (Fig. 8).

$$\frac{\partial h_{ap}}{\partial t} = r f_{ap} - q_{ap} \tag{3.12}$$

$$q_{ap} = \sum_{j} ap_j \max(h_{ap} - zap_j, 0) \tag{3.13}$$

where,

h_{ap}	Water storage depth of paddy field
q_{ap}	Outflow rate
ap	Tank model constant
zap	Tank model constant

Linear storage model for B soil layer

The linear storage model used for the water flux in B soil layer is:

$$\frac{\partial h_b}{\partial t} = I_b - q_b, \quad q_b = qh_b + qv_b \tag{3.14}$$

$$I_b = r(1 - \overline{f}_{al}) + u_c, \quad \overline{f}_{al} = \frac{\sum_l f_{al} A_l}{\sum_l A_l} \tag{3.15}$$

$$qh_b = kh_b \max(h_b - z_b, 0), \quad qv_b = kv_b h_b, \quad z_b = D_b(\lambda_b - \lambda_w) \tag{3.16}$$

$$u_b = \begin{pmatrix} h_b - d_b \\ 0 \end{pmatrix} \quad \text{when} \quad h_b - d_b \begin{pmatrix} \geq 0 \\ < 0 \end{pmatrix}, \quad d_b = \lambda_b D_b \tag{3.17}$$

where,

I	Inflow rate
h	Water storage depth
u	Return flow rate
qh	lateral outflow rate
qv	vertical outflow rate
kh	Soil constant for horizontal direction
kv	Soil constant for vertical direction
λ_w	Porosity contributing to outflow
A_l	Coverage area of l land-use category

When water level increases beyond the saturation storage water level, the excess water is sent back to the upper soil layer as u return flow.

Linear storage model for C soil layer

The linear storage model for C soil layer is:

$$\frac{\partial h_c}{\partial t} = I_c - q_c, \quad q_c = qh_c + qv_c \tag{3.18}$$

$$I_c = qv_b + u_d \tag{3.19}$$

Linear storage model for D soil layer

Linear storage model equation for D soil layer is similar to the equation for C soil layer but there is no return flow coming into D soil layer, which is the bottommost layer. Similarly, there is no vertical outflow from D soil layer.

$$\frac{\partial h_d}{\partial t} = I_d - q_d, \quad q_d = qh_d \tag{3.20}$$

$$I_d = qv_c \tag{3.21}$$

Kinematic wave model for river stream

The kinematic wave model used for each river grid in the hydrological model is:

$$\frac{\partial Ar}{\partial t} + \frac{\partial Qr}{\partial x} = qr \tag{3.22}$$

$$Qr = \alpha_r Ar^{4/3} \tag{3.23}$$

$$\alpha_r = \left(\frac{\sqrt{I}}{n}\right) \left(\frac{m}{\left(2\sqrt{1+m^2}\right)^2}\right)^{1/3} \tag{3.24}$$

$$qr = 2\frac{\sum_{l,l\notin p} q_{al} A_l}{\sum_l A_l} + \frac{q_{ap} A_{l,l\in p} + (q_b + q_c)A + q_w}{bl}, \quad A = \sum_l A_l \tag{3.25}$$

where,

Ar	Stream cross-section area
Qr	Outflow rate
qr	Lateral inflow rate
bl	Stream length
m	Stream slope gradient
I	Stream slope
n	Equivalent roughness of stream
A	Basin area excluding water bodies
q_w	Drainage discharge
l	Land-use categories
p	Paddy land-use category

The lateral inflow to the river grid contains flows from A, B, and C soil layers and drainage discharge.

3.3.4 *Snowfall and Snowmelt*

Snowfall and snowmelt are modeled by an energy balance at a single layer of snow. Differentiation between rain and snow is made by the relation shown in eq. 3.26. When near-surface air temperature is less or equal to the critical temperature, then snowfall occurs.

$$T_a > T_c \tag{3.26}$$

$$T_c = (11.01 - 1.5\,e) + 273.15 \tag{3.27}$$

where,

T_a	Near-surface air temperature
T_c	Critical temperature
e	Water vapor pressure

3.3.5 *Dam operation model*

Yodo River basin is a multi-purpose river basin regulated with a network of dam reservoirs that is used for flood attenuation, water supply and power generation. There are different sizes of dams in the Yodo River basin but six large dams have been selected for this study (shown in Fig. 35). The size and capacity of the six dams are shown in Table 1).

In general, the effect of dam reservoirs is included as actual outflow boundary conditions for past scenarios. But this method cannot be use for the future scenarios. To develop a generalized dam model, a simplified operation rule was modeled to simulate the actual dam operation. Since the regulation of water flow in the rivers needs to be considered to correctly predict the outflow
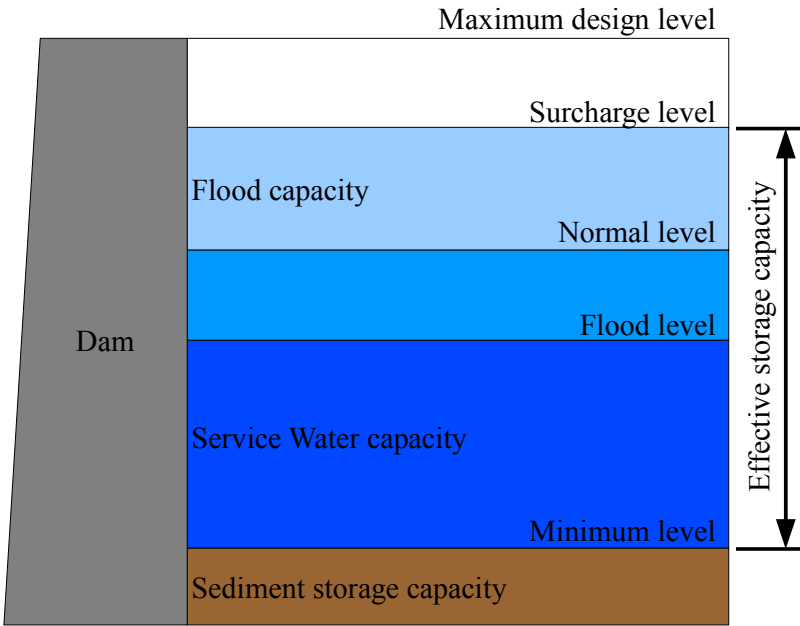
Figure 9: Structure and different water levels of a dam.

of the rivers, a simple water level fluctuating dam model was constructed, in which the desired water levels are set according to the normal water levels and flood water levels stipulated by the present dam operation rules (Fig. 9 and Table 2). The maximum allowed water level is the surcharge level and the water level is not allowed to decrease beyond the minimum level. According to the water levels set for the flooding and non-flooding seasons, the outflows of dams are adjusted such that the required water levels are maintained. In real dam operations, the weather reports and forecasts are referred by dam operators to predict the floods according to the precipitation rate in the dam basins. In the simplified dam model, the past and future precipitation forecasts are directly obtained from the meteorological input from the mesoscale model. The water levels are accordingly lowered to adjust for the flood. There are several modes of operation depending upon the intensity of precipitation and estimated flood (Sayama et al., 2005). But in the simplified model, only a single operation rule was applied so that the water level is adjusted if the precipitation intensity predicted by the meteorological model for the next day is more than 50 mm/day in the terrain grid of the dam.

Table 1: Database of six major dams of Yodo river basin for 2006.

DAMS	INTAKE AREA (KM^2)	TOTAL VOLUME ($\times 10^6$ M^3)	FLOOD CONTROL STORAGE[1] ($\times 10^6$ M^3)
Nango-araizeki	3848	27500.0	2221.0[2]
Amagase	4200	26.3	20.0
Takayama	615	56.8	35.4
Nunome	75	17.3	6.4
Hiyoshi	290	66.0	42.0
Hitokura	115	30.8	17.5

[1]From normal water level at flooding season to surcharge water level.

[2]Capacity of Biwa lake from standard water level of -0.3 m to design high-water level of 1.4 m.

Table 2: Different water levels of six major dams of Yodo river basin for 2006.

DAMS	WATER LEVELS	(EL M)[1]	
	SURCHARGE	NORMAL (NON-FLOODING)	NORMAL (FLOODING)[2]
Nangoaraizeki	1.4	0.3	-0.2 BSL m (6/16-8/31) -0.3 BSL m (9/1-10/15)
Amagase	78.5	78.5	72.0
Takayama	135.0	135.0	117.0
Nunome	287.3	284.0	280.6 (6/16-8/15) 279.2 (8/16-10/15)
Hiyoshi	201.0	191.4	178.5
Hitokura	152.0	149.0	135.3

[1]From Dam Database of Ministry of Land, Infrastructure and Transport, Japan.
[2]Flooding season is 6/16-10/15 if not stated.

VALIDATION AND ANALYSIS OF METEOROLOGICAL MODELS

4.1 INTRODUCTION

Prediction of the response of a river basin to climate change requires an integrated approach consisting of regional modeling of atmosphere and hydrology. Atmosphere is linked to land surface by precipitation and evapotranspiration. At the regional basin scale, the spatial variability of near-surface air temperature and precipitation are crucial for accurate prediction of runoff and overall hydrological cycle.

In this chapter, the suitability of using MM5 and WRF mesoscale meteorological models to produce high-resolution hydrometeorological variables is investigated and validation of the results of important hydrometeorological variables is also discussed. Firstly, MM5 mesoscale model is used to simulate meteorological variables in Osaka region to validate the use of high-resolution modeling in the highly urbanized city area situated in the Yodo River basin. The results of the MM5 model are evaluated quantitatively using statistical measures and the effect of different time scales on the meteorological variables is discussed.

In section 4.5, modeled precipitation in Yodo River basin is evaluated and validated against the observation data. As discussed in subsection 3.1.2, WRF mesoscale meteorological model is used to produce high-resolution hydrometeorological variables including mesoscale precipitation in Yodo River basin of Japan. Nesting of high-resolution mesh inside a coarse mesh produced a downscaled precipitation data with 3-km grid size. The 3-km gridded precipitation data was further downscaled to 1-km grid data according to the terrain structure. The spatial and temporal features of this precipitation data were validated with Radar GPV (Grid Point Value) data and observed station data.

4.2   DOMAIN AND GRID STRUCTURES

The Osaka prefecture region in Yodo River basin was selected as the target area for evaluating the MM5 model (Fig. 10). The area around Osaka was used as the finest domain area with a grid size of 1 km (Domain 3). This domain was nested inside a coarser domain with a grid size of 3 km (Domain 2). These domains were further nested in the coarsest domain of 9 km grid size covering nearly all of Japan (Domain 1).

Osaka is located slightly west of the middle of the Japanese archipelago and it is one of the largest metropolises in Japan and the center of western Japan. Osaka Prefecture consists of 33 cities, 10 towns and 1 village, including the City of Osaka (according to `http://www.epcc.pref.osaka.jp/center/english/environ/index.html`). Osaka Prefecture covers an area of 1,892 square kilometers, only 0.5 percent of the national land area, the second smallest among Japanese prefectures. Osaka extends from north to south and it is surrounded by mountains on three sides (terrain elevation is shown in Fig. 11). Its western face looks out to Osaka Bay and an alluvial plain spreads across the mouth of the Yodo River as it empties into the bay.

In the MM5 simulation, the simple ice scheme was used for the microphysics option. Similarly, Dudhia's longwave and shortwave radiation schemes were used. The Grell cumulus parameterization scheme and Medium-Range Forecast (MRF) PBL scheme (Hong and Pan, 1996) with multi-layer soil model (Dudhia, 1996) were used.

4.3   INPUT DATA

4.3.1   *Observation stations*

For evaluation of the simulated meteorological variables, the observation data were obtained from the "Air Pollution Continuous Monitoring Network Data Files" provided by Environmental Pollution Control Center, Osaka Prefecture. The air pollution monitoring network of Osaka covers the Osaka prefectural area with 20 air monitoring stations, and 11 auto exhaust monitoring stations. The monitored items are SO_2, particulate, oxidants, CO, NO, NO_2, hydrocarbons, meteorological parameters and traffic volume. So the Osaka prefecture
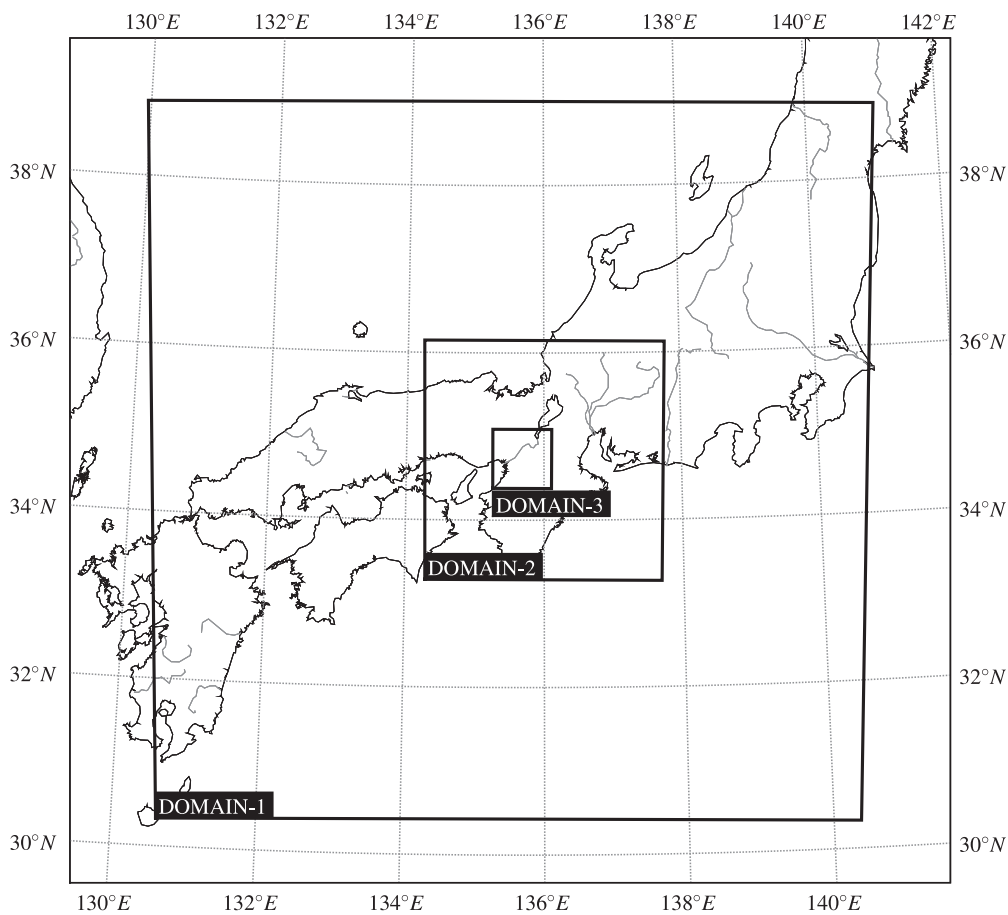
Figure 10: Nesting of model domains for MM5 model.
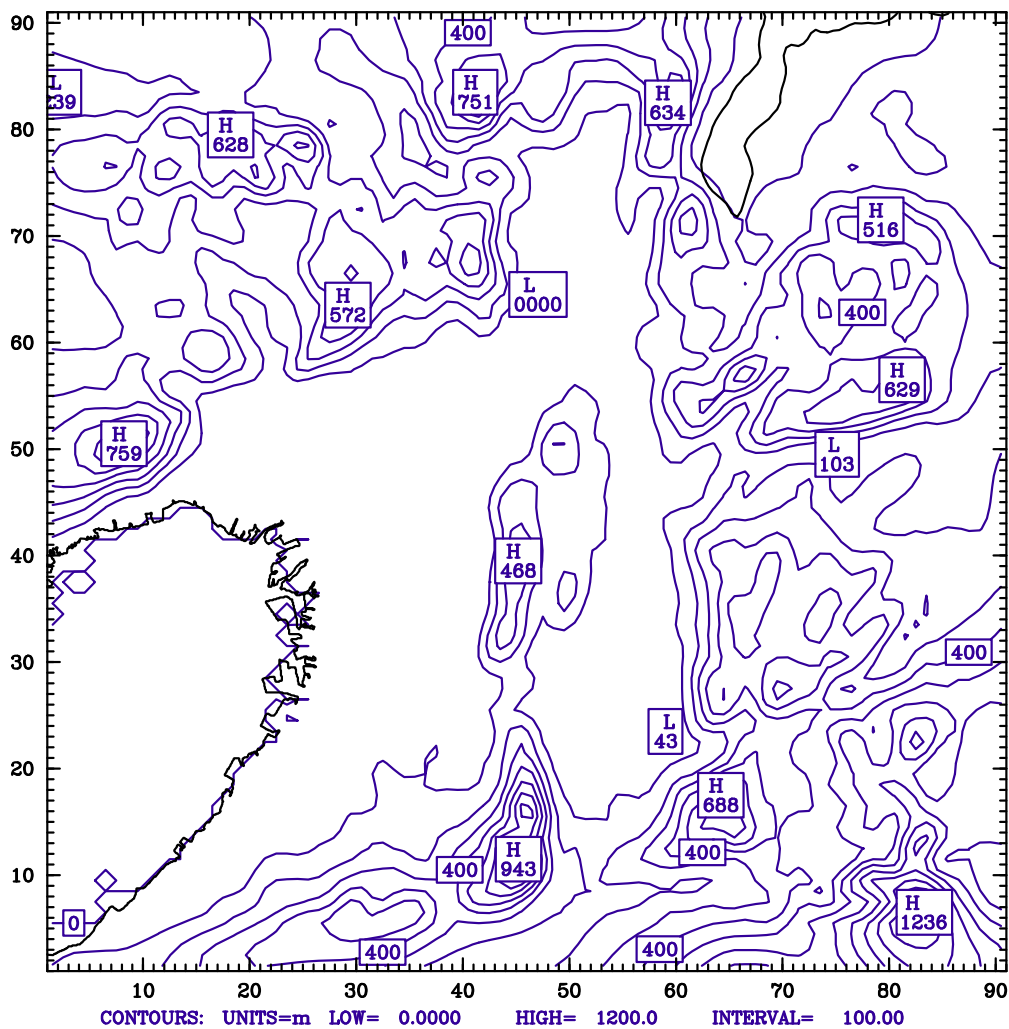
Figure 11: Terrain contour plot of Osaka and surrounding region.
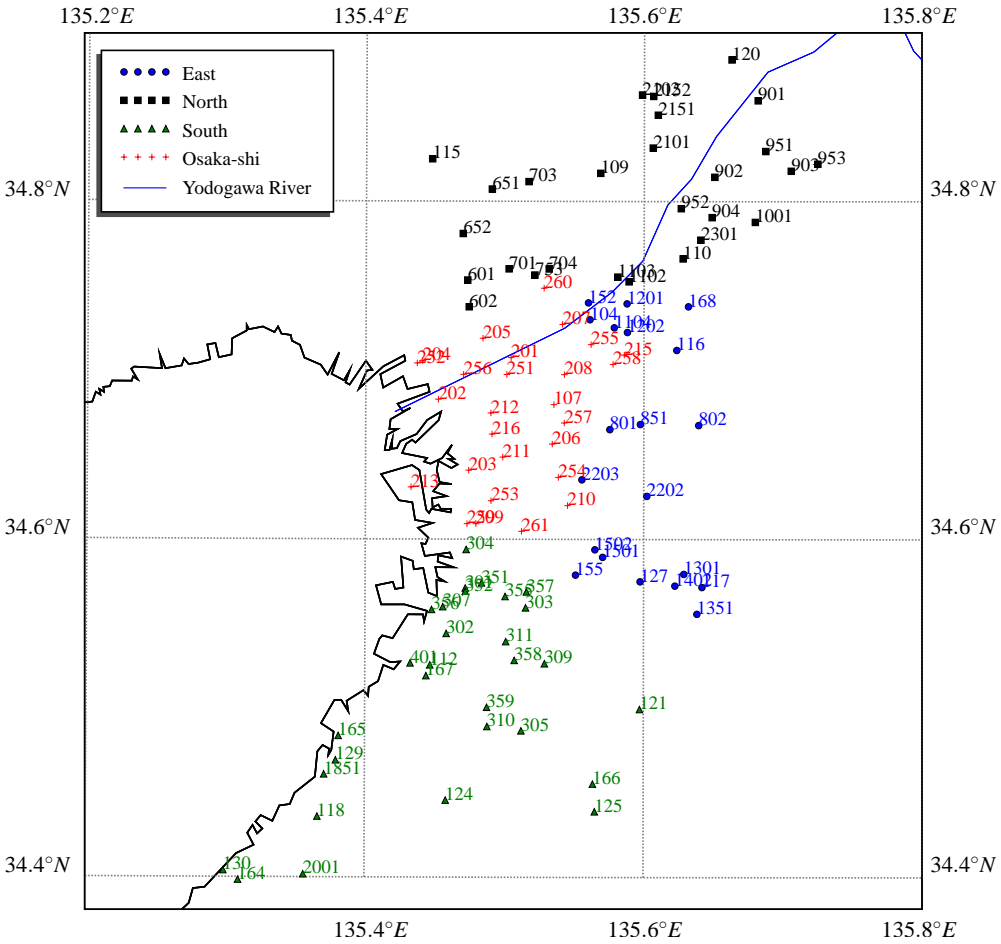
Figure 12: Observation stations of Osaka Prefecture.

has 31 air monitoring stations. Similarly, there are 94 stations in the various cities of Osaka. The online repository of Osaka prefecture and Osaka City (Osaka-shi) contains a well-managed set of observation data for more than 100 station points spread across the prefecture. Fig. 12 and Appendix A show the station points used in this study for the purpose of evaluating mesoscale model performance.

4.3.2 *Meteorological input data*

The MM5 model requires topography, land use and gridded atmospheric data. Several gridded data have been used to input meteorological data into the

MM5 model. The performance of MM5 may depend upon the spatial and temporal resolution of these data. MSM GPV (Mesoscale Grid Point Value) meteorological data from Japan Meteorological Agency (JMA) was used as the meteorological input data. The datasets obtained from the Mesoscale Model (MSM) has the following characteristics:

Time unit	UTC
Initialize time	0.00, 6.00, 12.00, 18.00 hours
Output interval	every 3 hours for the pressure levels
Area covered	22.4°N - 47.6°N ; 120°E - 150°E
Grid size	0.2×0.25 degrees horizontal resolution
Data format	Japan's domestic grid binary format (DGRB) defined by JMA (similar to GRIB format but much simplified)
P-levels (Pa)	97500, 95000, 92500, 90000, 85000, 80000, 70000, 50000, 40000, 30000, 25000, 20000, 15000, 10000

Available meteorological variables in MSM GPV datasets[1]:

z geopotential height (m)

u u-component of wind (m/s)

v v-component of wind (m/s)

w vertical velocity (m/s)

t temperature (°C)

h relative humidity (%)

r total precipitation or rain (at the surface) (mm/hr)

p_{msl} Pressure reduced to mean sea level (at the surface) (hPa)

REGRID program in MM5 creates meteorological fields on the mesoscale grid domain. REGRID contains two main programs called "pregrid" and "regridder". "Pregrid" pre-processes gridded, pressure-level meteorological

---

1 Out of these parameters, w and H are not available for 25000, 20000, 15000, 10000 pressure levels

fields from available datasets and puts the data in a binary intermediate format. "Regridder" takes the intermediate-format data and topographic data and creates 3-dimensional meteorological fields of wind, temperature, relative humidity, geopotential height, and 2-dimensional fields like sea-level pressure and sea-surface temperature.

The MSM GPV data was converted into the MM5's REGRID intermediate file format so that it can be used as input to the "regridder" directly without using the "pregrid" utility. The MSM GPV binary data was converted to ASCII text file by using the GPV Decoding Program provided in Meteorological Data Explorer (METEX) program. Then the text files were converted into the intermediate file format. In addition to these steps, some changes were made in the converter program to convert the MSM GPV data into the intermediate data files. Some of these steps were:

- The 97500 Pa level data was assumed to be 100000 Pa level data since there were no 100000 Pa level data in MSM GPV datasets. (The data can eventually be extrapolated to this pressure level, if needed.)

- Since the relative humidity field was missing in the pressure levels at 25000 Pa and below, the datasets at the 30000 Pa were used at these pressure levels (assuming that relative humidity is sufficiently constant at these high altitudes).

- The surface-level temperature data was used as the skin temperature (a skin temperature field represents the temperature of the surface of the earth, whether that surface is land or water).

Some of the limitations of using the MSM GPV datasets are:

- It can only be used for the Japanese and some of the nearby territories because it covers only the [22.4°N - 47.6°N ; 120°E - 150°E] area.

- It may not be possible to use all of the 3 hourly data of the MSM GPV datasets because several data are missing at 21 hours time period. So we can only use the 6 hourly data in these cases.

Validation of MSM GPV data

Since the high-resolution MSM GPV data is available for the Japanese region, the feasibility of using this data in the MM5 model was investigated using a

Figure 13: Time series comparison of u-component of wind between the MM5 output using MSM GPV and NCEP data with respect to observed data at Fujiiderashiyakusho station.

model test for the period of three months ($01/07/2004 - 30/09/2004$). Since the MSM GPV data has not been extensively used in the MM5 model, it was validated against the US NCEP (National Centers for Environmental Prediction) FNL (Final) Operational Global Analysis data by comparing the results with the observation data of Osaka Prefecture. The NCEP data is commonly used in mesoscale meteorological models like MM5 and WRF and it is available on 1.0 x 1.0 degree grids continuously at every six hours since 1999 (http://dss.ucar.edu/datasets/ds083.2/).

The time series outputs of the variables like u-component of wind (Fig. 13), v-component of wind (Fig. 14), and near-surface air temperature show the general trend of these variables in comparison with the observed values at different observation station in Osaka Prefecture region. The statistical analysis of the outputs using the MSM GPV and NCEP datasets (mean bias of wind components and near-surface air temperature are shown in Fig. 15 and 16) also indicate that u-component of the wind is slightly better simulated by the MM5 model while using the MSM GPV dataset. These and other outputs using both the MSM GPV and NCEP datasets show that the variables are generally well-simulated when using these datasets. Thus the MSM GPV datasets have been shown to have encouraging performance results while further research work is recommended for discovering the greater utility of this dataset in the field of atmospheric modeling and prediction.
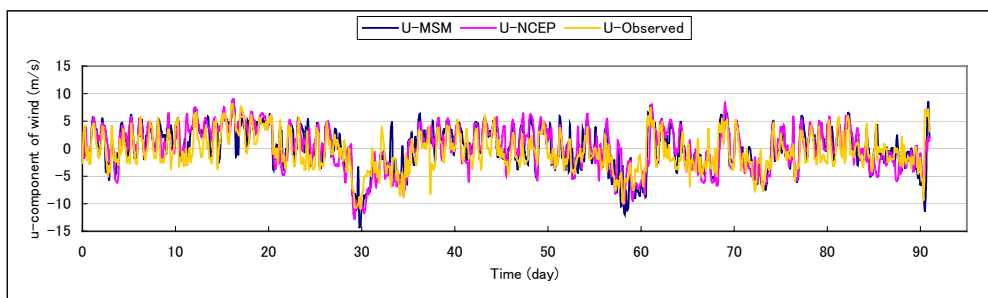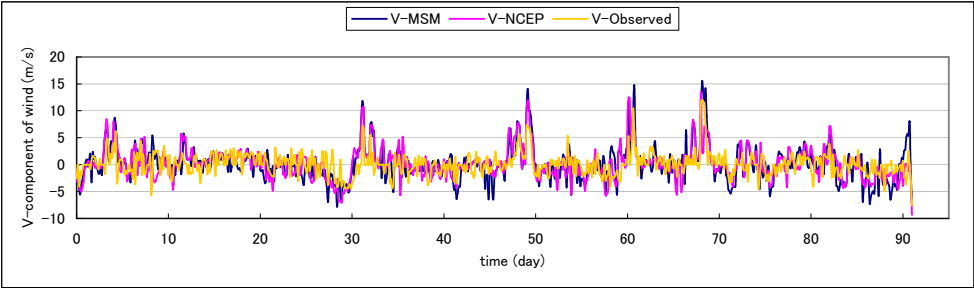
Figure 14: Time series comparison of v-component of wind between the MM5 output using MSM GPV and NCEP data with respect to observed data at Fujiiderashiyakusho station.
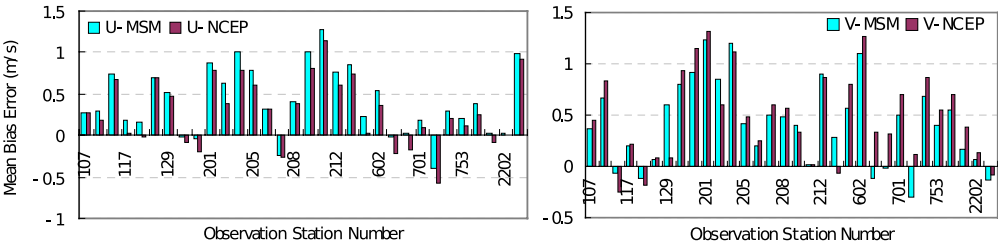
Figure 15: Mean bias error of the u-component and v-component of wind using the MSM GPV dataset and NCEP dataset.
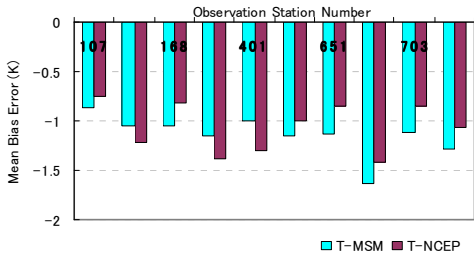
Figure 16: Mean bias error of the near-surface air temperature using the MSM GPV dataset and NCEP dataset.

4.4   VALIDATION OF METEOROLOGICAL VARIABLES

4.4.1   *Time series analysis of air temperature, wind and solar radiation*

A typical urban case is shown with the example of Kokusetsuoosaka (Station no. 107 in Fig. 12), which is located near the downtown area of Osaka City. The near-surface air temperature, wind speed, wind direction and solar radiation for the month of July 2002 are shown in Fig. 17. The diurnal variation in near-surface air temperature was well-predicted with some underpredictions in nighttime temperature. The urban heat island effect could have increased the nighttime observed air temperature. From the incident solar radiation time series, it can be inferred that solar radiation was well simulated on most days by MM5 except few times like on July 9. The wind speed plot shows a strong wind period during July 6, 14, 15, 16, 25 and 26. The strong winds on July 14 to 16 might have been the effect of a typhoon passing in the nearby Pacific Ocean region. MM5 seems to have captured the diurnal patterns as well as the maximum and minimum wind speeds for July 2002. The wind directions are also predicted with adequate accuracy.

4.4.2   *Statistical analysis of air temperature and wind*

Various quantitative statistical measures used in the evaluation of meteorological models were calculated to evaluate the results from MM5 model. These statistical measures are mathematically expressed by eq. 4.1 to eq. 4.5 (Yu et al., 2006; Zhang et al., 2006). Some of the metrics are inherently deficient due to the problems of asymmetry and bias. In other words, some metrics give relatively less priority to the underprediction of a variable than its overprediction. Moreover, some metrics show a large inflation due to a few instances in which the observed quantity in the denominator of the expression is quite low relative to the bulk of the observations. The mean bias is useful for measuring the overall over- or underestimation by the model. Other metrics like mean absolute gross error are useful for observing the spread of the departure between the simulated and observed data. The normalized mean bias (NMB, eq. 4.4) has the advantage of avoiding inflated values, since the normalization is achieved by dividing by the sum observed concentrations instead of the
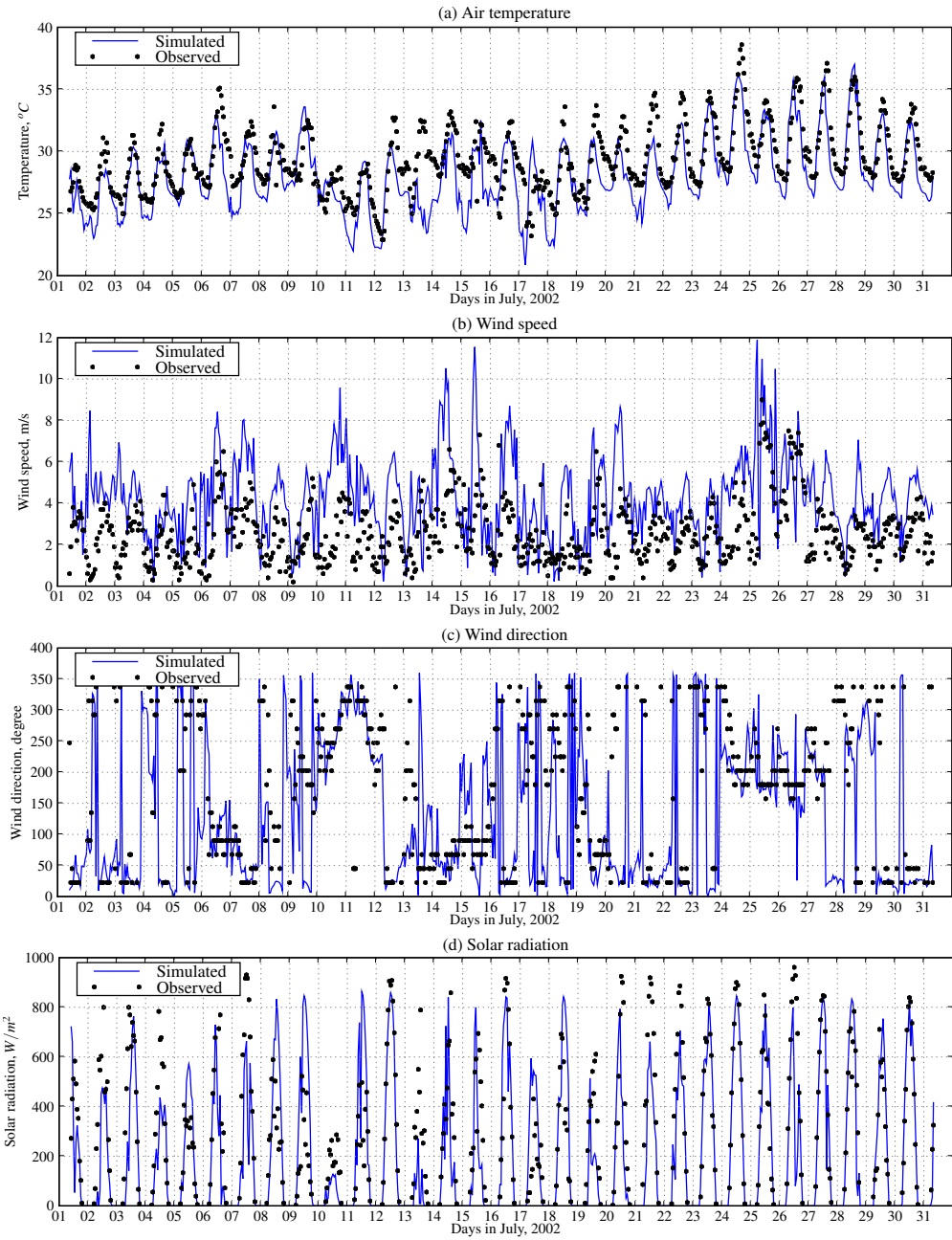
Figure 17: Meteorological fields (near-surface air temperature, wind speed, wind direction and incident solar radiation) for Station no. 107.

individual observations, which can inflate some other metrics when they are applied to low concentrations. But these also suffer from asymmetry between the bounds of overprediction and underprediction. Yu et al. (2006) have proposed a new set of unbiased symmetric metrics for evaluation of atmospheric models. One of them is normalized mean bias factor (NMBF, eq. 4.5). If NMBF is positive, the model overestimates the observations by a factor of NMBF+1. It has the advantage of avoiding dominance by the low values of observation and maintaining adequate evaluation symmetry.

In the following equations, M_i and O_i are model-simulated and observation data at time and location i respectively. N is the number of pairs of data. Similarly, the average values are given as

$$\overline{M} = \frac{1}{N} \sum_{i=1}^{N} M_i \quad and \quad \overline{O} = \frac{1}{N} \sum_{i=1}^{N} O_i$$

1. Correlation Coefficient (Range: -1 to 1)

$$r = \frac{\left\{ \sum_{i=1}^{N} (M_i - \overline{M})(O_i - \overline{O}) \right\}}{\left\{ \sum_{i=1}^{N} (M_i - \overline{M})^2 \sum_{i=1}^{N} (O_i - \overline{O})^2 \right\}^{\frac{1}{2}}} \tag{4.1}$$

2. Mean Bias (Range: -∞ to +∞)

$$MB = \frac{1}{N} \sum_{i=1}^{N} (M_i - O_i) = \overline{M} - \overline{O} \tag{4.2}$$

3. Mean Absolute Gross Error (Range: 0 to +∞)

$$MAGE = \frac{1}{N} \sum_{i=1}^{N} |M_i - O_i| \tag{4.3}$$

4. Normalized Mean Bias (Range: -1 to +∞)

$$NMB = \frac{\overline{M}}{\overline{O}} - 1 \tag{4.4}$$

5. Normalized Mean Bias Factor (Range: -∞ to +∞)

$$NMBF = \begin{cases} \dfrac{\overline{M}}{\overline{O}} - 1 & for \quad \overline{M} \geq \overline{O} \\[2ex] 1 - \dfrac{\overline{O}}{\overline{M}} & for \quad \overline{M} < \overline{O} \end{cases} \tag{4.5}$$

The statistical measures in Table 3 show that the near-surface air temperature is well simulated by MM5. The correlation coefficients are quite large and in the range of 0.79 to 0.87. MB and NMB show that all the temperatures are underpredicted to some extent. In MM5, the finer grids are better than the coarser grids with a difference of nearly 2% between domain 1 and domain 3 in most of the biases. NMBF shows that domain 3 of MM5 underpredicts by the factor of 1.02. Overall, finest grid of MM5 fares slightly better in terms of biases and gross error.

For U-component of horizontal wind, Table 4 shows that domain 1 is better than domain 2 and 3 in terms of MB, NMB and NMBF whose values are 0.38, 0.81 and 0.81. For V-component, Table 5 shows that the finer grids perform better in contrast to the results of U-component, but MM5 overpredicts the V-component. Since U- and V-components can have both positive and negative values, it can underestimate wind speed bias due to positive and negative values offsetting each other. Moreover, these wind components have very small values that can magnify errors to unrealistic values. So it is difficult to evaluate the wind results simply by the statistical measures. Even in the case of wind speed and wind direction, there can be over- or underpredictions when wind direction is larger than 180 degrees.

4.4.3 *Time scale analysis of air temperature and wind*

The effect of time scales on meteorological variables can be analyzed by spectral decomposition of the time series and studying the inherent intra-day, diurnal and longer-term time scales in those time series. The relative contributions of these time scale components associated with different physical processes can be used to evaluate the performance of meteorological models. The highest and lowest resolvable frequencies are determined by the sampling interval and the length of the data record (Hogrefe et al., 2001b). Since the simulation time period is one month, we can only resolve time scales of about 10 days.

Table 3: Quantitative statistical performance for air temperature using 1-hr data.

VARIABLES[a]	MM5 DOMAINS[b]			CRITERIA[c]
	D1	D2	D3	
Count[d]	16560	16560	16560	
MB	-1.26	-0.98	-0.70	
CORCF	0.79	0.79	0.80	
MAGE	1.75	1.64	1.53	
NMB	-0.04	-0.03	-0.02	$\leq 35\%$
NMBF	-0.04	-0.03	-0.02	$\leq 35\%$

(a) Defined in eq. no. 4.1 to eq. no. 4.5.

(b) D1 is 9-km domain, D2 is 3-km domain and D3 is 1-km domain.

(c) Zhang et al. (2006).

(d) Total number of data pairs from all the observation stations and 1-hr data .

Table 4: Quantitative statistical performance for U-component of wind using 1-hr data.

VARIABLES	MM5 DOMAINS			CRITERIA
	D1	D2	D3	
Count	48872	48872	48872	
MB	0.38	0.41	0.40	
CORCF	0.72	0.68	0.67	
MAGE	1.46	1.59	1.65	
NMB	0.81	0.86	0.85	$\leq 35\%$
NMBF	0.81	0.86	0.86	$\leq 35\%$

Table 5: Quantitative statistical performance for V-component of wind using 1-hr data.

VARIABLES	MM5 DOMAINS			CRITERIA
	D1	D2	D3	
Count	42066	42066	42066	
MB	0.57	0.43	0.40	
CORCF	0.59	0.55	0.53	
MAGE	1.63	1.69	1.75	
NMB	1.45	1.09	1.01	$\leq 35\%$
NMBF	1.45	1.09	1.01	$\leq 35\%$

Considering this limitation, only the intra-day scale, diurnal scale and longer-term scale have been used in this study. The intra-day scale has frequencies less than 12 hours, diurnal scale has frequencies around 24 hours and longer-term scale contains all the frequencies above the diurnal scale. The frequency bands were determined (Rao et al., 1997; Hogrefe et al., 2001b), and the clean separations between intra-day, diurnal and longer-term scales were confirmed from the periodograms using the Fast Fourier Transform (FFT) technique (not shown here). The Kolmogorov-Zurbenko (KZ) filter method is a widely used technique for the separation of different time scales of meteorological variables (Eskridge et al., 1997). Besides having a powerful and efficient separation characteristics, KZ filter method can be applied to datasets having missing observation data as well. In order to determine the time scale frequencies, the meteorological data were analyzed without using the logarithmic scale (Hogrefe et al., 2001b; Rao et al., 1997).

For meteorological variables, the relative contribution of the different temporal components to the total time series can be examined from the variances of the components (Hogrefe et al., 2001a). In Domain 3 (1-km grid) of MM5 for July 2002, Fig. 18 shows the contribution of different time scale components of time series of near-surface air temperature and wind speed using the percentage contribution of variance of each component to the total variance. Both the observed and simulated contribution of diurnal time scale to the total variance indicate a strong diurnal influence on air temperature. The contribu-
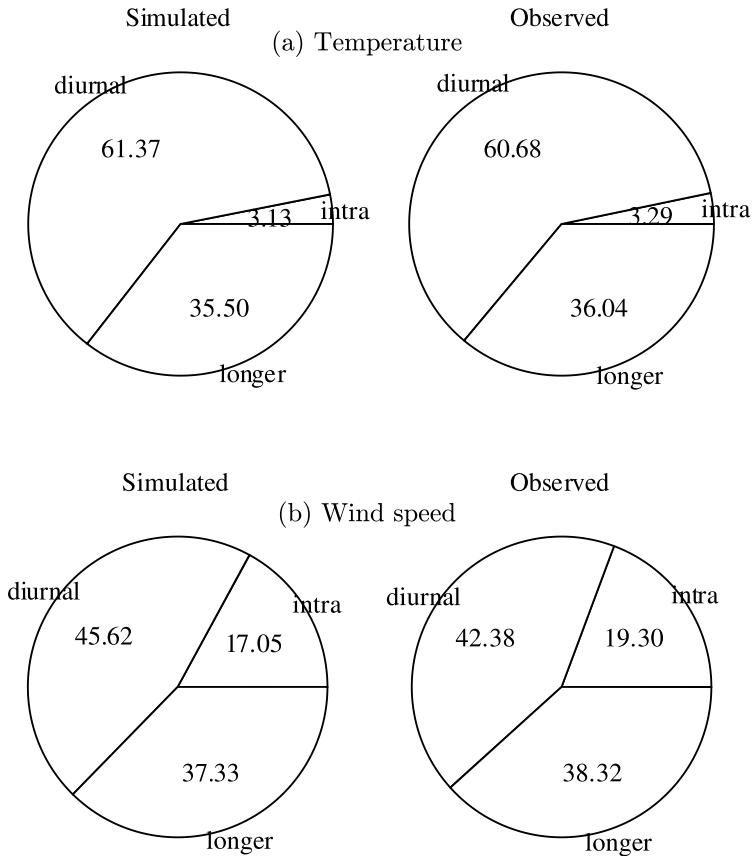
Figure 18: Contribution of different time scales to the total variance of (a) near-surface air temperature and (b) wind speed. The values are shown as percentage of contribution of time scale component to the total variance.

tions of intra-day, diurnal and longer-term components are differing from the observed values by 0.95, 1.01 and 0.99 times respectively for the temperature time series and by 0.88, 1.07 and 0.97 times respectively for the wind speed time series. It indicates that the intra-day components differ the most from the observed values. Though one would expect the intra-day component to have larger underpredictions than this result (Hogrefe et al., 2001a), the use of very high resolution (1-km) grid and high resolution meteorological analysis data could have been one of the factors behind this improvement. The wind speed is also being influenced by diurnal forcings but the contribution of intra-day component is nearly 6 times than that of air temperature. Ohsawa et al. (2007) reported that the maximum wind speed due to southerly sea breeze are underpredicted by MM5 even in fine domains of nearly 1 km grid size and that a better representation of diurnal variation is necessary in the summertime in regions with complex terrain. This situation is improved in the present study because four dimensional data assimilation (FDDA) is not used and so a significant loss in the contribution of diurnal variations is avoided. In addition, the contribution of intra-day component has increased due to the absence of smoothing of intra-day variations by FDDA, and the local wind circulations being captured at very fine resolution of 1 km.

The correlation coefficient between the simulated and the observed time scale components is helpful in identifying the spatial information of the model performance. The correlation coefficients for near-surface temperature (Fig. 19) are consistently high over 0.8 over all the observation stations of Osaka. Diurnal component is the best-simulated time series component with correlation coefficients higher than 0.9. The longer-term component has also high values (>0.7) but the intra-day component has small correlation coefficients less than 0.3, especially in the stations near the west coast. The correlation coefficients for wind speed (Fig. 19) are very small in all the stations (<0.2) and the longer-term component has better coefficient values among the time series components. This result is typical of summertime wind, which is affected by model representation of the boundary layer mixing processes and PBL growth and transition periods (Gilliam et al., 2006). The diurnal component of wind speed shows some relatively higher correlation coefficients (0.6 to 0.7) in the stations around the Yodo River, which, among other reasons, may be due to complex land use pattern in the region.
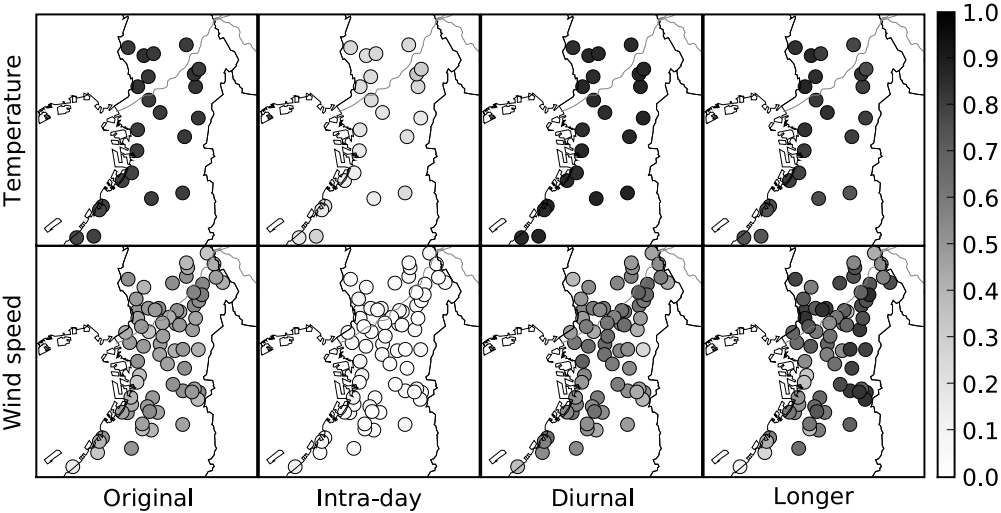
Figure 19: Correlation between simulated and observed temperature and wind speed for different time scales. The light gray line from the top right corner is Yodo River.

4.5   VALIDATION OF PRECIPITATION IN YODO RIVER BASIN

4.5.1   *Domain and grid structures*

Yodo River basin (Fig. 20) is one of the major basin areas in Japan and it influences and controls the water cycle of the Kinki region of Japan, which contains large cities like Osaka, Nara and Kyoto. Seta River originates from Lake Biwa and flows through Kyoto Prefecture as Uji River. Katsura River from Kyoto Prefecture and Kizu River from Mie Prefecture merge with Uji River to form Yodo River in Osaka Prefecture, which then finally flows into Osaka Bay.

The heterogeneity in orography of Yodo River basin requires a high spatial resolution in precipitation results from WRF. The spatial scale in the order of 1-km is generally required in these types of mesoscale studies. To keep balance between the computational cost of such high-resolution simulation and the required resolution in the result, the 3-km grid precipitation data is further downscaled using subgrid downscaling technique.
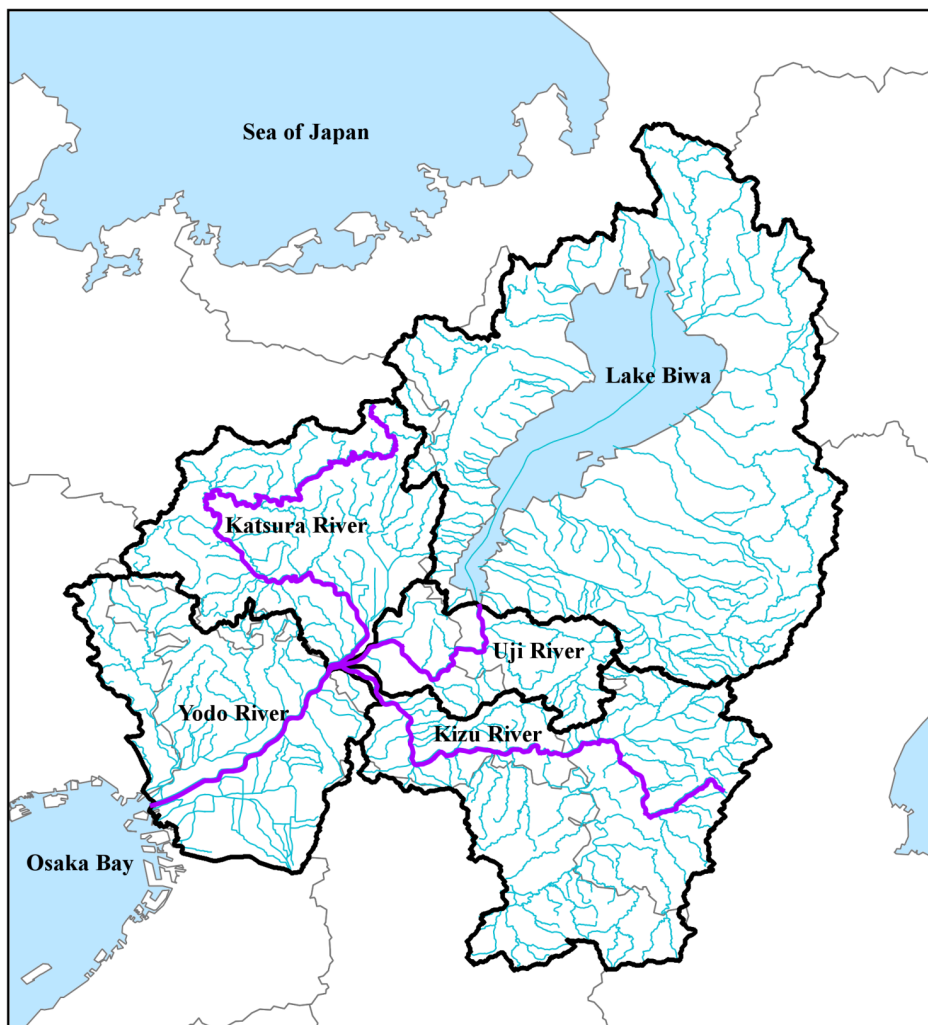
Figure 20: Sub-basins of Yodo River basin with major rivers. Thick black lines are the boundaries of the sub-basins.

Table 6: WRF parameters and options

PARAMETER/OPTION	VALUE
Nesting	One-way with 3 domains
Domain-1 size	50 × 50 mesh with 27-km mesh size
Domain-2 size	46× 46 mesh with 9-km mesh size
Domain-3 size	52 × 52 mesh with 3-km mesh size
Vertical grid	35 full levels with top level at 5 kPa
Microphysics	WSM 3-class simple ice
Cumulus	Kain-Fritsch scheme
Planetary boundary layer	YSU scheme
Land surface	Noah land surface model
Longwave radiation	RRTM scheme
Shortwave radiation	Dudhia scheme

4.5.2   *WRF model data and parameters*

Some important options selected in this work are shown in Table 6. Precipita-
tion field is mainly affected by the microphysics and cumulus parameterization.
Dynamic or stratiform precipitation is obtained from microphysics scheme and
convective precipitation is obtained from cumulus parameterization scheme.
Cumulus parameterization generally has greater impact in the precipitation
over landmass, and microphysics option has greater effect in the diurnal pre-
cipitation pattern in oceans (Koo and Hong, 2008). WRF Single-Moment 3-class
microphysics scheme is sufficient for long-term simulation with grid sizes
greater than 3-km because it is a computationally efficient scheme with ice and
snow processes suitable for mesoscale grid sizes. Similarly, Kain-Fritsch cumu-
lus parameterization scheme is a deep and shallow convection subgrid scheme
that can be efficient and suitable for mesoscale modeling. Since sea surface
temperature (SST) also affects the precipitation events in long-term simulations
(Kang and Kimura, 2003), SST was daily updated using the 0.5-degree NCEP
real-time global analysis SST (http://polar.ncep.noaa.gov/sst/ophi/).
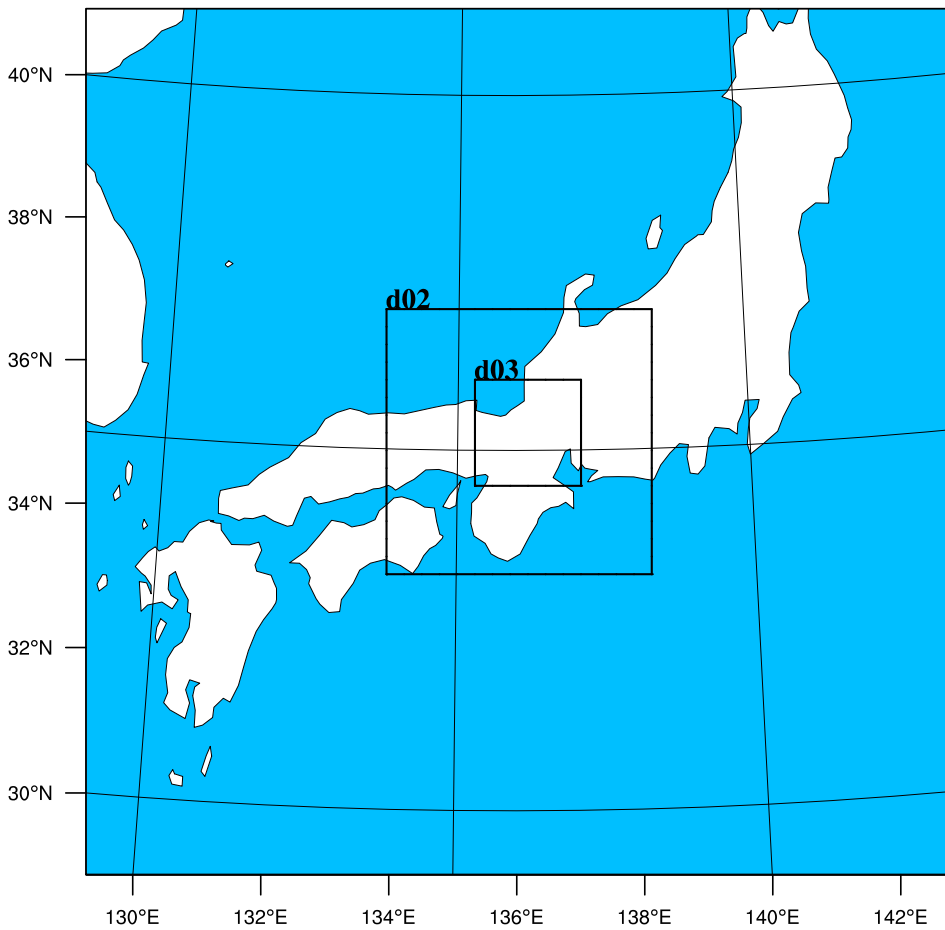
Figure 21: Nesting of three domains in WRF model. The total area is Domain-1, 'd02' is Domain-2 and 'd03' is Domain-3.

Though both MSM GPV and NCEP Global Analyses data (see subsection 4.3.2 for data description) could be used to drive WRF model, NCEP data was chosen as boundary condition and initial condition for WRF simulation because real-time global analysis SST data was also available in case of NCEP data. NCEP Global Analyses data was dynamically downscaled to 3-km grid domain containing the Yodo River basin using one-way nesting of 3-km gridded Domain-3 inside 9-km gridded Domain-2, which was again nested inside 27-km gridded Domain-1 (Fig. 21).

4.5.3 *Method*

In order to calculate precipitation input data for hydrological modeling, WRF (Weather Research and Forecasting) mesoscale meteorological model is used to predict long-term mesoscale precipitation in the Yodo River basin. It is essential for the model to correctly simulate the accumulated precipitation and the rate of precipitation in the basin and sub-basin areas in all the seasons of the year. Mesoscale precipitation from WRF is obtained for 3-km grids, and then downscaled to 1-km subgrids as described below in this subsection. This data is then validated against the conventional areal observation data and meteorological radar precipitation data in order to assess the usability of the WRF precipitation in the hydroclimate modeling of climate change scenarios in Yodo River basin. Since the precipitations at sub-basin levels are important for calculating river flow rates, precipitation rates in the sub-basins are also compared with radar data.

Radar precipitation data are convenient for validation of gridded meteorological precipitation output because they have generally higher resolution than the observation networks of precipitation and the spatial distribution of precipitation is available across all the terrain types. Heavy precipitation events simulated by mesoscale meteorological models can be validated using radar precipitation (Sugimoto and Hirakuchi, 2003). Radar precipitation is especially useful in regions with mountainous terrain, where orographic rainfall is difficult to measure with conventional methods.

The 1-km mesh synthetic radar GPV (Grid Point Value) data provided by Japan Meteorological Agency contain the radar images of echo intensity and echo height over nearly whole region of Japan. The radar network of Japan has 20 meteorological radars spread throughout the country and some of these are Doppler radars. The radar data are combined from these radars and finally the data are corrected according to the observed precipitation data obtained from AMEDAS (Automated Meteorological Data Acquisition System) surface observation network. The precipitation rate is made available in GRIB2 format at time step of 10 minutes. Since the volume of such 10-minute data is large for one-year calculation, only hourly radar data were used to validate the hourly output of WRF.

The observed precipitation data in Yodo River basin described in subsection 6.3.1 of chapter 6) is also used to validate the WRF precipitation results. The areal observed precipitation data generated by widely used Thiessen polygon method (subsection 6.3.1) will be referred to as 'SDP data' throughout this chapter.

Subgrid downscaling of WRF precipitation

The 3-km grid precipitation data from WRF is downscaled to 1-km subgrids using the terrain height correction equation (Eq. 4.6). Eq. 4.6 was adapted from Kondo (1994) and estimated correction coefficient for Yodo River basin was used.

$$P_1 = P_3(1 + k(H_1 - H_3)) \tag{4.6}$$

where,

P_1	Precipitation at 1-km subgrid (mm)
P_3	Precipitation at 3-km WRF grid (mm)
H_1	Terrain height at 1-km subgrid (m)
H_3	Terrain height at 3-km WRF grid (m)
k	Correction coefficient (0.05/100 m^{-1})

In order to consider the difference in precipitation due to different terrain heights of 3-km (Fig. 22a) and 1-km grids (Fig. 22b), Eq. 4.6 was used.

4.5.4 *Total basin precipitation*

The accumulated precipitation from Domain-2 of WRF (Fig. 23a) shows an overall overprediction of precipitation compared to Radar GPV and SDP. The nested Domain-3 having 3-km grid shows a large improvement over Domain-2 precipitation result (Fig. 23b). The WRF precipitation from Domain-3 shows a very good simulation result when compared with the Radar GPV data. The overall daily rate of precipitation is accurately predicted by WRF except a slightly different rate of precipitation in August 2006, though the monthly precipitation amount is nearly same in both the Radar GPV and WRF output.
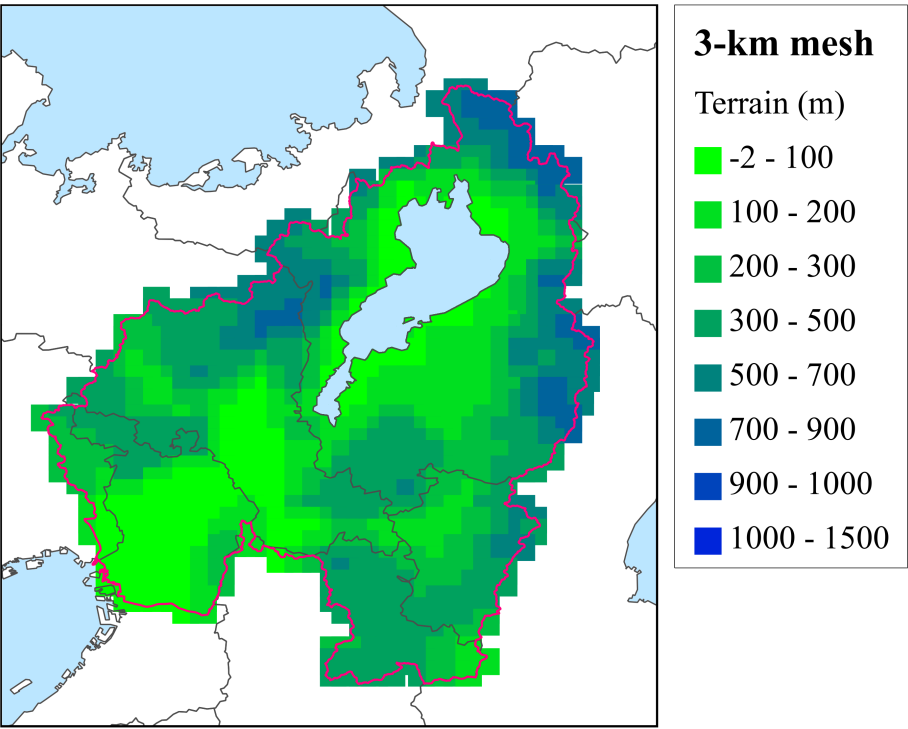
(a) 3-km mesh grid.
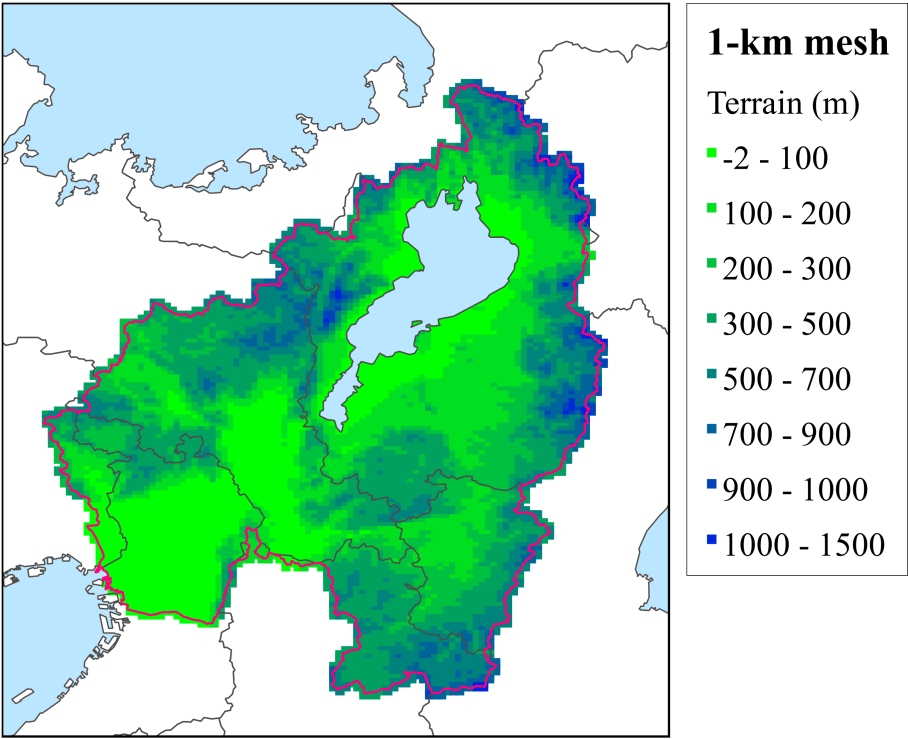
(b) 1-km mesh grid.

Figure 22: Terrain height of Yodo River basin.

Individual precipitation events are also generally well reproduced by WRF. The SDP data produces dry bias when compared to Radar GPV in nearly all the months. The underestimation by SDP data is especially pronounced in August, which may be due to the lack of representation of local downpour and rainfall events in the Yodo River basin. The spatial heterogeneity of localized rainfall events may not have been captured by observations stations, which represent the Thiessen polygons in the observation network. In August, these local rainfall events are captured by WRF but the time period of rainfall occurrence is different than the Radar GPV precipitation. The use of areal average precipitation in SDP data makes it difficult to fully capture the spatial distribution of precipitation. But the correction of SDP precipitation using elevation-rainfall relationship has improved the dry bias in the original SDP precipitation (not shown in figure).

The heaviest precipitation occurred in July and Domain-3 of WRF shows good agreement with the Radar GPV precipitation data. But SDP data shows some underestimation. Overall, the total basin precipitation and monthly precipitation in all the seasons were well simulated in 3-km grid Domain (Domain-3) of WRF.

When WRF precipitation in Domain-3 is downscaled with Eq. 4.6, only a slight dry bias is observed when compared with Radar GPV. This is expected due to the averaging of subgrid terrain heights into a single 3-km terrain height, which can lead to slightly higher terrain height in the lower terrain. Though the downscaled 1-km WRF results show a slight underprediction compared to Radar GPV, it helps to improve the areal distribution of precipitation.

The spatial maps of precipitation in Fig. 24 show a strong orographic effect on precipitation in all the cases. This orographic effect is especially recognizable in the mountainous outskirts of the Yodo River basin. The precipitation distribution at 1-km spatial resolution could not be exactly reproduced by WRF at 1-km grid scale (Fig. 24d) but the sub-basin scale precipitation is reasonably reproduced (see sub-section 4.5.5).

In the southern region of Yodo River basin covering urban region of Osaka, a markedly higher precipitation is present in Radar GPV, which is likely affected by the unusually high precipitation detected by the meteorological radar situated in the Osaka Prefecture region. The relatively less amount of observed precipitation in SDP data (Fig. 24d) in the Osaka Prefecture region gives a fair indication that the Radar GPV precipitation data in the Osaka Prefecture
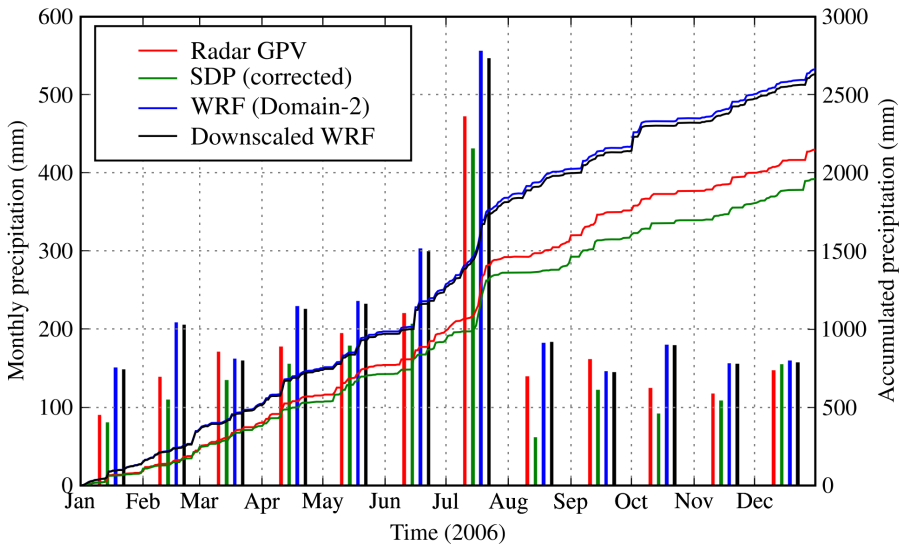
(a) Domain-2.
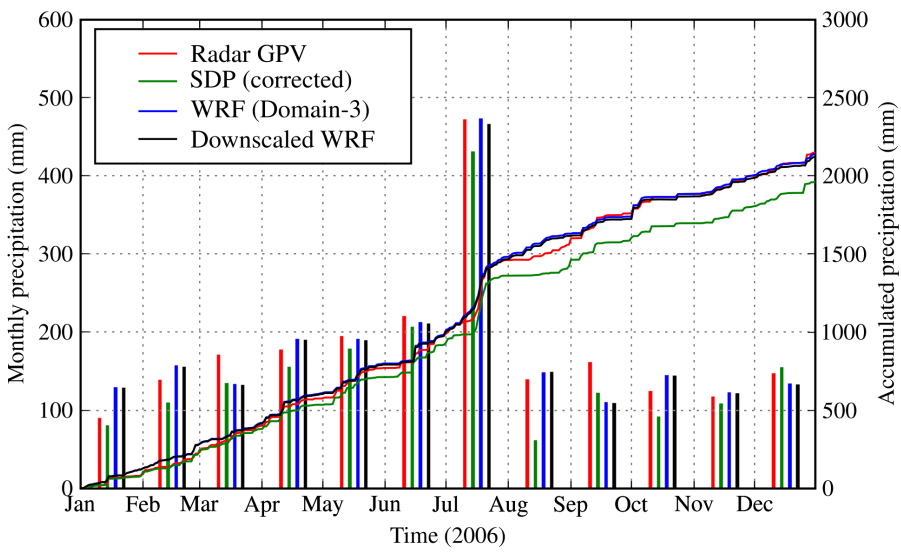
(b) Domain-3.

Figure 23: Comparison of precipitation in Yodo River basin. SDP (corrected) is the precipitation after correction using Eq. 4.6. Downscaled WRF is the WRF precipitation after downscaling with Eq. 4.6.

region is unusually higher than expected. Though a more comprehensive correction in the radar data is required, we can safely assume that the Radar GPV data is slightly larger than usual in the mid-Osaka region.

In the southeastern region of Yodo River basin, the total precipitation shows some dry bias in 3-km WRF results when compared to Radar GPV and SDP data. This dry bias is present due to lower terrain height in 3-km grid compared to the 1-km grid (Fig. 22). It can also be slightly reduced by downscaling the data to 1-km by considering the orographic effect.

In the central region of Yodo River basin containing the Uji River basin, Radar GPV shows a high precipitation region, which is underestimated by SDP data. WRF is better in simulating this high precipitation region.

In Lake Biwa, SDP data and WRF Domain-3 show lower precipitation amount compared to the Radar GPV data. On the other hand, SDP data and WRF Domain-3 show some high precipitation area in the upper region of Katsura River basin.

Overall, WRF produces better spatial distribution of yearly precipitation in the Yodo River basin than the SDP data when compared with Radar GPV.

4.5.5 *Sub-basin precipitation*

The monthly evolution of precipitation in the sub-basins of Yodo River basin is shown in Fig. 25. In the high precipitation month of July, downscaled WRF shows more than 150 mm of underprediction at Uji River basin when compared to Radar GPV. Since the size of Uji River basin is relatively small compared to Biwa basin, a slight overprediction by WRF in Biwa basin causes the overall underprediction in the Yodo River basin to be small (Fig. 23b).

Precipitation in Yodo River sub-basin is underpredicted by WRF except in October. Similarly, precipitation in Kizu River basin is underpredicted in some months. These underpredictions may be partly attributable to the unusually high precipitation produced by Osaka meteorological radar in some parts of these basins.

Precipitation in Uji River basin is underpredicted in all the months except January and October. This underprediction in Uji River basin is more pronounced in the heavy precipitation time period of July.
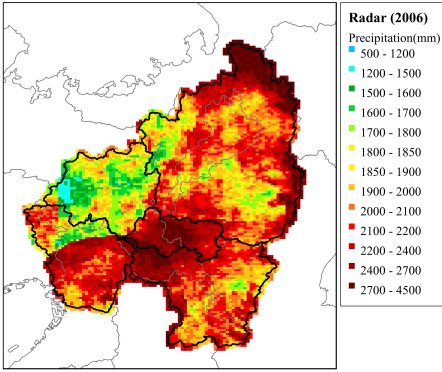
(a) Radar GPV.
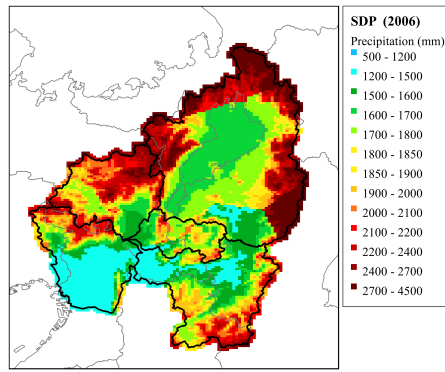
(b) SDP observed precipitation generated by Thiessen polygon method.
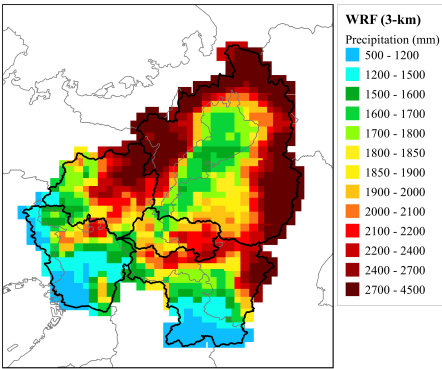
(c) WRF Domain-3 with 3-km grid.
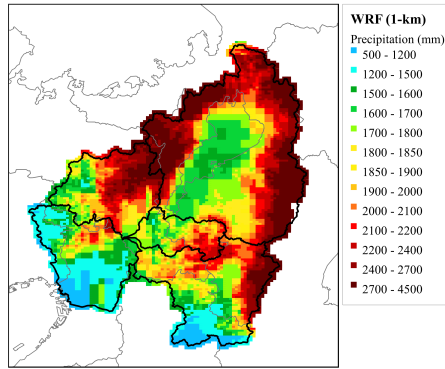
(d) WRF Domain-3 downscaled to 1-km grid.

Figure 24: One-year precipitation map for Yodo River basin in 2006.
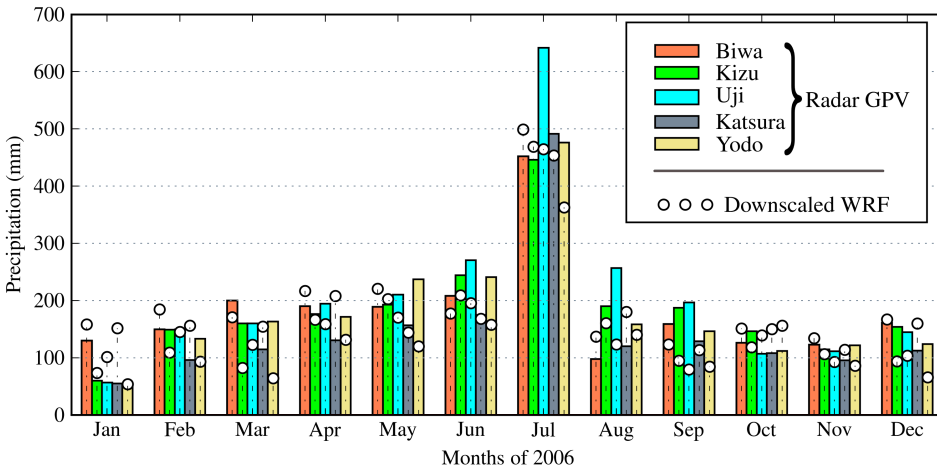
Figure 25: Monthly precipitation in sub-basins of Yodo River basin.

In Katsura River basin, precipitation is generally overpredicted except in May, June, July and September. The larger values of precipitation in WRF result is mainly due to the heavy precipitation events generated by WRF in the northern region of Katsura River basin (Fig. 24c).

Biwa sub-basin is the largest sub-basin in Yodo River basin and orographic effect on precipitation is large in the mountainous region of this sub-basin. WRF is able to generally predict this orographic effect. WRF precipitation in Biwa sub-basin is generally over-predicted in 2006 except in March, June and September. Due to its largest contribution to the total basin precipitation, Biwa sub-basin has an overall contribution of wet bias to the total precipitation of Yodo River basin. Biwa sub-basin and Katsura River basin, which are closer to Sea of Japan than other basins, show largely wet bias in 2006. Kizu River basin, Uji River basin and Yodo River basin have overall dry bias.

4.6 CONCLUSION

The meteorological fields were evaluated against the observation data in the Osaka and Yodo River region to validate the use of MM5 and WRF mesoscale meteorological models for high-resolution mesoscale meteorological modeling of Yodo River basin. After validation with observed data, the mesoscale models were found be applicable for high-resolution estimation of meteorological variables in Yodo River basin.

High-resolution MSM GPV meteorological data and US NCEP (National Centers for Environmental Prediction) FNL (Final) Operational Global Analysis data were used for driving mesoscale meteorological models. Both of these data were found to be applicable to mesoscale meteorological modeling in Japan.

Regarding air temperature results, MM5 simulated the diurnal variation of near-surface air temperature with high correlation and daily maximum temperatures were well reproduced as well. Moreover, finer grids produced better results, with the 1-km domain showing the best overall results. For the components of wind, diurnal variations were well reproduced with some overpredictions.

The time scale components of the meteorological fields (temperature and wind) were evaluated against the observation data in the Osaka prefecture region using the MM5 model. The time scale analysis reveals a strong influence of spatial distribution on the meteorological outputs. The intra-day scales for wind are relatively less well-represented than the other time scales by the MM5 model, and thus, a more accurate represented land use and vegetation can be recommended for the terrains of Osaka. The contribution of intra-day component to the overall variability of air temperature was found to be well simulated though correlation coefficient was low (<0.4) compared to the best simulated diurnal component.

To validate high-resolution gridded precipitation data for modeling and forecasting the hydroclimate of Yodo River basin, WRF mesoscale model was successfully used to produce high-resolution precipitation data with 3-km grid size. The WRF precipitation was subsequently downscaled to 1-km grid size to refine the spatial distribution of precipitation, and then it was validated with Radar GPV and SDP observation network precipitation data. One-year simulation with WRF indicates that WRF is able to capture the total accumulated precipitation in all the sub-basins of Yodo River basin. The temporal evolution of precipitation is also well simulated with some wet bias in Biwa sub-basin, which is the largest sub-basin in Yodo River basin. The spatial distribution of precipitation was generally well captured in the mountainous terrain where orographic effect on precipitation is significant. Overall, the mesoscale precipitation generated by WRF is found to be well suited for modeling and forecasting the hydroclimate and climate change scenarios of Yodo River basin.

VALIDATION AND ANALYSIS OF URBAN CANOPY MODEL

5.1 INTRODUCTION

This chapter investigates the effects of urban heat island phenomenon in Osaka, Japan (see Fig. 28 for terrain structure of the region), using real meteorological conditions. State-of-the-art WRF model, coupled with urban canopy model, is modified by including the gridded anthropogenic heat emission data of Osaka for meteorological modeling of Osaka region in order to assess the contribution of urban canopy effect and anthropogenic heat emission towards the formation of urban heat island.

The spatial and temporal development of urban heat island is complicated by the complex distribution of urban structure and anthropogenic heat emission at local and urban scales. Diurnal anthropogenic heating profiles have been used in mesoscale models to use anthropogenic heat flux as a heat source, which is evenly-distributed in the surface layer (Fan and Sailor, 2005; Lin et al., 2008). Though previous findings have pointed out the improvement in urban heat island simulation using only the area-averaged anthropogenic heat and land-use parameters in a meteorological model, this study uses gridded high-resolution urban land use data and hourly gridded anthropogenic heat map of Osaka to validate the importance of anthropogenic heat and urban canopy model in the heat island phenomenon in Osaka.

Though WRF (Weather Research and Forecasting) model is good at predicting daytime air temperature, it has a tendency to underestimate urban nocturnal air temperature (Kusaka and Hayami, 2006). This can adversely affect the simulation of nocturnal heat island. To add the contribution of heat from an urban canopy, WRF is coupled with an urban canopy model. A detailed urban land-use map to be used for urban canopy modeling is developed and used, and a gridded emission map consisting of spatial and

Table 7: Important WRF parameters and schemes used in urban canopy modeling.

PARAMETER/SCHEME	MODEL SETTING
Nesting	One-way
Cumulus	None
Microphysics	WSM 3-class simple ice
Planetary boundary layer	YSU scheme
Land surface	Noah land surface model
Longwave radiation	RRTM scheme
Domains	3-km and 1-km grids
Time period	August 8-14, 2007

seasonal distribution of anthropogenic heat emission for better representation of urban heat emission.

5.2 SETUP AND MODIFICATION OF METEOROLOGICAL MODEL

5.2.1 *WRF model parameters and domains*

Parameters and schemes shown in Table 7 were used to run the WRF model in a 1-km gridded domain nested inside a 3-km gridded domain (Fig. 26). Vertical grid structure was configured with 24 terrain-following eta levels. The topmost level was set at 100 hPa and the thickness of the first and second levels from the land surface were about 25 and 65 meters respectively.

The initial conditions for the WRF grid were obtained by preprocessing the high-resolution MSM GPV meteorological data (described in subsection 4.3.2) from Japan Meteorological Agency.

Soil moisture and temperature below ground level required for the Noah land surface model were obtained from the FNL (Final) Global Analyses on 1.0 x 1.0 degree global grids provided by NCEP (National Centers for Environmental Prediction).

One-way nesting was utilized to solely observe the effect of using anthropogenic heat and urban canopy model in the 1-km grid. The boundary

conditions for the 1-km grid are provided by the larger mother domain having 3-km grid structure (Fig. 26).

5.2.2 *Inclusion of the effect of anthropogenic heat*

Anthropogenic heat is considered to be directly vented into the atmosphere. So anthropogenic heat flux may be directly introduced into the thermodynamic equation as an additional source term at the first level above ground (Ichinose et al., 1999).

Though urban canopy model in WRF contains a simple diurnal representation of anthropogenic heat emission, this feature was disabled because it cannot represent the actual spatio-temporal emission pattern of anthropogenic heat. So, an explicit representation of hourly gridded anthropogenic heat data was used in the PBL scheme.

YSU (Yonsei University) PBL scheme (Hong et al., 2006) in the WRF model is the next generation of the MRF PBL commonly used in MM5 model, and it uses an explicit treatment of the entrainment layer at the PBL top in addition to countergradient terms to represent fluxes due to non-local gradients. YSU PBL scheme is modified in order to include anthropogenic heat as an additional source term at the first level above ground. Eq. (5.1) is the thermodynamic equation based on YSU PBL scheme.

$$\frac{\partial C}{\partial t} = \frac{\partial}{\partial z} \left[K_c \left(\frac{\partial C}{\partial z} - \gamma_c \right) - (\overline{w'C'})_h \left(\frac{z}{h} \right)^3 \right] \tag{5.1}$$

where,
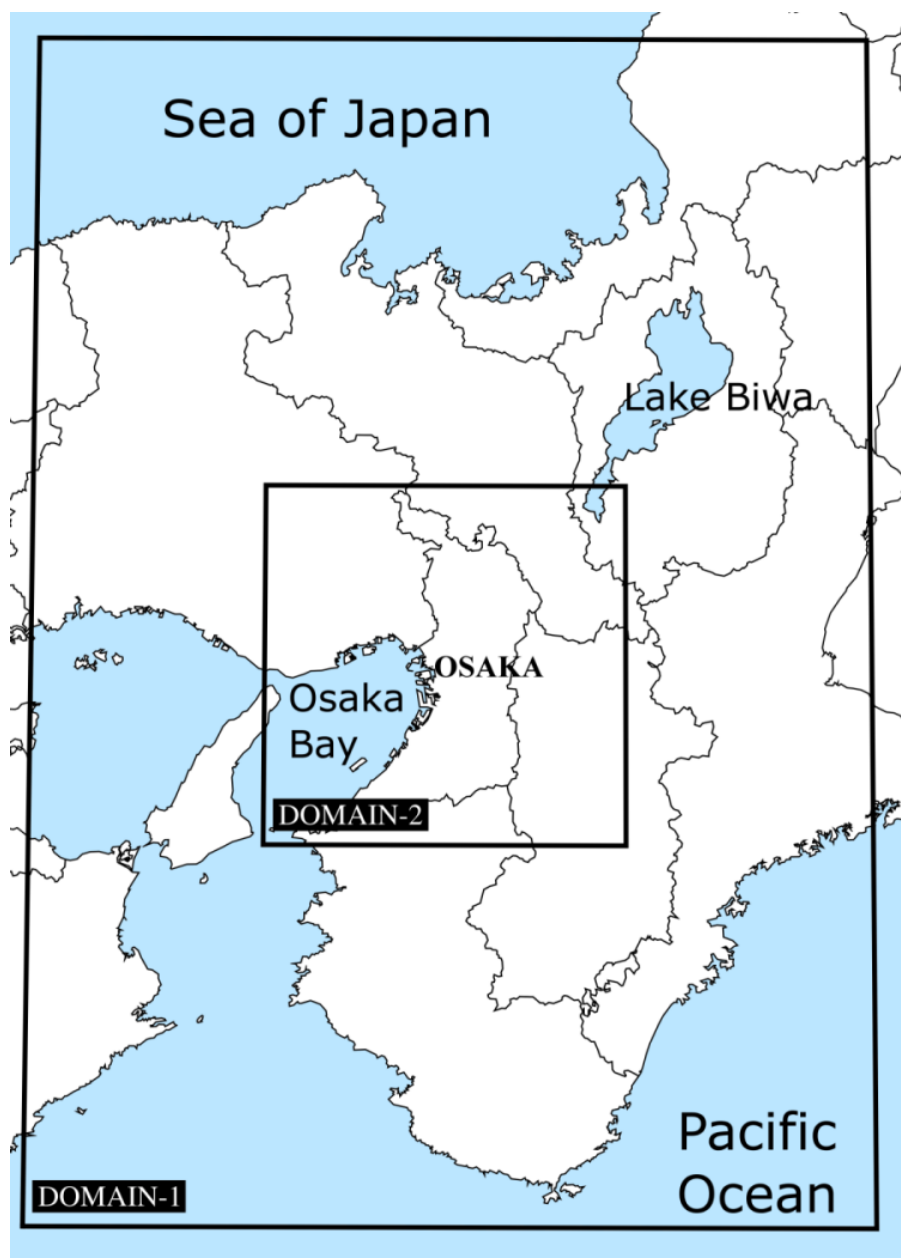
Figure 26: Domain configuration used in WRF model coupled with urban canopy model. Domain-1 is the mother domain having 3-km grid structure. Domain-2 is the nested domain having 1-km grid structure, which also contains the Osaka region.

C	θ, q
θ	Potential temperature
q	Mixing ratio for water vapor, cloud, ice
z	Height from the surface
h	Height of boundary layer
K_c	Exchange coefficient
$(\overline{w'C'})_h$	Flux at the inversion layer
$(\overline{w'C'})_h \, (z/h)^3$	Asymptotic entrainment flux term at the inversion layer
γ_c	$b \dfrac{(\overline{w'C'})_0}{w_{so} \, h}$ (correction to the local gradient that incorporates the contribution of the large-scale eddies to the total flux)
b	6.8 (coefficient of proportionality)
$(\overline{w'C'})_0$	Surface flux
w_{so}	Mixed-layer velocity scale at $z = 0.5 \, h$

In the numerical formulation of potential temperature equation, the equation for the bottom layer (layer 1) is given as

$$(1 + \delta_1)\theta_1^{n+1} - \delta_1 \theta_2^{n+1} = \theta_1^{n-1} + \delta_1 \mu_1 + \beta \tag{5.2}$$

where,

δ_k $(2\Delta t\, K_{k-1})/(\Delta \hat{z}_{k-1}\, \Delta \bar{z}_k)$

$\Delta \hat{z}_k$ Distance between θ_{k+1} and θ_k

$\Delta \bar{z}_k$ Distance between $\bar{\theta}_{k+1}$ and $\bar{\theta}_k$

μ_k $\alpha\, \Delta \hat{z}_k$

α $-\gamma - (\overline{w'\theta'})_h (z/h)^3 K^{-1}$

β $\dfrac{2\Delta t\, (\overline{w'\theta'})_0}{\Delta \bar{z}_1 \rho\, C_p}$

C_p Specific heat of dry air at constant pressure

ρ Dry air density

Let H_{as} be the sensible anthropogenic heat flux. Then, the additional forcing due to sensible anthropogenic heat flux is

$$F_{as} = \frac{2\Delta t\, H_{as}}{\Delta \bar{z}_1 \rho\, C_p\, \Pi} \tag{5.3}$$

where Π is Exner function.

This additional forcing due to sensible anthropogenic heat flux is added as a source term in eq. 5.2.

With similar treatment, latent anthropogenic heat flux, H_{al}, is included in the bottom layer of the moisture equation. The additional forcing due to latent anthropogenic heat flux is

$$F_{al} = \frac{2\Delta t\, H_{al}}{\Delta \bar{z}_1 \rho\, L\, \Pi} \tag{5.4}$$

where L is latent heat of vaporization.

5.3   INPUT DATA

5.3.1   Urban land-use data

In urban canopy model of WRF, the urban land-use has to be sub-categorized according to various parameters like building height, building coverage and urban fraction in each grid cell. For this, urban category was divided into

three sub-categories, viz., high-density residential, medium-density residential, and low-density residential (Fig. 29).

1997's 100-m National Digital Information data were used to obtain the 1-km land-use distribution for other non-urban land use categories.

Detailed Digital Information (10-m Grid Land Use) data obtained from Japan Map Center for the Kinki region were used to create a detailed urban land-use map needed for urban canopy model.

Average building height and building coverage data are available in Osaka City Mesh Data. To obtain building height data for urban canopy model, the building height data from Osaka City Mesh Data were associated with the 10-m grid urban land-use data from Detailed Digital Information. From these data, the building height was calculated at each of the 1-km grid cells by averaging the height of the buildings falling on those grid cells.

5.3.2 *Urban canopy model parameters*

The important parameters of the urban canopy model are selected for the model region so that they reflect the actual urban canopy structure and properties (Table 8). Urban fraction was calculated as

$$FRC\_URB = A_{URBAN}/A_{GRID} \tag{5.5}$$

where,

A_{URBAN} Area covered by urban region

A_{GRID} Area of the whole grid

Building coverage ratio is calculated as

$$R = A_{BUILDING}/A_{URBAN} \tag{5.6}$$

where,

$A_{BUILDING}$ area covered by the buildings in the grid
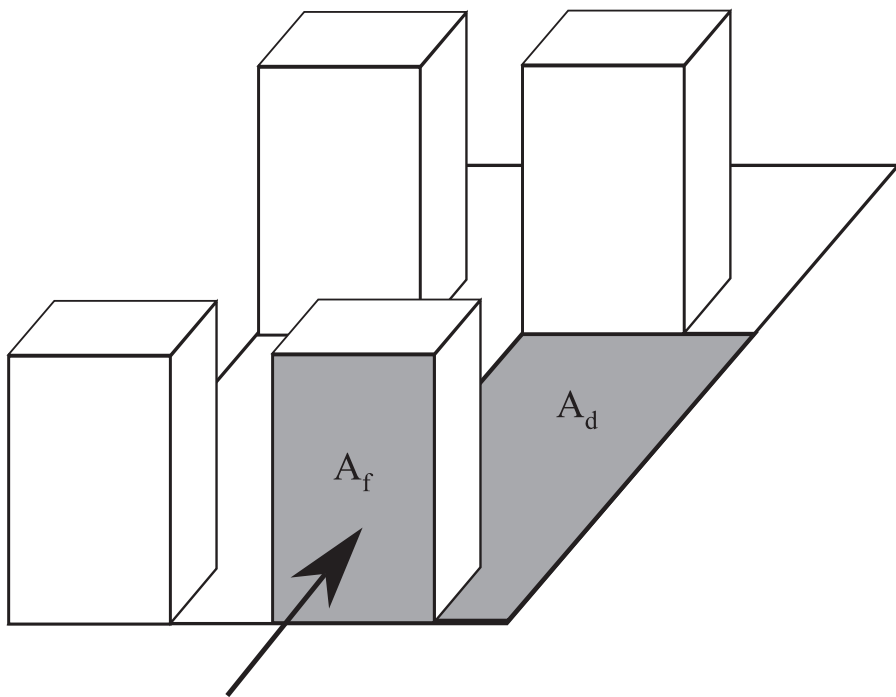
Figure 27: Model representation of urban canopy for calculation of building volumetric parameter. A_f is the frontal surface area of the building exposed to the horizontal wind flow (shown by arrow) and A_d is the underlying surface area for a single canopy.

Building volumetric parameter (AS) is one of the parameters used in the calculation of canopy wind while balancing the obstacle drag force and the local shear stress in an uniform canopy. It represents the ratio of building surface area facing the wind to the volume of space. A_f is the frontal surface area of the building exposed to the horizontal wind flow and A_d is the underlying surface area for a single canopy (Fig. 27). Thus,

$$AS = A_f/(A_d \times ZR) \tag{5.7}$$

where ZR is the building height. The A_f/A_d ratio is also referred to as frontal area density (Macdonald, 2000).

In this simulation study, urban land-use was sub-categorized according to the urban fraction of each grid cell. As can be inferred from Table 8, the sub-categorization using building height is not worthwhile in the case of Osaka

region due to small differences in building heights among the different urban types. So urban land-use category has been sub-categorized according to the evenly distributed urban fraction data.

The grid-scale flux for urban grid fraction is calculated by urban canopy model and the rest of the non-urban fraction is calculated by Noah land surface model of WRF. Then the total flux is calculated as

$$F = FRC\_URB * F_{URBAN} + (1 - FRC\_URB) * F_{NON-URBAN} \tag{5.8}$$

where,

F	Total flux
F_{URBAN}	Flux calculated by urban canopy model
$F_{NON-URBAN}$	Flux calculated by Noah land surface model

Urban canopy is divided into roof, wall and road surfaces. Important characteristic properties of these three surfaces used in urban canopy model of WRF are shown in Table 9.

5.3.3 *Anthropogenic heat flux*

The hourly anthropogenic data in 1-km grids for the Kinki region are available (Narumi et al., 2002) (see Fig. 30 for a typical example of gridded anthropogenic heat flux data used in the model region). The yearly average of anthropogenic heat fluxes from vehicle and railroads is used in the present study. Similarly, August average of anthropogenic heat flux from the release of waste heat from building and commercial energy consumption is used. There are sensible and latent anthropogenic heat fluxes available that are separately processed and ingested in the WRF model.

The gridded anthropogenic data are interpolated to the WRF grid structure by a preprocessing program called WPS (WRF Preprocessing System), and then included in the thermodynamic equation (subsection 5.2.2).

Table 8: Important parameters of urban canopy model depending on land-use category.

NAME	UNIT	LOW DENSITY RESIDENTIAL	MEDIUM DENSITY RESIDENTIAL	HIGH DENSITY RESIDENTIAL
Building Height	m	7.5	8.1	8.2
Roughness length above canyon for momentum	m	0.75	0.81	0.82
Roughness length above canyon for heat	m	0.75	0.81	0.82
Zero plane displacement height	m	1.5	1.62	1.64
Building coverage ratio	-	0.46	0.49	0.50
Normalized building height	-	0.37	0.40	0.41
Drag coefficients by buildings	-	0.1	0.1	0.1
Building volumetric parameter	1/m	0.25	0.30	0.35
Moisture availability on roof, building wall and road	-	0	0	0
Urban fraction	-	0.52	0.79	0.92

Table 9: Important properties for roof, wall and road surfaces of urban canopy.

NAME	UNIT	PLANE	VALUE
Heat capacity	cal/cm^3/°C	roof	0.5
		wall	0.5
		road	0.5
Thermal conductivity	cal/cm/sec/°C	roof	0.004
		wall	0.004
		road	0.004
Surface albedo		roof	0.1
	-	wall	0.1
		road	0.1
Surface emissivity	-	roof	0.97
		wall	0.97
		road	0.97
Roughness length for momentum	m	roof	0.1
		wall	0.1
		road	0.1
Roughness length for heat	m	roof	0.1
		wall	0.1
		road	0.1
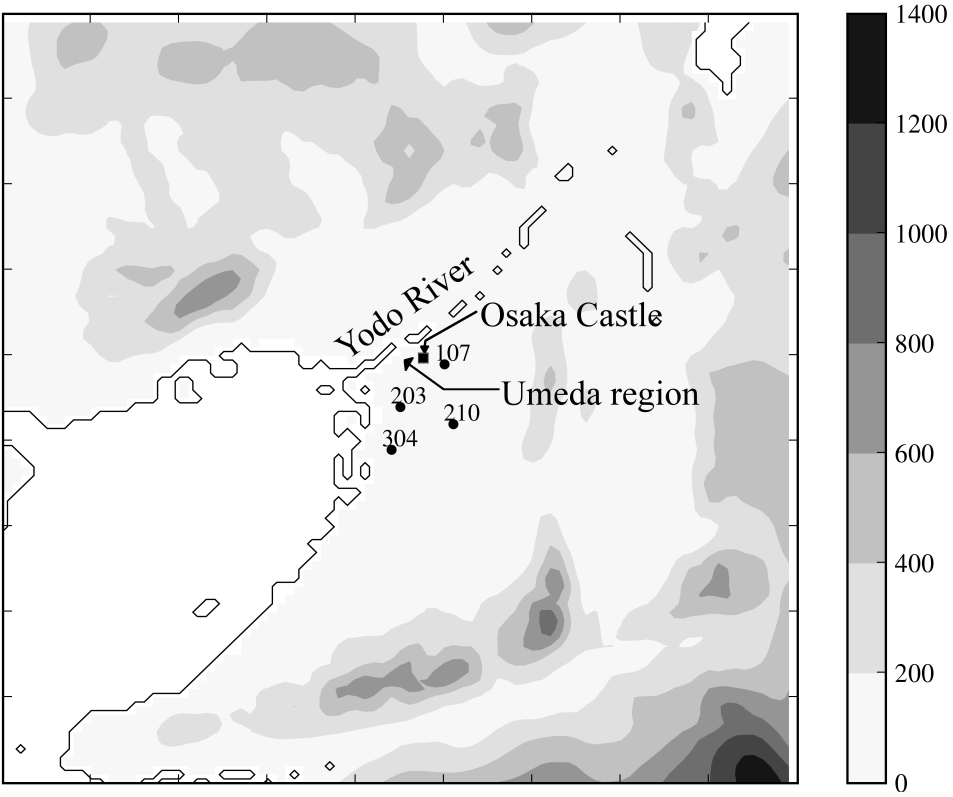
Figure 28: Terrain height (in meter) of the model region. 107, 203, 210 and 304 (see also Appendix A) are the observation stations used for comparison with the model results. The shown region is the same region as Domain-2 in Fig. 26.
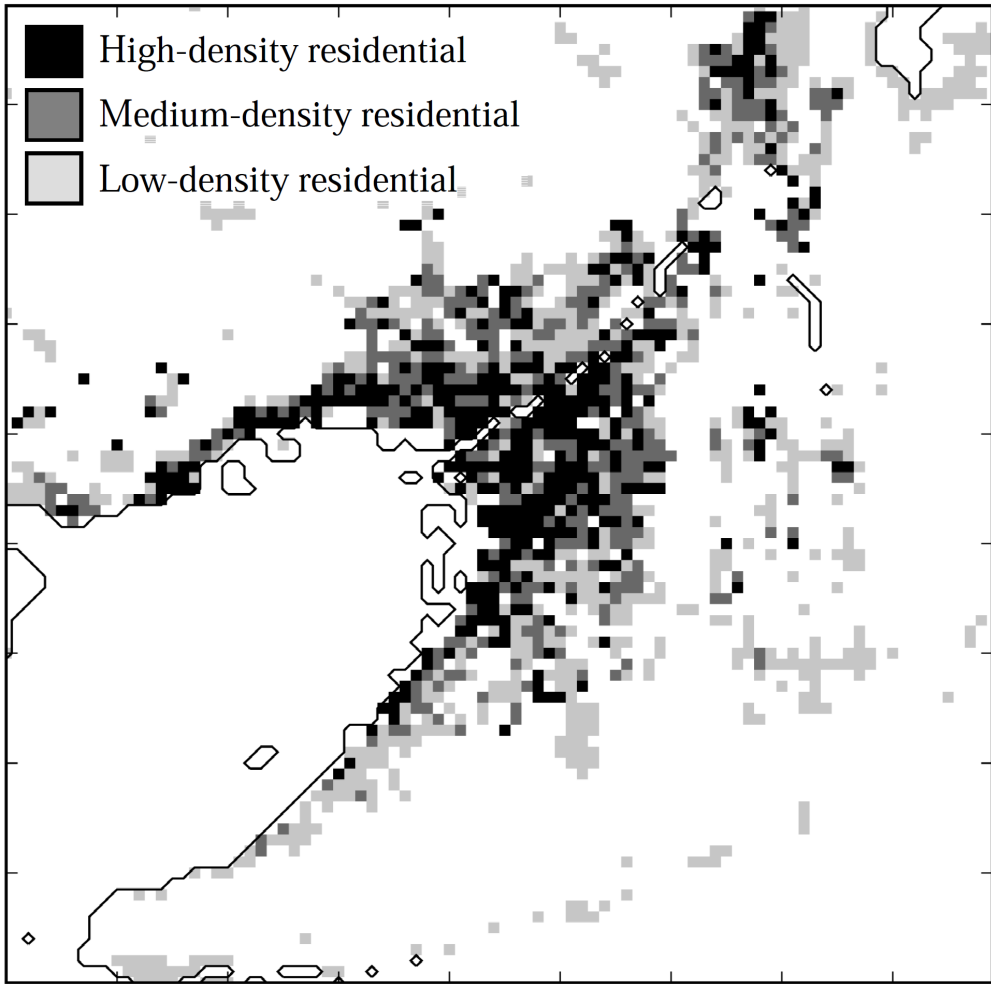
Figure 29: Sub-categories of urban land-use in model for Kinki region. The shown
region is the same region as Domain-2 in Fig. 26.
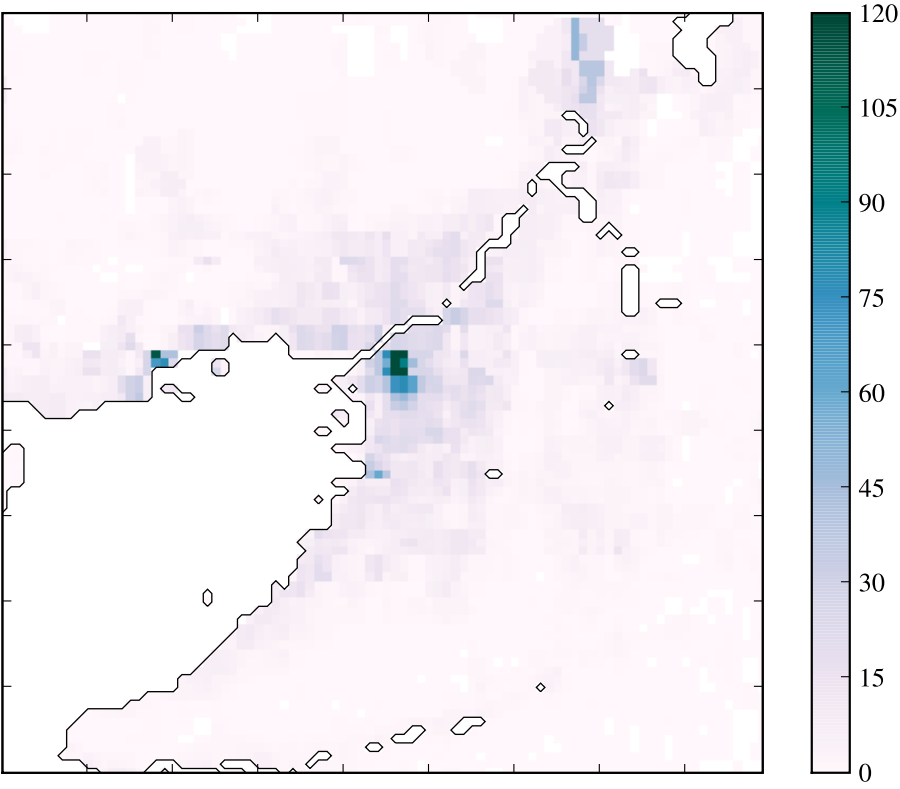
Figure 30: Sensible anthropogenic heat flux (W/m^2) of Kinki region at 2000 JST. The shown region is the same region as Domain-2 in Fig. 26.

5.4   CHANGE IN NEAR-SURFACE AIR TEMPERATURE

5.4.1   *Area-averaged spatial change in air temperature*

Stable and generally non-precipitating week of August (8-14), 2007 was selected for the highly urbanized Osaka City to observe the urban heat island effect. To quantify the urban heat island effect over a long period of time, one-week average of near-surface air temperature was analyzed. Four scenarios were developed, viz.,

DEFAULT: WRF only,

AH: WRF with anthropogenic heat (AH),

UCM: WRF with urban canopy model (UCM), and

AH+UCM: WRF using both anthropogenic heat and urban canopy model.

The results discussed here are one-week average of near-surface air temperature for each hour of the day (Fig. 31). The three columns in Fig. 31 depict the near-surface air temperature difference of AH, UCM, and AH+UCM scenarios with respect to the default case. These near-surface air temperature results are for Osaka City only. From Fig. 31, some important results are discussed here.

In AH-Default case, near-surface air temperature increases prominently in Osaka City from 2000 JST to 0700 JST. The maximum increase over this region is seen at 0700 JST. At daytime, an increase in near-surface air temperature at the high-anthropogenic heat spot in and around Umeda region is generally observed.

In UCM-Default case, near-surface air temperature increases over the entire Osaka City region from 2200 JST to 0600 JST, except over the Osaka Castle area where near-surface air temperature is generally not affected by urban canopy. The maximum increase over this region is seen at 0300-0400 JST. From 0900 JST to 1800 JST, near-surface air temperature slightly decreases, especially in the northern and eastern Osaka City. This localized cooling effect may be attributed to the effect of urban canopy as well as the green spaces like parks and suburban vegetation interspersed in the urban setting of Osaka City.

In (AH+UCM)-Default case, using both anthropogenic heat and urban canopy model, prominently high increase in near-surface air temperature is
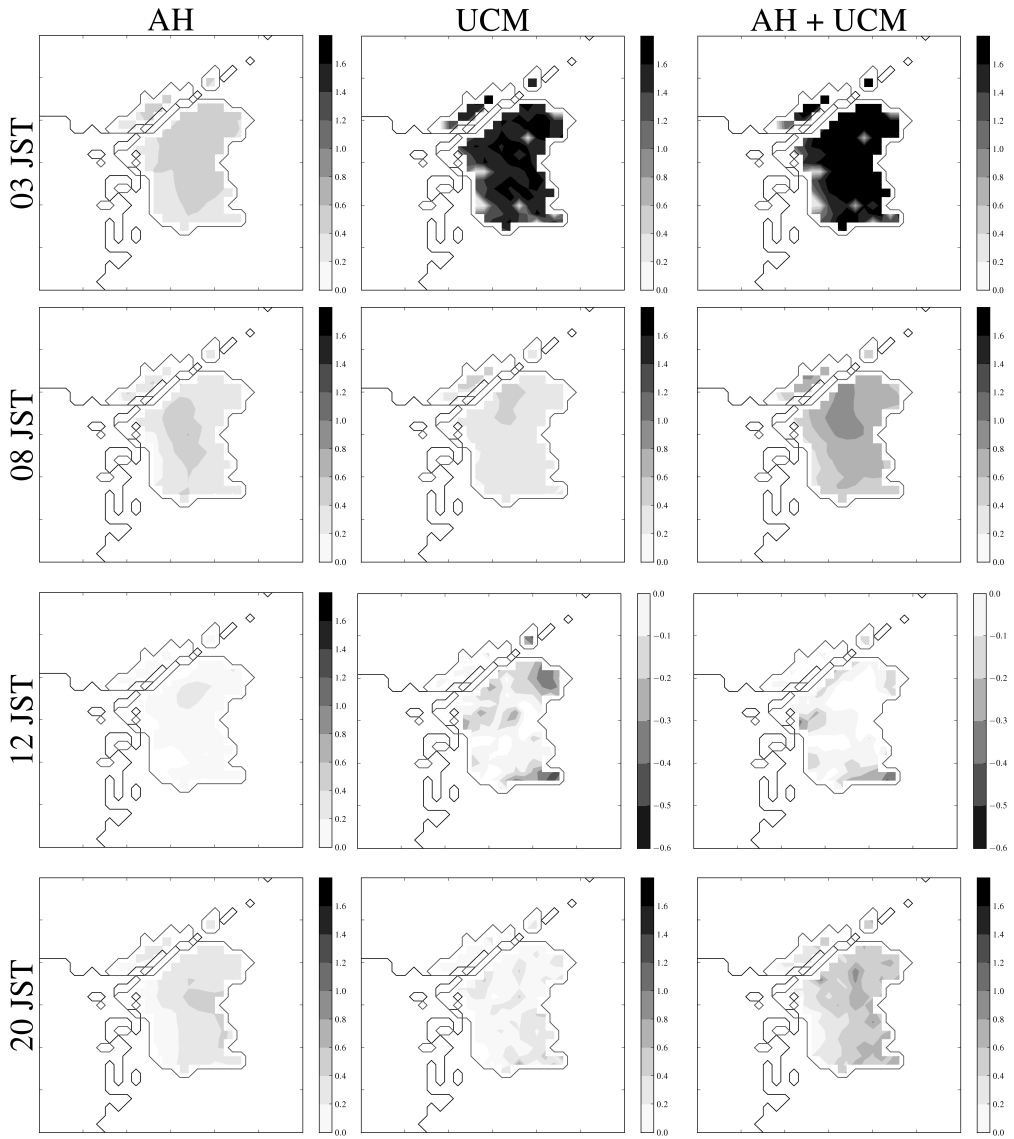
Figure 31: Time-varying difference plots of the near-surface air temperature differences (deducting the values of the default case from the three other cases) in Osaka City. Only selected hours are shown. UCM and (AH+UCM) cases at 1200 JST have scales different than that of the other cases, and in these two figures, darker shades represent cooling effect mainly due to urban canopy. In the left column, four points are observation stations in Osaka City.

Table 10: Maximum and average differences in near-surface air temperature for three simulation cases.

CASES	MAXIMUM DIFFERENCE (K)	AVERAGE DIFFERENCE (K)
AH – Default	0.8	0.2
UCM – Default	2.2	0.7
(AH+UCM)-Default	2.5	0.8

observed from 2100 JST to 0700 JST. Compared to UCM-Default case, localized increase in near-surface air temperature is observed from 0000 hour to 0500 JST in and around the high-anthropogenic heat region. From 0900 JST to 1800 JST, the cooling effect of UCM is partly canceled by the introduction of anthropogenic heat.

Table 10 shows the largest changes in the near-surface air temperature of the AH, UCM and (AH+UCM) cases with respect to the default case. The UCM case shows a higher contribution to the rise in the air temperature than the AH case. Nevertheless, AH case shows an appreciable increase in air temperature, especially at nighttime. Overall, using both AH and UCM in WRF, maximum of 2.5 K increase in near-surface air temperature is observed.

To observe the effect of introducing anthropogenic heat and urban canopy effect on the improvement of overall performance and accuracy of WRF model, the simulated area-averaged time series of Osaka City were compared with the area-averaged observed time series at observation points (see Fig. 28 and Appendix A). Since the WRF simulation result for each grid in the domain is a volume-averaged value for that grid, the comparison of area-averaged time series seems to be more meaningful in this context. Since we are observing time series for a very fine grid resolution of 1 km, the fine differences arising from local effects and grid structure can adversely affect the comparison with individual stations. In Fig. 32, the area-averaged time series of urban grids in Osaka City are investigated with respect to the observed time series. For the default case, the area-averaged time series plot shows underprediction at nighttime on most of the days. One of the reasons for this underprediction is that the anthropogenic heat generated in the urban region is not well

represented in the WRF model. Another reason is that the urban canopy effect is not represented in the default configuration of WRF model. After using anthropogenic heat and urban canopy model in the WRF model, we see an appreciable increase in the nighttime near-surface air temperature on all the days of the week. When compared with the observed data, the simulation of nighttime air temperature is greatly improved by using anthropogenic heat and urban canopy model in all days except at nighttime between August 12 and 13. Between August 8 and 11, the daytime air temperature is underestimated by the WRF model. One of the main causes of this underestimation can be the model not being able to fully reproduce the synoptic conditions prevalent on those days. The model simulation overpredicts air temperature at nighttime only between August 12 and 13, which may have been caused by the model being unable to fully represent the sudden drop in temperature accompanied with an increase in wind speed in Osaka City. Though rest of the days had good results for nighttime air temperature, a use of a larger domain to nest the 1-km domain can be recommended so that synoptic and regional scale phenomena may be better included in the boundary conditions.

In contrast, only a relatively small amount of near-surface air temperature increases at nighttime in non-urban grids of Osaka City. This small increase in nighttime temperature in non-urban grids reflects the effect of large number of urban grids surrounding the non-urban grids. In non-urban grids, it must be pointed out that the actual grid points are surrounded, and hence, affected by different types of urban atmosphere in the Osaka City region. Overall, the complex regional setting of Osaka City, in which greenspaces and open spaces are irregularly interspersed in the urban setting, influences the local climate to create complex temperature patterns.

5.4.2   *Time-averaged air temperature time series*

To ascertain the diurnal average pattern of near-surface air temperature in Osaka City, the one-week time series at different stations were averaged to 24-hour time series. This type of averaging can eliminate the intra-day time scale fluctuations that are inherent in air temperature results (Shrestha et al., 2008), and thus a clear diurnal pattern can be observed.
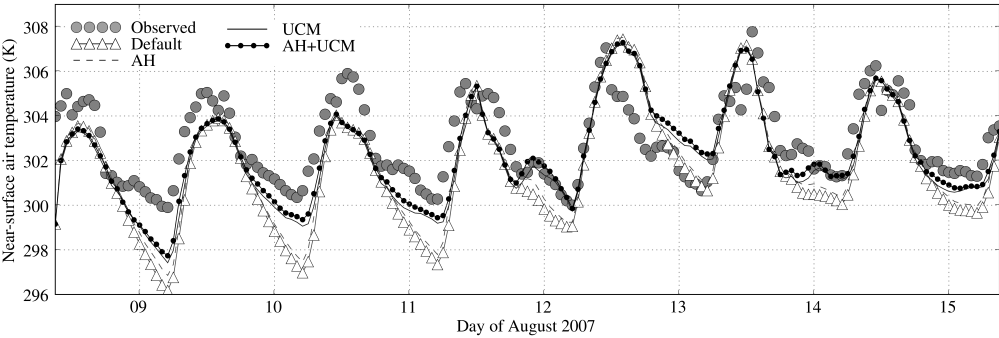
Figure 32: Area-averaged time series of near-surface air temperature for the different scenarios compared with the observed data in the urban grids of Osaka City.

Four stations in Osaka City having observation data (see left column in Fig. 31 and Fig. 28) have been selected for one-week averaged time series analysis of urban heat island (Fig. 33). The gross error gets reduced when using AH and UCM. This improvement is mainly attributable to the increase in the nighttime near-surface air temperature when using anthropogenic heat and urban canopy.

Osaka City has a complex land-use area, and it consists of a combination of highly urban region, Yodo River, greenspaces and open spaces including the Osaka Castle region. Fig. 33 clearly demonstrates that the inclusion of urban canopy effect and anthropogenic heat sources produce better air temperature results at nighttime. On the other hand, in daytime, a small cooling effect is observed due to the inclusion of urban canopy model. This cooling effect seems to have been partially canceled by the effect of anthropogenic heat emission. Thus we can observe a complex effect of anthropogenic heat emission and urban canopy structure on the near-surface air temperature of highly irregular land-use area of Osaka City.

5.5 CHANGE IN PRECIPITATION

Urban heat island effect is predominantly investigated in the urban region by studying radiation, urban air temperature and boundary layer development. Investigation of urban rainfall and its change due to urban heat island effect is

Figure 33: Time series of near-surface air temperature at four stations in Osaka City (see Fig. 28 and Appendix A) for the different scenarios compared with the observed data obtained from Japan Meteorological Agency.

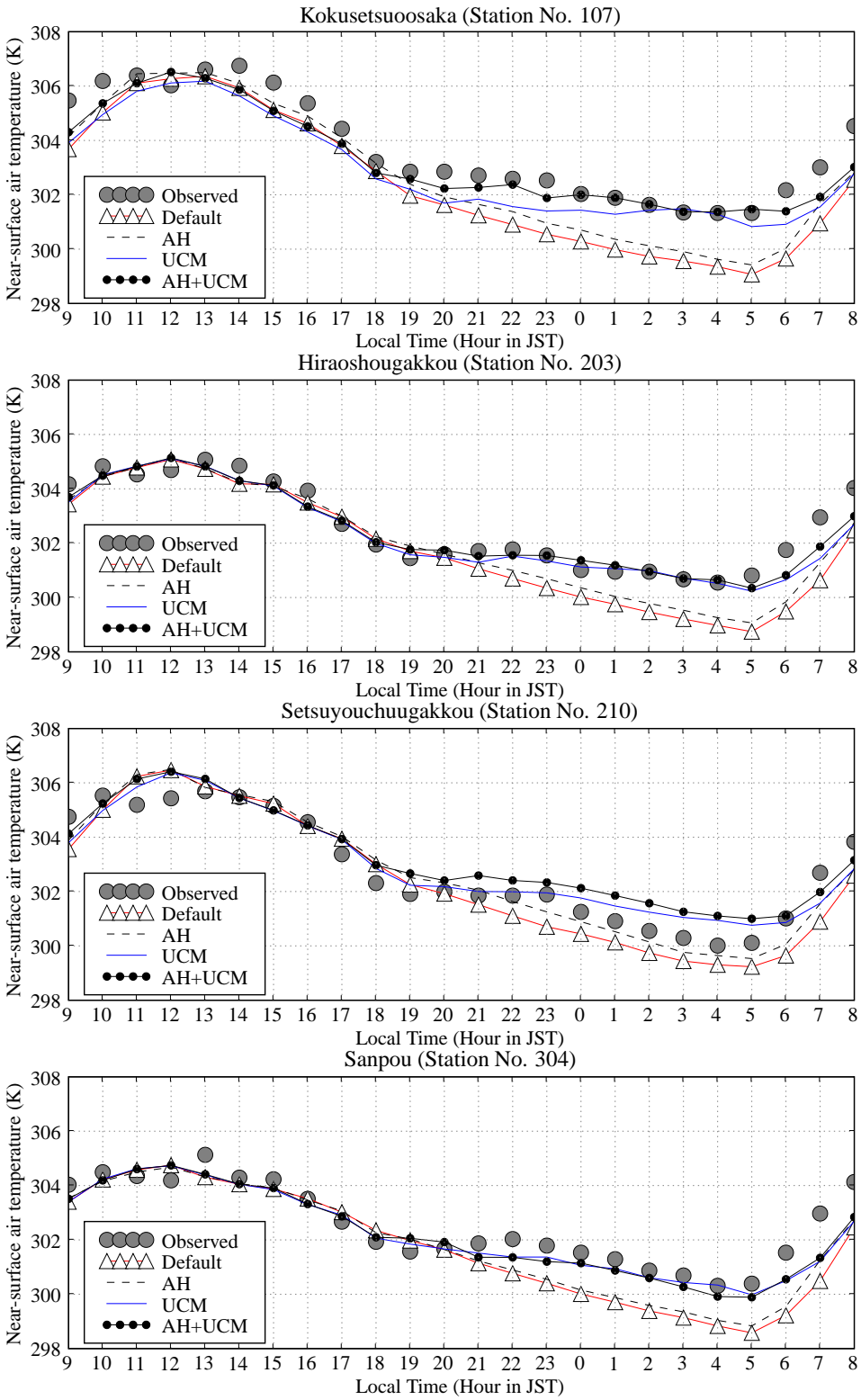relatively less compared to the study of urban air temperature profile (Lowry, 1998).

To demonstrate the effect of urban heat island on urban precipitation, a short discussion on the change in urban precipitation during the different scenarios described in subsection 5.4.1 is given here. Fig. 34 shows precipitation map during some of the rainy periods during the one-week simulation period of August 2007. Since fairly non-precipitating days were selected in this study, only a few hours of precipitation can be observed. Even in these few hours, the effects of anthropogenic heat and urban canopy are clearly visible. Precipitation pattern in the northern parts of Osaka region is mainly changed due to the introduction of anthropogenic heat flux and urban canopy effect. Maximum of nearly 10 mm or greater changes in precipitation were observed. Since the synoptic forcings have been kept same in all the scenarios, the convective and orographic effects may have caused precipitation changes and the results apparently point towards the urban-induced rainfall variability introduced by urban heat island effect.

5.6 CONCLUSION

To impart a realistic modeling approach to the investigation of the effects of urban canopies and anthropogenic heat flux in an urban setting, WRF mesoscale model, coupled with an urban canopy model, was modified to accommodate the gridded hourly anthropogenic heat flux data. The WRF modeling system was then used to simulate one-week summertime scenarios of 2007 using one-way nesting of 1-km grid domain inside a 3-km grid domain. The scenarios include the default WRF model scenario, WRF coupled with urban canopy model scenario, WRF with anthropogenic heat scenario, and finally WRF coupled with both urban canopy model and anthropogenic heat scenario.

For summertime, area-averaged time series of Osaka City and one-week average of the diurnal variation of near-surface air temperature in observation stations clearly demonstrates the effect of anthropogenic heat, especially at nighttime with a maximum increase of 0.8 K in Osaka City. The urban heat island effect of urban canopy is also confirmed with overall increase in near-surface air temperature at nighttime with maximum increase of 2.2 K,
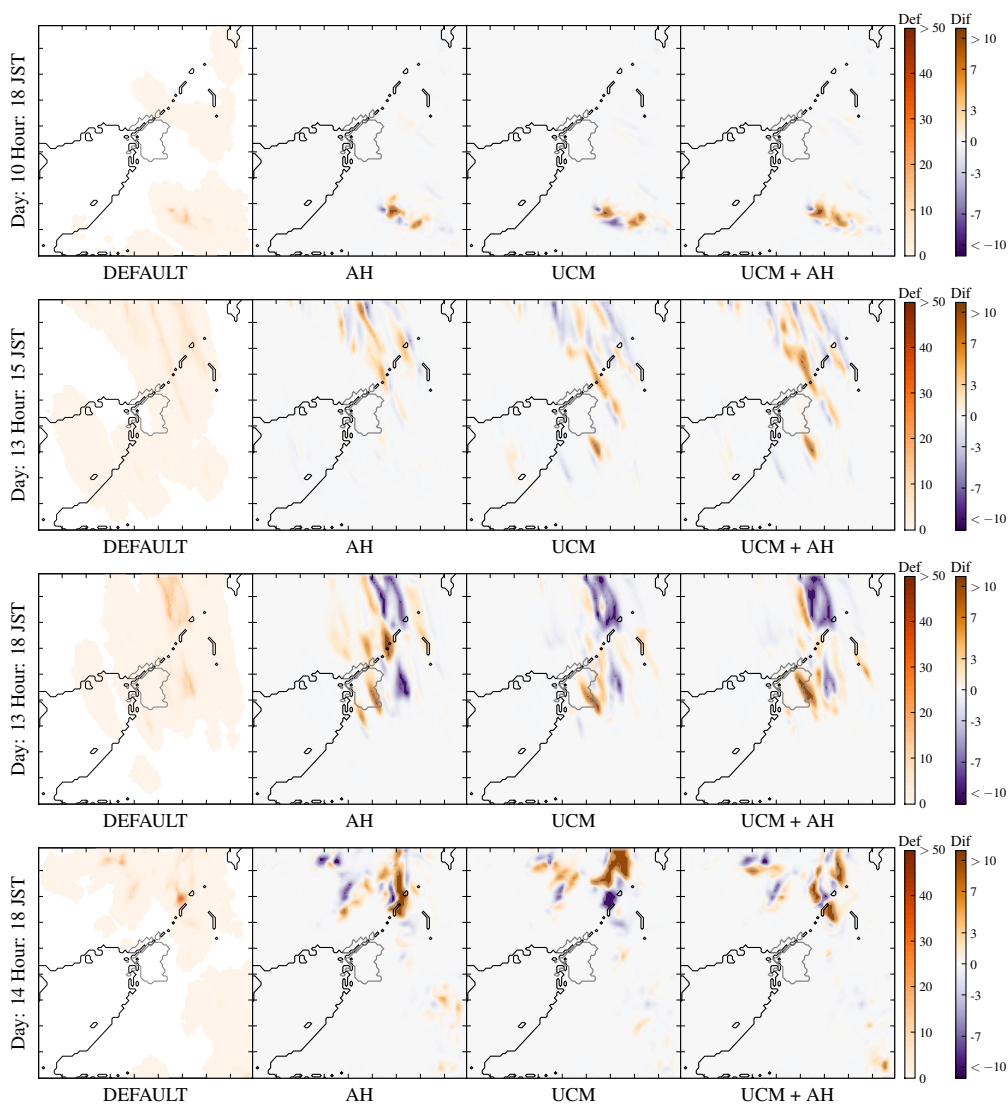
Figure 34: Precipitation in Default case, and changes in precipitation in AH, UCM and AH+UCM cases during the rainy periods of August 2007. Default case shows the precipitation in the domain ("Def" colorbar with millimeter scale). AH, UCM and AH+UCM cases show the change in precipitation with respect to Default case ("Dif" colorbar with millimeter scale). In AH, UCM and AH+UCM cases, brownish red color represents increase and blue color represents decrease in precipitation compared to Default case.

but with a relatively small decrease at daytime. Using both urban canopy model and anthropogenic heat, the nighttime near-surface air temperature is further increased with maximum increase of 2.5 K at regions with high-anthropogenic heat emission, thus simulating a better representation of urban heat. Additionally, in the daytime, the cooling effect of urban canopy is partially canceled out by anthropogenic heat forcing.

Due to the complex land-use pattern consisting of tall buildings, residential area, greenspaces, open spaces, parks, and recreational spots, the diurnal pattern of atmospheric temperature in Osaka City is intricately associated with the urban canopy structure as well as the anthropogenic heat emitted from urban sources. Thus, using WRF model, we obtain an average increase of near-surface air temperature of 0.2 K when anthropogenic heat is considered, 0.7 K when urban canopy is considered, and 0.8 K when both anthropogenic heat and urban canopy structure are taken into account.

The changes in precipitation due to the effect of urban heat island were concisely demonstrated. Overall, the change in diurnal temperature profile and change in precipitation pattern are shown to be important effects of urban heat island in the Osaka region of Yodo River basin. In consequence, the water resource in Yodo River basin is likely to be affected by urban heat island effect.

In this chapter, urban heat island effect during summertime was substantially demonstrated in the Osaka region of Yodo River basin. But it is also desirable to inspect such urban effect during other seasons. When the whole-year urban scenario can be simulated by the modified mesoscale modeling approach, the effect of urbanization can be included in the study of water resources in Yodo River basin. Though the subsequent chapters do not include the urban canopy effect demonstrated in this chapter, the application of such urban effects in the future research is highly recommended.

6

VALIDATION AND ANALYSIS OF HYDROLOGICAL
MODEL

6.1 INTRODUCTION

Yodo River basin is a mesoscale type of river basin. Basin area of mesoscale
river basins can reach from several hundreds to several thousands of square
kilometers (Krysanova and Becker, 1999) and high-resolution hydrological
modeling is required to study the impact of meteorological and climate
changes on water resources of such mesoscale river basins. The mesoscale
hydrological modeling requires finer spatial and temporal resolutions than
the large-scale hydrological modeling. The land-use and precipitation data are
also required to have high resolution.

Physically-based distributed hydrological modeling is suitable for assess-
ing hydrology of mesoscale basins. The important model components of
such distributed hydrological models consist of evapotranspiration, surface
runoff, sub-surface water flow, groundwater flow, river channel flow, reservoir
operations, water intake, sewerage disposal, interflow in the soil, and so on.

In Yodo River basin, high-resolution distributed hydrological modeling
approach is used to simulate the water flow and river discharge in response to
the changing hydrometeorological variables in the basin.

6.2 DOMAIN AND GRID STRUCTURES

Yodo River basin is gridded into 8242 square grids having 1 km x 1 km resolu-
tion (Fig. 35). Each grid in the basin contains terrain data and river network
flow direction that channels water flowing in the rivers. The evapotranspira-
tion model is used to solve surface energy balance in each of the basin grids. In
Lake Biwa, lake model has not been used to simulate the lake hydrodynamics.
So, in the rainfall-runoff model, only 7557 grids, excluding those of Lake Biwa,

are used in the simulation. The input streams into Lake Biwa are directly led out from the outlet of the lake.

Distributed hydrological model (section 3.3) was used to simulate the response of Yodo River basin to meteorological forcings for one-year period of 2006 using evapotranspiration model, rainfall-runoff model and dam reservoir model.

6.3   INPUT DATA

6.3.1   *Observed precipitation data*

One of the conventional methods of calculating areal average rainfall from observation station network is the Thiessen polygon method (Thiessen, 1911). In this method, perpendicular bisectors are drawn for each line joining a station with its neighboring stations. This method is simple and practical for regions having precipitation observation network. On the other hand, in the regions having a complex terrain structure and orographic precipitation, it may underestimate the overall rainfall. To correct this problem, several rainfall-elevation relationships have been proposed in the literature (Daly et al., 1994; Drogue et al., 2002; Mölders et al., 1996; Running et al., 1987), including the effect of wind on precipitation (Suzuki et al., 2003). To generate gridded precipitation for distributed hydrological modeling, the SDP (Surface Daily Product) observation station data provided by Japan Meteorological Agency were used to find areal average precipitation in the Yodo River basin. The SDP observation data also contains other hydrometeorological variables like air temperature, wind speed, water vapor pressure, sunshine duration, and so on. Ten observation stations were selected for the generation of Thiessen polygons (Fig. 36). Then the daily average precipitation data were calculated using Thiessen polygon method.

When the observation stations are generally in the low terrain region, the orographic effect on precipitation can be included in the precipitation data using any suitable terrain elevation correction methods. To consider the heterogeneity in terrain structure in Yodo River basin, terrain height correction method shown in Eq. 4.6 was applied to the areal average precipitation data
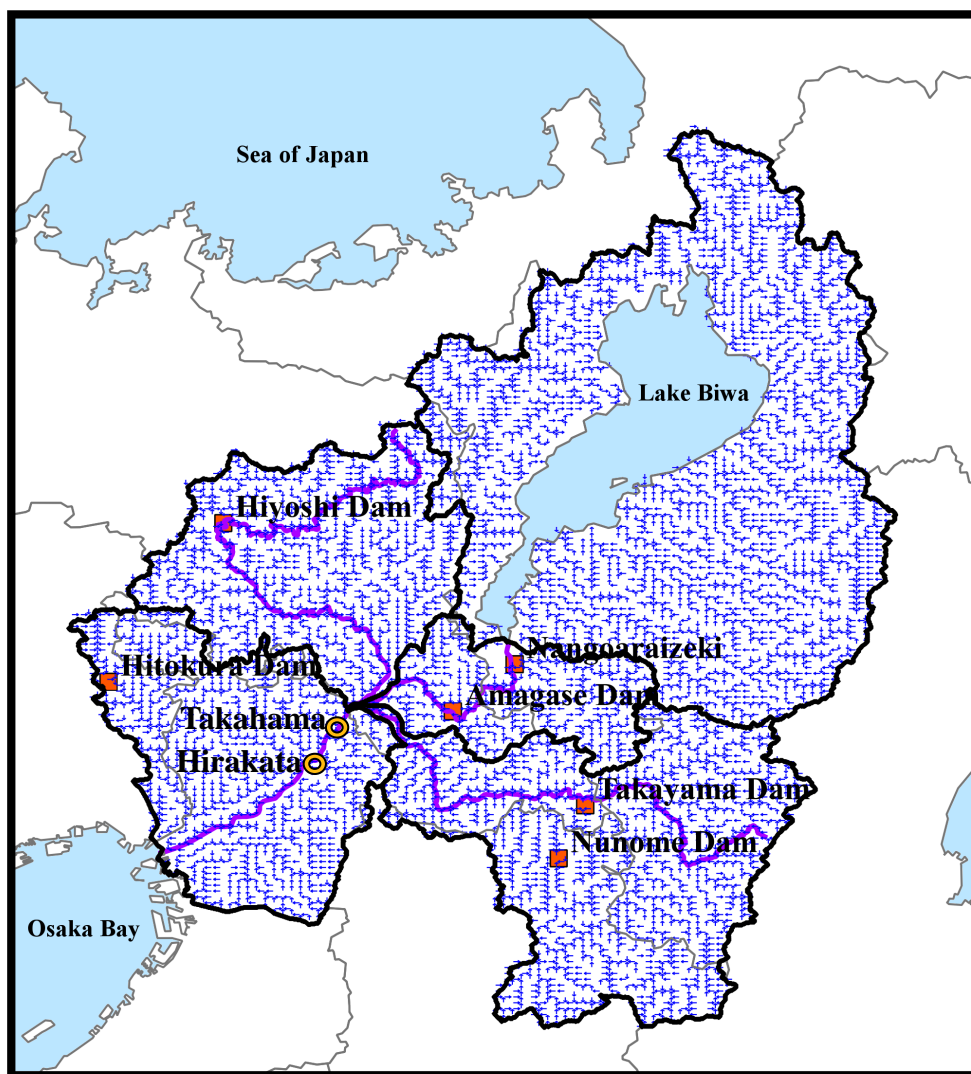
Figure 35: Yodo River basin grid structure with flow directions. Square symbols are dams and circles represent two observation stations.
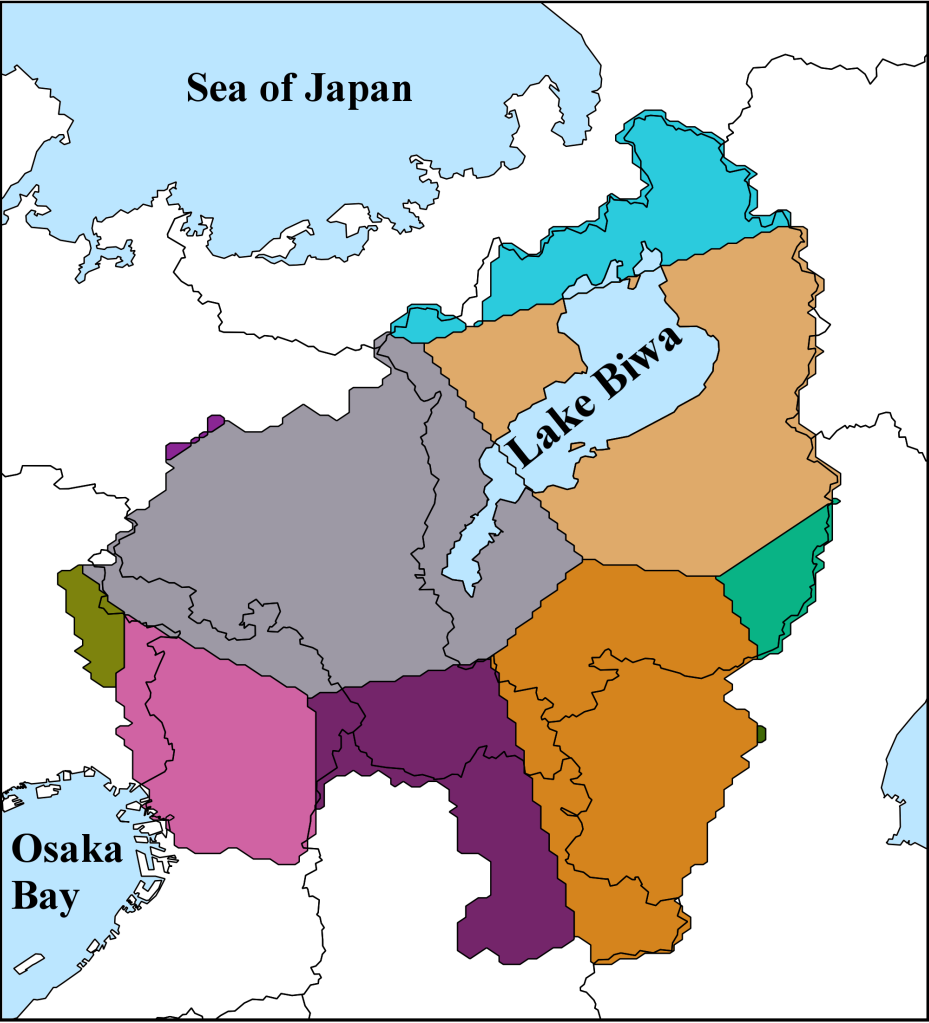
Figure 36: Thiessen polygons for observed precipitation in Yodo River basin.

to generate 1-km resolution gridded precipitation distribution. Henceforth, this corrected SDP precipitation data will be referred to as 'SDP data' only.

6.3.2 *Other input data for evapotranspiration model*

Besides precipitation, the following input variables are required to run evapotranspiration model:

- Near-surface air temperature

- Near-surface wind speed

- Surface pressure

- Water vapor pressure

- Incoming shortwave radiation flux at surface

The input data needed for all these input variables also gridded into the Yodo River basin domain by using Thiessen polygon method described in subsection 6.3.1.

Near-surface air temperature

Near-surface air temperature was obtained from the SDP observation station data provided by Japan Meteorological Agency, and it was used in the calculation of sensible heat flux (eq. 3.7) and latent heat of vaporization (eq. 3.5). Just like in the case of precipitation, terrain height correction was applied to air temperature data. The correction coefficient used to consider the effect of terrain on air temperature was 0.65 K per 100 m.

Water vapor pressure

Water vapor pressure was also obtained from SDP observation data, and it was used in the calculation of air density and near-surface specific humidity in bulk transfer equation for moisture (eq. 3.6).

Incoming shortwave radiation flux at surface

Actual sunshine duration obtained from SDP observation data was used to calculate daily incoming shortwave radiation flux at surface. Empirical

relationship between incoming solar radiation at surface and extraterrestrial radiation is:

$$R_S \downarrow = R_{S0} \downarrow \ \left(a + b \frac{N}{N_0} \right) \tag{6.1}$$

where,

$R_S \downarrow$	Incoming shortwave radiation
$R_{S0} \downarrow$	Extraterrestrial radiation
N	Actual sunshine hours
N_0	Day length
a and b	Empirical numerical parameters

The regressional parameters a and b were set at 0.244 and 0.511 respectively. The actual sunshine hours data is provided in the SDP observation station data. $R_{S0} \downarrow$ is the assumed amount of solar radiation coming to the surface without the influence of the atmosphere. N_0 is day length, or the theoretical maximum duration of sunshine hour between dawn and sunset.

Wind speed

Near-surface speed was also obtained from SDP observation data, and it was used in the bulk transfer equation for moisture (eq. 3.6).

Parameters for evapotranspiration model

Some important parameters for the five types of land-use surfaces used in the surface energy balance equation of the evapotranspiration model are shown in Table 11. Since the surface properties of paddy fields change during irrigation and non-irrigation periods, different set of parameters are used for these two periods. For Yodo River basin, the irrigation period is estimated as 120-270th days of a year. Anthropogenic heat flux is set at an average value of 80 Wm^{-2} for the Yodo River basin area.

Table 11: Parameters for evapotranspiration model in Yodo River basin.

LAND-USE	BULK TRANSFER COEFFICIENT	EVAPORATION EFFICIENCY	ALBEDO
Forest	0.002	0.7	0.1
Paddy - irrigation period	0.005	0.7	0.15
Paddy - non-irrigation period	0.0008	0.3	0.2
Crop field	0.0008	0.2	0.2
Urban	0.0001	0.2	0.3
Water bodies	0.001	1.0	0.06

Irrigation period: 120-270$^{\text{th}}$ days of a year

6.3.3 *Data and parameters for runoff model*

Precipitation and evapotranspiration quantities simulated by the evapotranspiration model are used as input data in the HydroBEAM runoff model. Water intake and release for water supply, water use, hydroelectric plants, and irrigation purposes are also used as input into the runoff model. The sewerage and wastewater flow data are also used for the corresponding grids. Dam operation rules (subsection 3.3.5) are used to control the water level and storage in the six majors dams (Fig. 35).

Important soil layer and model parameters used in the runoff model are shown in Table 12.

6.4 VALIDATION OF RIVER DISCHARGE

6.4.1 *Dam outflow*

Dam network in Yodo River basin is highly regulated using several complex operation rules such as ordinary operation, preliminary release operation,

Table 12: Soil layer and model parameters for runoff model in Yodo River basin.

PARAMETER		VALUE
Equivalent	Paddy	-
roughness	Crop field	0.300
$(m^{-1/3}s)$	Forest	0.700
	Urban	0.030
	River channel	0.035
Direct runoff	Paddy	1.0
percentage	Crop field	0.21
from surface	Forest	0.3
	Urban	0.737
Soil layer depth	A	0.3
(m)	B	1.0
	C	2.5
	D	10.0
Porosity (%)	All soil layers	10.0
Linear storage	B soil layer horizontal runoff coefficient	0.03
model constant	C soil layer horizontal runoff coefficient	0.007
(1/d)	D soil layer horizontal runoff coefficient	0.0039
	B soil layer vertical runoff coefficient	0.11
	C soil layer vertical runoff coefficient	0.013
	D soil layer vertical runoff coefficient	0.0
Tank model	A1: runoff coefficient (1/d)	1.0
constant	Z1: hor. runoff boundary height (mm)	300.0
(*ap* and *zap*	A2: hor. runoff coefficient	0.17
in eq. 3.12)	Z2: hor. runoff boundary height	DPD[1]
	A3: hor. runoff coefficient	0.0
	Z3: hor. runoff boundary height	0.0

[1]Desired Ponding Depth

Table 13: Comparison of modeled and observed annual outflow from dams in Yodo River basin in 2006.

DAM	OUTFLOW ($m^3 \times 10^6$)	
	OBSERVED	FROM MODEL
Amagase	3523.7	3494.2
Hiyoshi	360.9	396.2
Takayama	474.6	474.3
Nunome	56.5	61.6
Hitokura	95.2	50.3

emergency operation, peak attenuation operation and post-flood operation (Sayama et al., 2005). The microscale studies of reservoir effects on the water resource of river basins require exhaustive classification of dam operation rules to simulate the actual practices in dam control. In this study, the dam operations have been simplified (subsection 3.3.5) to focus on the overall response of mesoscale Yodo River basin to atmospheric forcings and climate change.

Table 13 shows the comparison between the modeled and observed annual outflow from the six major dams in Yodo River basin. The observed outflows from the dams have been provided by Ministry of Land, Infrastructure and Transport, Japan (`http://www2.river.go.jp/dam/index.html`, in Japanese). The outflow for Nangoaraizeki dam has not been included because of data unavailability. The hydrological model reasonably reproduces the actual observed outflows in all the dams. The dam outflows are slightly overpredicted at Hiyoshi and Nunome dam but some underpredictions of outflow are present at Amagase and Hitokura dam.

The slight overpredictions in annual outflow amount at Hiyoshi and Nunome dams can also be visualized from the hydrographs in Fig. 37. The overall slight overprediction of outflow at Hiyoshi and Nunome dams can be attributed to some peaks larger than the observed discharge peak values in rainy season of June and July. The largest peak discharge at Nunome is overpredicted by nearly 20 cumec.

At Amagase dam, though the annual discharge is slightly underpredicted by the hydrological model, the maximum discharge peak in July is overpredicted by more than 1000 cumec and the ensuing low discharge periods are also generally overpredicted by the model. Some of these overpredicted peak discharges shown by the hydrological model may be attributed to underrepresentation of peak attenuations during actual dam operations at Nangoaraizeki and Amagase dam reservoirs that regulate the outflow from Lake Biwa into Uji River. Another reason for the overprediction in Amagase dam peak discharges may be that the lake hydrodynamics of Lake Biwa has not been considered in the present model, and hence, the outflow from Lake Biwa is possibly overpredicted due to the lack of consideration of residence time in the lake. Though the peak discharge in July is also overpredicted at all the dams except at Hitokura dam, most of the peak discharges are modeled by the hydrological model with sufficient levels of correlation, which are evident from hydrographs in Fig. 37.

6.4.2 *River discharge at observation stations*

The Water Information System database provided online by Ministry of Land, Infrastructure and Transport, Japan (http://www1.river.go.jp/, in Japanese) contains many observation stations in Yodo River basin. But, at present, most of the observation stations have missing data in 2006. Hence, only two observation stations, viz., Hirakata and Takahama (Fig. 35) are validated with the observed data (Fig. 38). In Hirakata station, only the high discharge peak in July 2006 was available in the observed river discharge data.

Takahama station is situated in the Yodo sub-basin and receives river discharge from Biwa, Uji, Katsura and Kizu sub-basins (Fig. 20). Hirakata station lies even further downstream than Takahama station in the Yodo River flowing in the Yodo sub-basin. Though the maximum river discharge in July could not be compared with the observed data at Takahama station, rest of the river discharge in 2006 is well-simulated by the hydrological model in Takahama station with some slight underpredictions in spring season. The highest peak discharge during July 2006 is reasonably predicted at Hirakata station with the observed discharge being overpredicted by nearly 1000 cumec. This over-
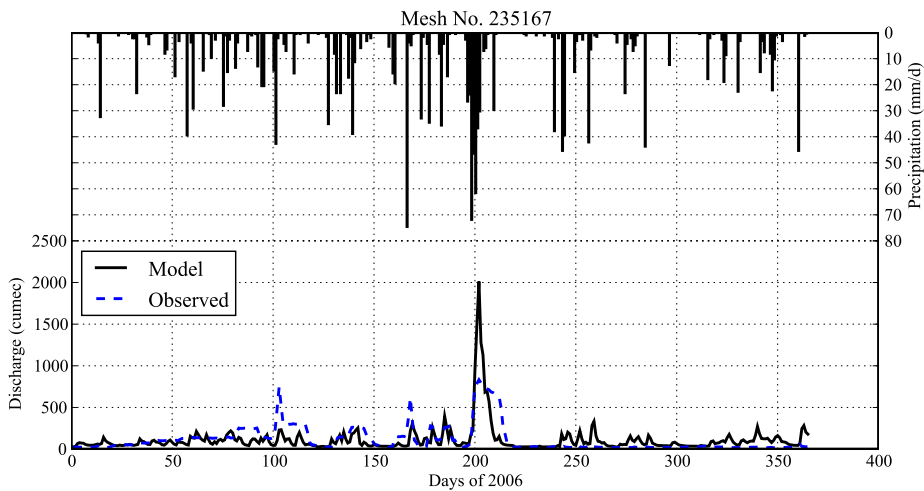
(a) Amagase dam.
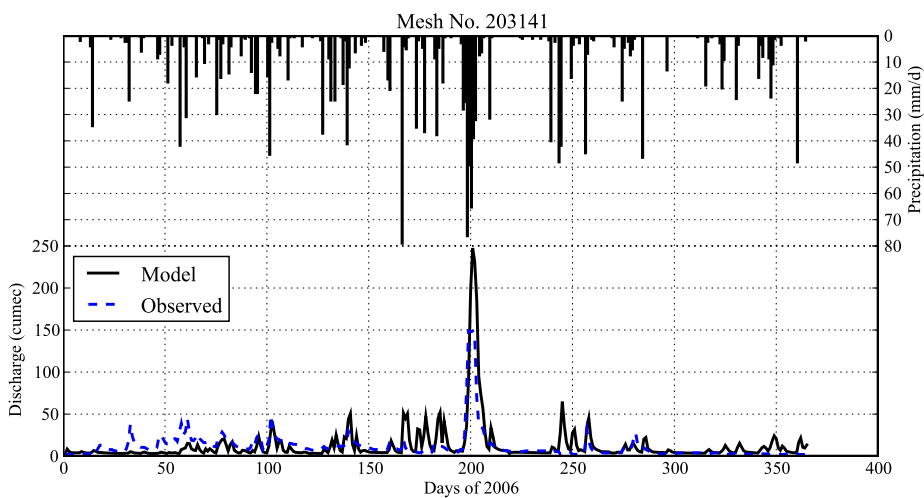
(b) Hiyoshi dam.
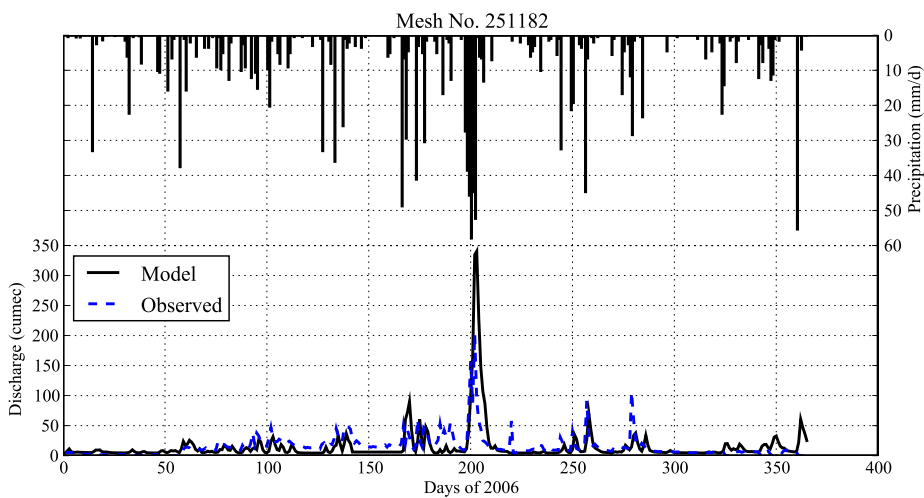
(c) Takayama dam.

Figure 37: Hydrographs for five dams of Yodo River basin in 2006.

(d) Nunome dam.

(e) Hitokura dam.

Figure 37: Hydrographs for five dams of Yodo River basin in 2006.

prediction in maximum peak discharge in July is most probably due to the overprediction of dam outflow from the upstream Amagase dam.
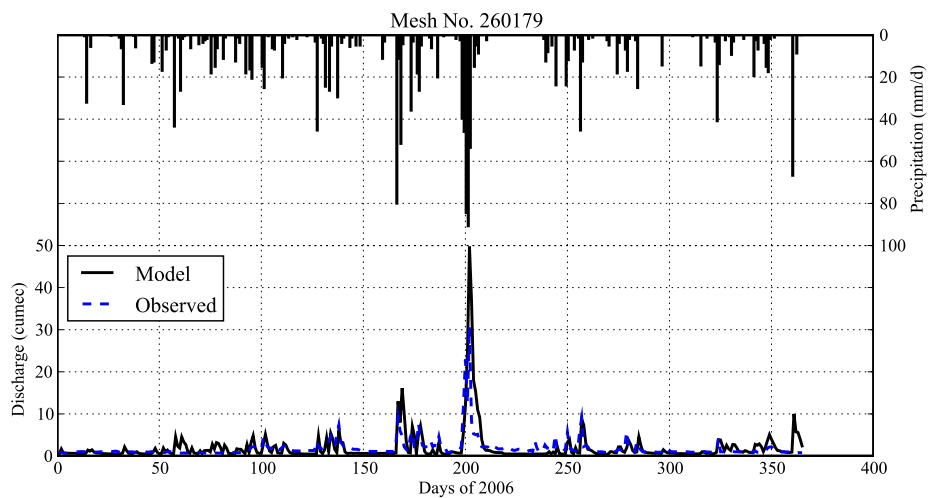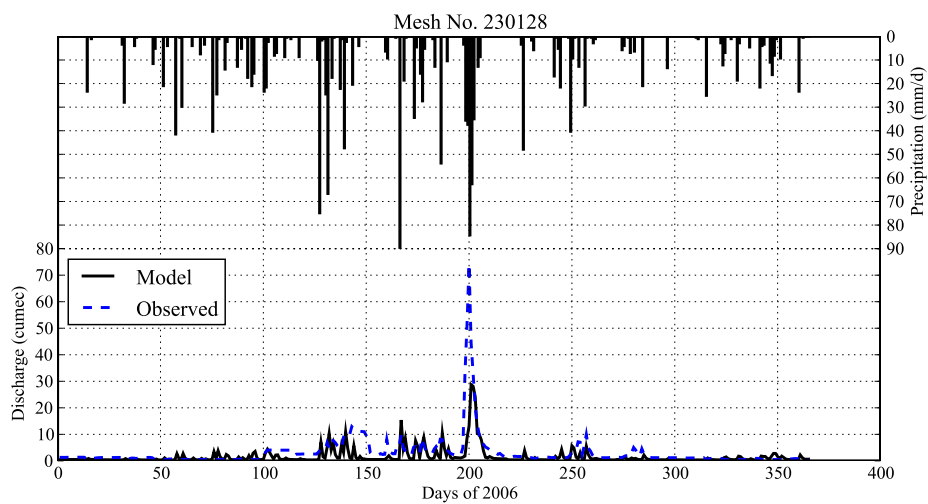
6.5 VALIDATION OF DAM MODEL

To validate the simplified dam model used in the hydrological model to simulate the reservoir operation in six major dams in Yodo River basin, the observed water levels at those dams (http://www2.river.go.jp/dam/index.html, in Japanese) were compared with the simulated water levels (Fig. 39). The patterns of water level fluctuations in all the dams were well-simulated by the dam model used in the hydrological model. The change in water levels during transition period between the flooding and non-flooding seasons was also predicted with sufficient accuracy. Since the actual dams operations are complex and are manually changed according to different existing weather conditions, the water levels from the simplified dam model used in this study do not exactly fit with the observed water levels. Some short-period changes in water levels may not be reproduced at all by the present dam model. For example, some of the periodic fluctuations in the water levels at Amagase dam are smoothed by the dam model. Similarly, at Hiyoshi dam, the sudden increase in dam water level at highest peak discharge in July 2006 could not be reproduced by the dam model. Similarly, the temporary drop in water level in the second half of August 2006 in Hiyoshi dam was also not reproduced. The reason for this non-reproducibility might be the simple precipitation limit used in the model to determine flooding (subsection 3.3.5). It should also be noted that the transition periods between flooding and non-flooding seasons have regular patterns in the modeled water levels, but the actual dam operations may differ from this somewhat idealized but expected transition in dam water levels.

Regardless of the above-mentioned differences between the simulated and observed water levels in the dams of Yodo River basin, the overall trend of dam water levels are sufficiently well-reproduced by the simplified dam model for application of the hydrological model in the assessment and prediction of water resources at mesoscale.
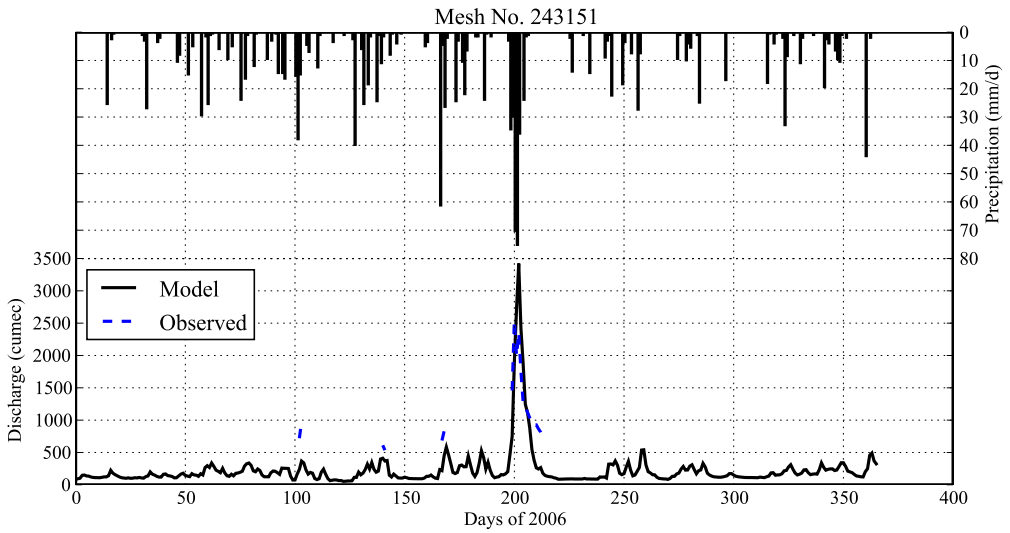
(a) Hirakata observation station.
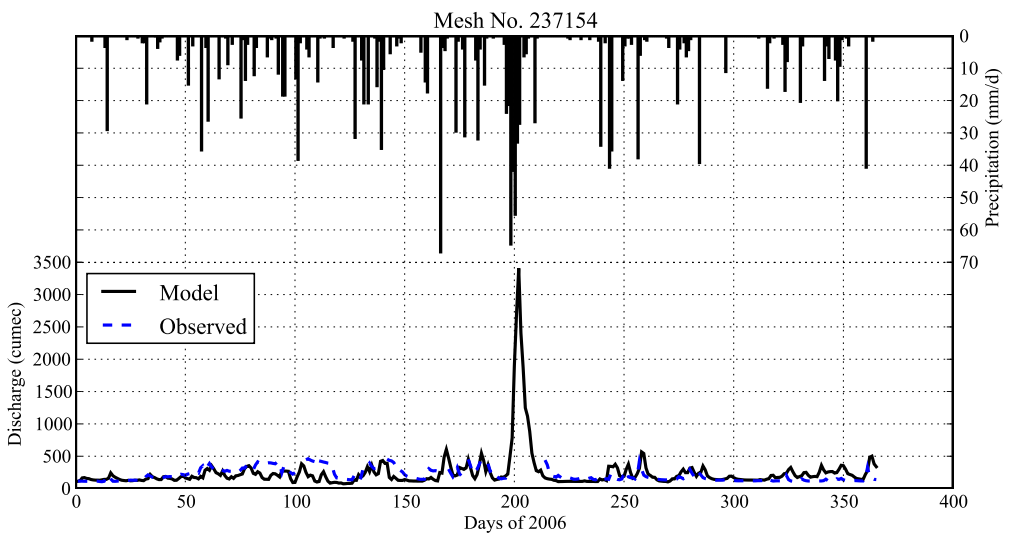
(b) Takahama observation station.

Figure 38: Hydrographs for two observation stations of Yodo River basin in 2006.
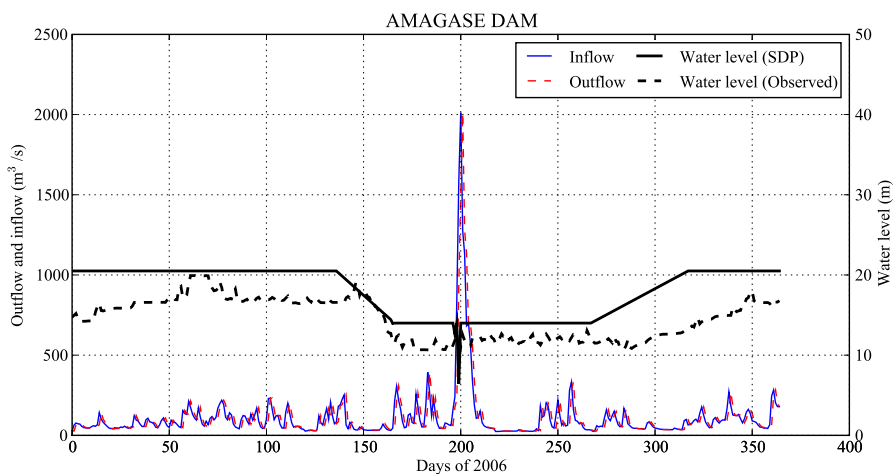
(a) Amagase dam.
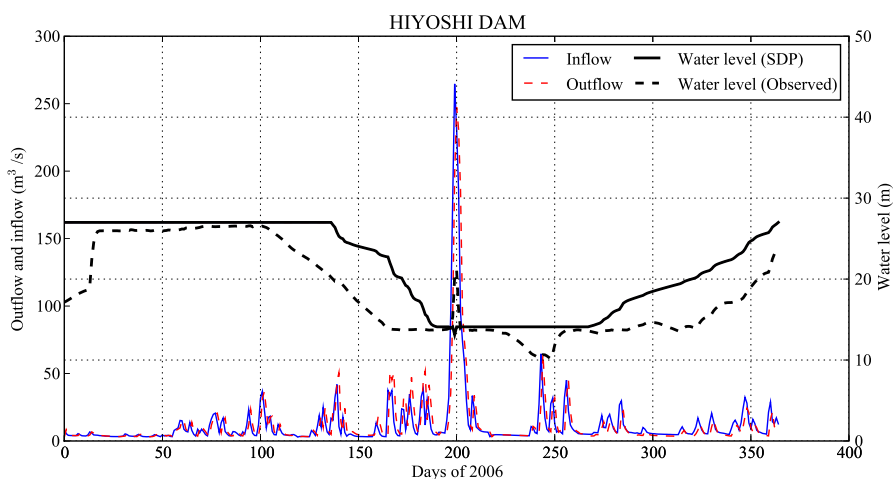
(b) Hiyoshi dam.
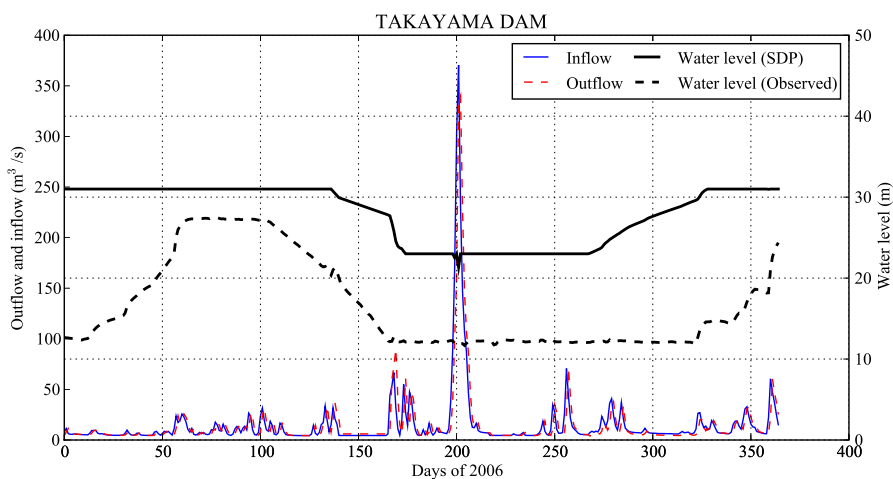
(c) Takayama dam.

Figure 39: Inflow, outflow and water level for five dams of Yodo River basin in 2006.
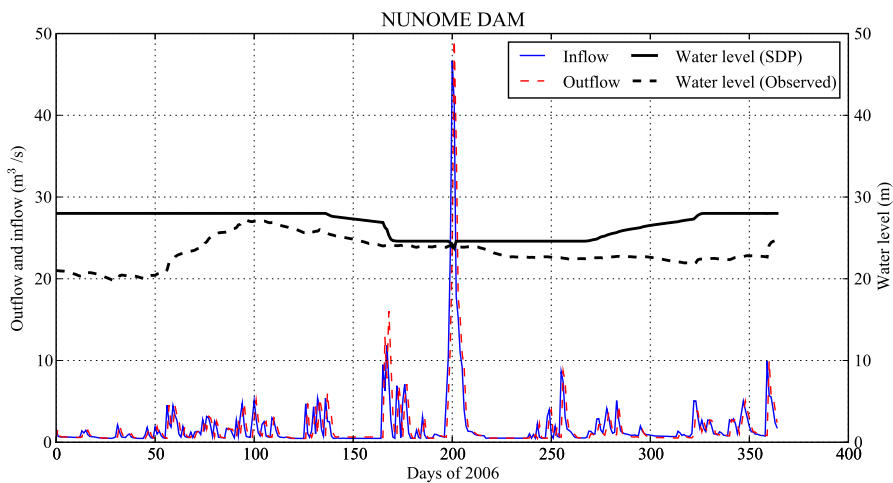
(d) Nunome dam.
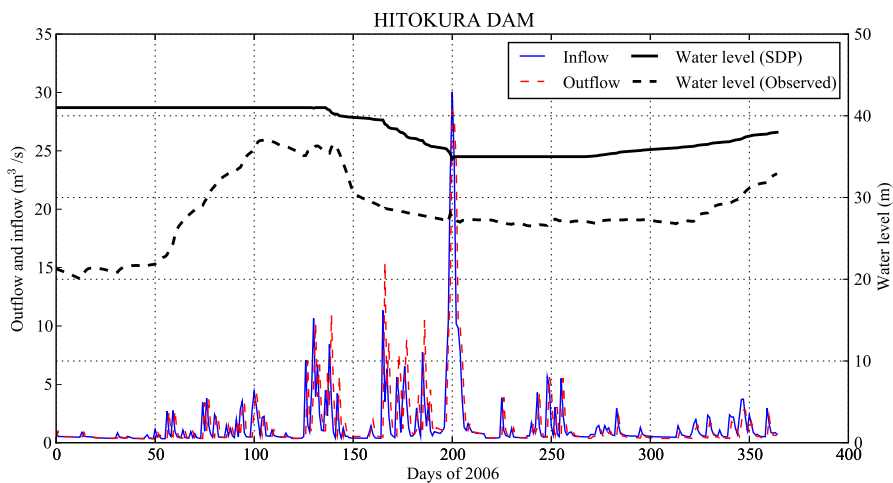
(e) Hitokura dam.

Figure 39: Inflow, outflow and water level for five dams of Yodo River basin in 2006.

6.6 CONCLUSION

Distributed high-resolution hydrological model was used to simulate the response of Yodo River basin to the atmospheric forcings in 2006. The hydrological modeling consisted of evapotranspiration, surface runoff, sub-surface water flows in the soil layer and river channel flows as the main sub-models. Precipitation data, required to run the model, was obtained by Thiessen polygon method from ten observation stations in the Yodo River region. A simplified dam model was also used in the rainfall-runoff model to simulate the reservoir operations in the highly regulated dam reservoir network in Yodo River basin.

Outflows from the dams and river discharge at the observation stations were found to be reasonably simulated by the hydrological model. The reservoir effect on basin water flow was also adequately simulated. The objective of predicting the effects of atmospheric and climate changes on the water resources of Yodo River basin can be reliably fulfilled by using the distributed hydrological modeling approach presented in this chapter.

HYDROLOGICAL SIMULATION OF YODO RIVER BASIN BY COUPLED HYDROMETEOROLOGICAL MODEL

7.1 INTRODUCTION

The distributed hydrological modeling approach used in chapter 6 can be improved in two respects:

1. The resolution of the input data can be increased by replacing the SDP observation data by meteorological output from an atmospheric or meteorological model.

2. The hydrological model can be adapted for predicting and assessing the future water resource scenarios by using the atmospheric forcings from the future climate projections.

Both of these desired improvements point towards the use of modeled hydrometeorological data as input to the hydrological model. One simple way of obtaining the hydrometeorological data is to directly downscale the global climate data obtained from General Circulation Models (GCMs). One main disadvantage of using this method is that the very fine spatial resolution required by hydrological models cannot be realistically obtained from the very coarse GCM outputs. To circumvent this problem we need atmospheric models with better spatial and temporal resolutions. Regional and mesoscale meteorological models are better suited for providing more accurate and high-resolution input data to the distributed hydrological models. The regional and mesoscale models are generally run by using initial and boundary conditions obtained from meteorological analysis and reanalysis data, and GCM data. Thus the regional and mesoscale models dynamically downscale the global climate variables to regional and local scales.

Since Yodo River basin has a mesoscale basin structure, the distributed hydrological modeling at a spatial scale of 1 km x 1 km shown in chapter 6 is required to resolve the terrain and land-use of the basin. It was shown in

chapter 4 that WRF mesoscale meteorological model could be successfully used to produce precipitation data at the desired spatial resolution for hydrological modeling. In this chapter, WRF model is used to produce all the meteorological variables required by the hydrological model. The hydrological simulation of Yodo River basin is then carried out for 2006 by coupling the WRF model with the distributed hydrological model described in chapter 3. Since the objective is to study the effect of change in climate and atmospheric forcings on the water resource of Yodo River basin, this chapter uses the one-way coupling approach in which the meteorological variables from mesoscale meteorological model are used as input to the hydrological model. Then the river discharge results are compared with the results of chapter 6, in which observation data were used as input to hydrological model.

7.2   INPUT DATA

7.2.1   *WRF precipitation data*

Non-convective precipitation is calculated by microphysics model in WRF and convective precipitation is calculated by cumulus parameterization. The sum of convective and non-convective precipitation from WRF is then used as the total precipitation input for the hydrological model.

7.2.2   *Other input data for evapotranspiration model*

All the input variables are readily available from WRF output except the water vapor pressure. Air temperature at 2 m. is used as near-surface air temperature. Similarly, horizontal wind vector components, u and v, at 2 m. are used to calculate near-surface wind speed.

Water vapor pressure

From WRF output, surface pressure (P) and water vapor mixing ratio at 2 m. (q) are extracted, and then water vapor pressure is calculated by using eq. 7.1.

$$e = \frac{q\,P}{0.622 + q} \tag{7.1}$$

Incoming shortwave radiation flux at surface

In the hydrological model, sunshine duration is used to calculate daily incoming shortwave radiation flux at surface. Since we are calculating daily average fluxes, we can directly use the daily average values of incoming shortwave radiation from WRF without using the regressional relation between sunshine duration and incoming shortwave radiation.

Wind speed

Horizontal wind vector components, u and v, at 2-m height are used to calculate near-surface wind speed. Firstly, the 10-m wind vector components are used to find wind speed at 10-m height using the formula, $\overline{V}_{10} = \sqrt{u^2 + v^2}$. This conversion of wind vector components into wind speed was carried out using ncap2 (NetCDF Arithmetic Processor) tool provided by NetCDF Operator (NCO, http://nco.sourceforge.net/) suite of programs that contains command-line tools to analyze and manipulate NetCDF files. Then, using the wind profile based on the Monin and Obukov similarity theory, 10-m wind speed was converted to 2-m wind speed using eq. 7.2, which is based on the work by Högström (1988).

$$\overline{V}_2 = \overline{V}_{10} - \frac{u_*}{k} \left[\ln\left(\frac{z_{10}}{z_2}\right) - \psi_m(z/L) \right] \tag{7.2}$$

$\overline{V}_2$	Wind speed at 2 m
$\overline{V}_{10}$	Wind speed at 10 m
u_*	Friction velocity
k	von Kármán's constant
z_{10}	Height at 10 m
z_2	Height at 2 m
ψ_m	Integral of universal function of momentum
L	Monin-Obukov length

The 2-m wind speed can be compared with the original wind speed from WRF at 10-m height in Fig 40. As expected, the wind speed has decreased
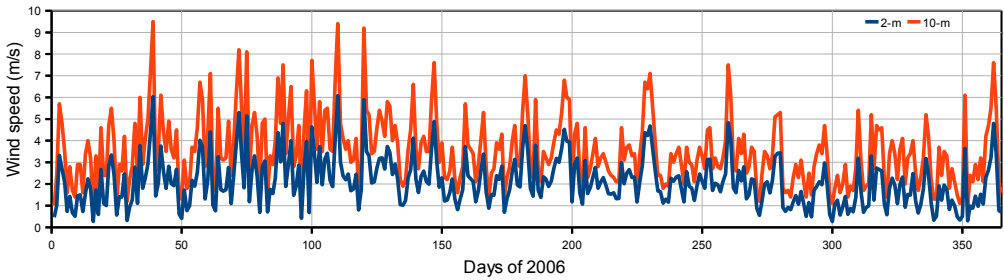
Figure 40: Wind speed obtained from WRF at 10-m height and converted wind speed at 2-m height.

when scaled to 2 m from 10m height. In comparison to the minimum wind speeds, the maximum wind speeds have reduced by large amounts, and in some instances, peak values have increased by nearly 3 m/s.

7.3   COUPLING OF METEOROLOGICAL AND HYDROLOGICAL MODEL

WRF mesoscale model is one-way coupled in offline mode with the hydrological model of Yodo River basin. That means, several WRF output variables are used as atmospheric forcings in distributed hydrological model without considering the feedback from hydrological model to WRF mesoscale model. The offline mode indicates that the passing of data between the models occurs without any synchronous operation between the two models under consideration. In other words, the models are run separately with the coupling of the models occurring in between the operation of the two models. This kind of coupling is sometimes called "loose coupling." WRF mesoscale model is first run to simulate the hydrometeorological variables like air temperature, precipitation, surface pressure and incoming solar radiation. Then the required hydrometeorological variables are downscaled and appropriately converted into the data format required by the hydrological model. Since the grid structure of WRF mesoscale model and hydrological model differ from each other, this kind of offline coupling requires the conversion of data from meteorological grid coordinate system to the hydrological basin grid system.

Basin grid information

The grid structure of Yodo River basin in the hydrological model is represented by nearly 1 km x 1 km GIS grid system, which is also known as Japanese 3D Mesh. In the hydrological model, each grid is given a unique Mesh ID to represent the sequence of channel flow in the basin. Besides a Mesh ID, these grids have 3D Mesh ID as well. A list of Mesh ID and 3D Mesh ID for 8242 grid mesh of Yodo River basin is created. Longitude and latitude information for each of the grid mesh is available in a GIS shapefile that contains 3D Mesh ID and corresponding geographical coordinates. Using GRASS GIS (`http://grass.itc.it/`), geographical coordinates (latitude/longitude) of basin grid meshes are tabulated against corresponding Mesh ID using the 3D Mesh ID data that are common between the GIS shapefile and the basin grid data.

WRF grid information for each basin mesh

A Fortran program called `read_wrf_nc` (described in `http://www.mmm.ucar.edu/wrf/OnLineTutorial/Tools/read_wrf_nc.htm`) is available in WRF software to look into the NetCDF binary format (`http://www.unidata.ucar.edu/software/netcdf/`) output data produced by WRF. This program is slightly modified to obtain X/Y coordinates of WRF for each of the grid mesh of Yodo River basin. The latitude/longitude information from the previous step for each Mesh ID of Yodo River basin are used as input to `read_wrf_nc` program to produce a list containing Mesh ID and corresponding WRF X/Y coordinates.

Extraction of meteorological variables from WRF output

As noted in subsection 6.3.2, hydrological model requires daily precipitation, near-surface air temperature, near-surface wind speed, surface pressure, water vapor pressure and incoming shortwave radiation flux at surface as input. The required output data from WRF are extracted from the WRF output files using a Python program that utilizes Climate Data Management System (CDMS, `http://www2-pcmdi.llnl.gov/cdat`) library to access NetCDF variables. Then the extracted WRF output variables are processed as described in section 7.2. Since the WRF precipitation data Domain-3 (Fig. 21) is at 3-km resolution, they

are downscaled to 1-km resolution required by the hydrological model using
the method described in subsection 4.5.3. Other variables are obtained at basin
grids corresponding to the nearest grid in the WRF output data. Subsequently,
the thus-obtained hourly meteorological data for all the 1-km x 1-km grid
mesh of Yodo River basin are averaged into daily average values and then
written into the input data files required by evapotranspiration model of the
hydrological model.

7.4   RIVER DISCHARGE IN YODO RIVER BASIN FROM COUPLED HYDROM-
   ETEOROLOGICAL MODEL

The observed river discharges in Yodo River basin were used in chapter 6
to validate the use of the distributed hydrological model at basin-scale level.
Here, the use of the coupled hydrometeorological model is validated so that
the WRF hydrometeorological variables can be used instead of observation
data in the distributed hydrological model as input data. This facilitates the
use of high-resolution gridded data from WRF to be used in the hydrological
model and the future basin scenarios can also be studied using the projected
variables from WRF mesoscale model. The limited availability of observation
data in Yodo River basin can be overcome by coupling the WRF mesoscale
model in one-way mode to drive the basin-scale hydrological simulations.

Since observation data were limited to dam data and two observation
stations, the validation is done with these data only. Table 14 shows the
comparison of total annual outflow discharge from five dams in 2006 be-
tween observed data, hydrological model using SDP data, and the coupled
hydrometeorological model described in this chapter. All the dam outflows
are comparatively similar between the hydrological model using SDP data
and the coupled hydrometeorological model. Amagase dam shows slightly
larger overprediction in the coupled model than the hydrological model using
SDP data. These overpredictions can also be observed from some larger peaks
in coupled model output in Fig. 41. The couple hydrometeorological model
is even better at predicting maximum peak discharge of July 2006 at most of
the places than the original hydrological model using SDP data. At Hiyoshi,
Takayama and Nunome dams, the maximum peak discharge in July is better
represented by the coupled hydrometeorological model. But at Hitokura

Table 14: Comparison of annual outflow from dams in 2006 between observed data, hydrological model using SDP data, and coupled hydrometeorological model.

DAM	OUTFLOW $(m^3 \times 10^6)$		
	OBSERVED	SDP	WRF
Amagase	3523.7	3494.2	4348.2
Hiyoshi	360.9	396.2	442.7
Takayama	474.6	474.3	302.8
Nunome	56.5	61.6	41.7
Hitokura	95.2	50.3	29.2

"WRF" column is the result of coupled hydrometeorological model. "SDP" column is the result of hydrological model using SDP observation data (chapter 6).

dam, the maximum peak discharge in July is even more underpredicted by the coupled model than the hydrological model using SDP data. Moreover, May-June peak discharges at Hitokura dam are also more underpredicted by the coupled model than the hydrological model using SDP data.

In the case of two observation stations used in the validation of coupled hydrometeorological model, the maximum peak flow at Hirakata station and the overall annual discharge at Takahama station are predicted by the coupled model without any appreciable deterioration from the performance of the original hydrological model using SDP data (Fig. 42). In fact, the maximum discharge peak in July 2006 at Hirakata tends to be better simulated by the coupled hydrometeorological model.

Generally speaking, the coupled hydrometeorological model tends to reasonably produce good river discharge results that are more or less comparable with the results from the hydrological model using SDP data. We might even see some improvements in the simulation of very high peaks of river discharge by using the coupled hydrometeorological model, when compared with the standalone hydrological model using SDP observation data.
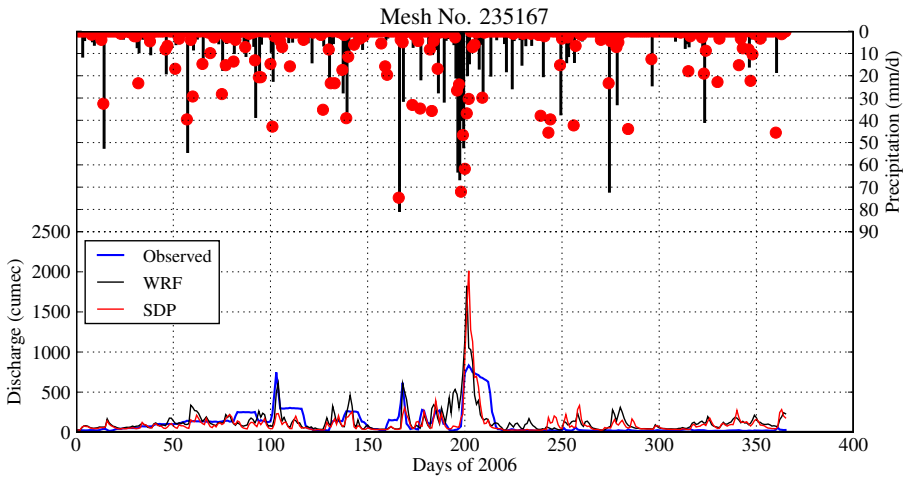
(a) Amagase dam.

(b) Hiyoshi dam.
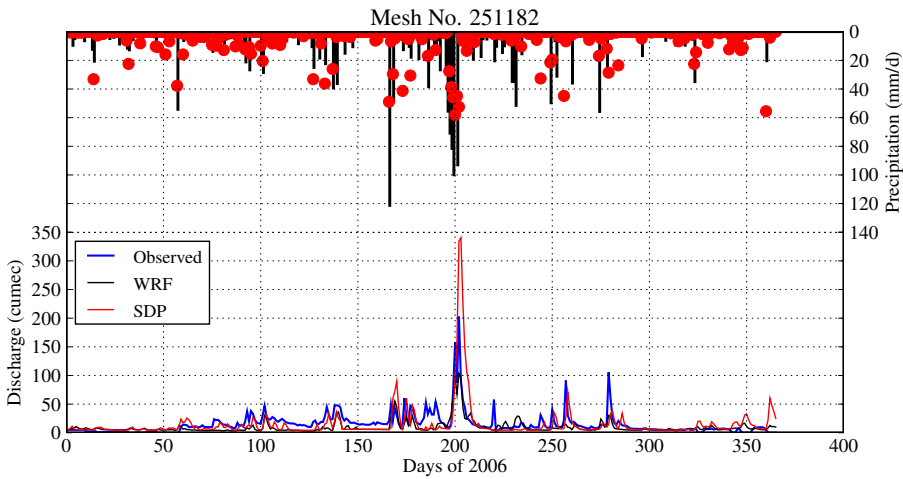
(c) Takayama dam.

Figure 41: Hydrographs for five dams in Yodo River basin using coupled hydromete-
orological model.
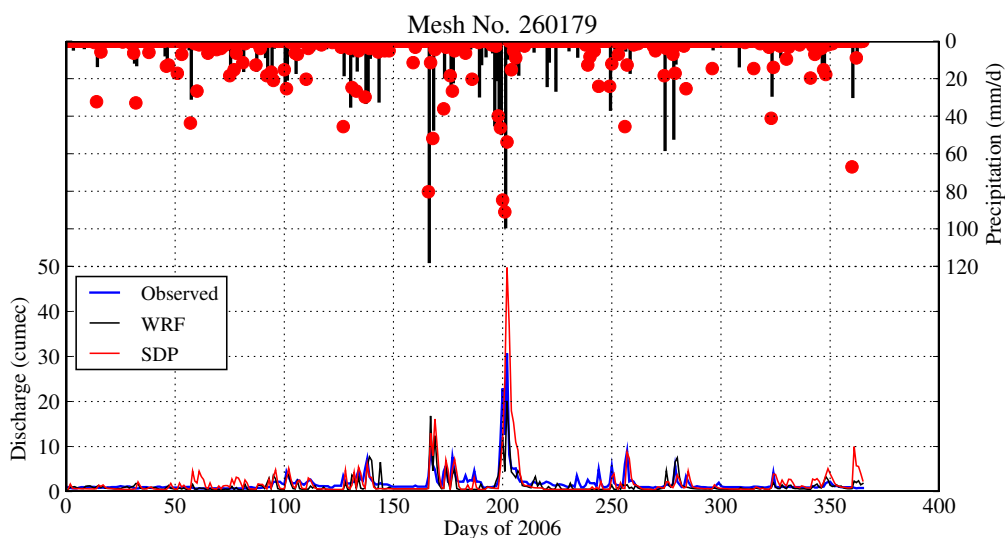
(d) Nunome dam.
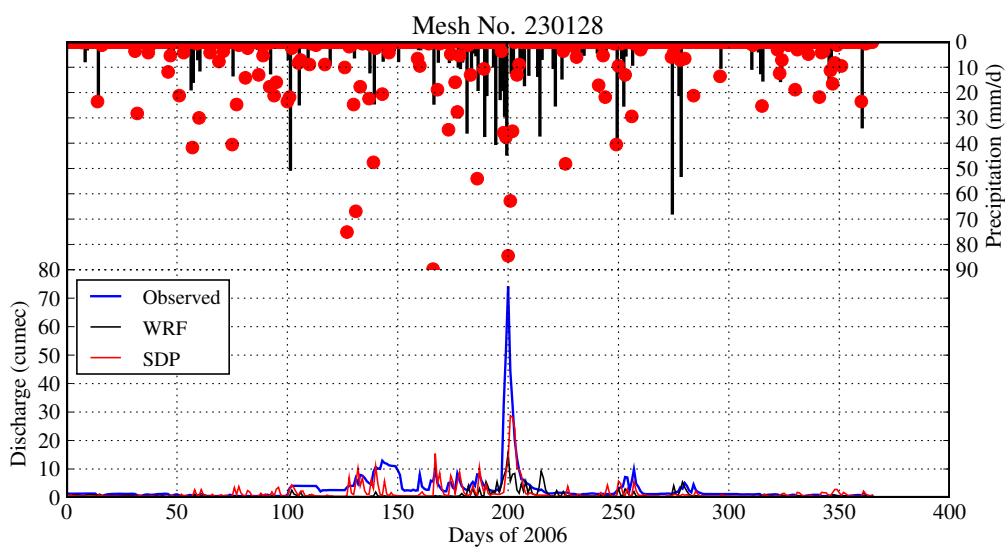
(e) Hitokura dam.

Figure 41: Hydrographs for five dams in Yodo River basin using coupled hydromete-orological model. "WRF" line is the result of coupled hydrometeorological model. "SDP" line is the result of hydrological model using SDP observation data (chapter 6).

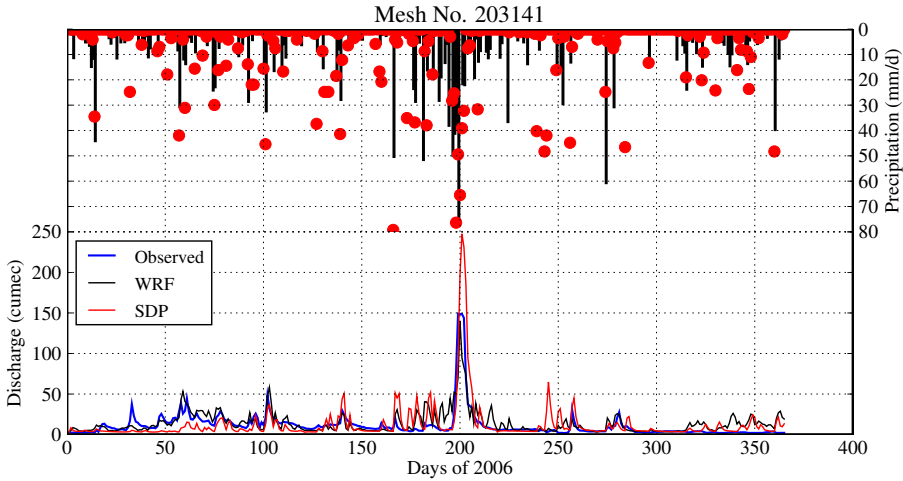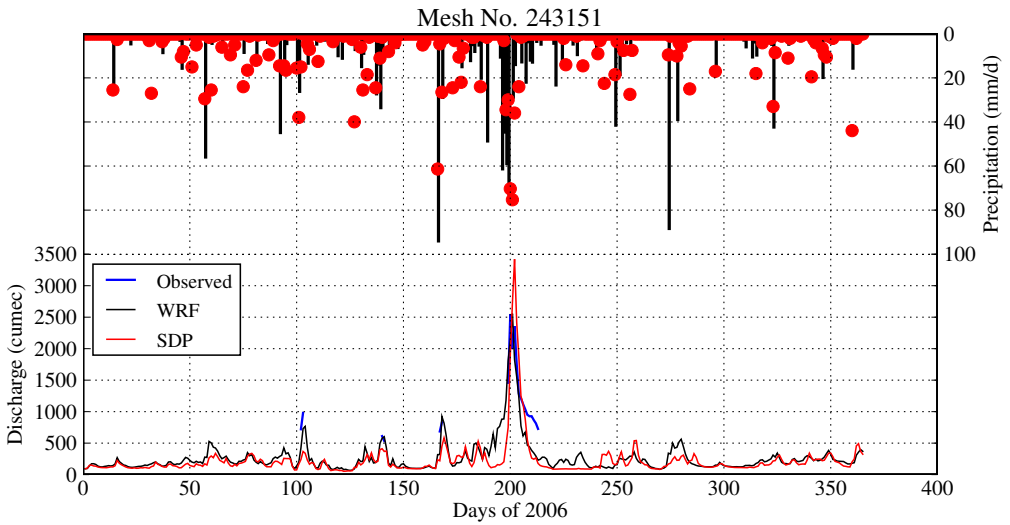(a) Hirakata observation station.
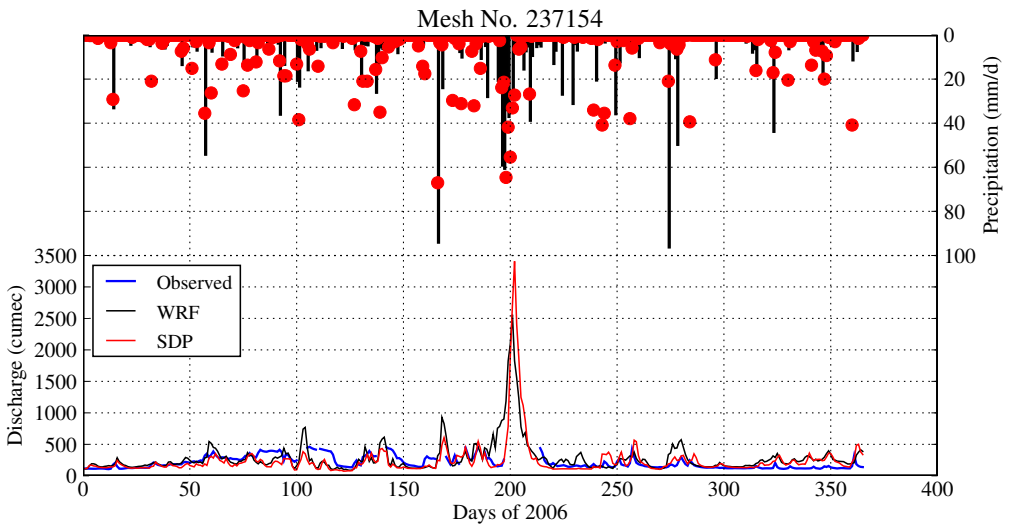
(b) Takahama observation station.

Figure 42: Hydrographs for two observation stations using coupled hydrometeorological model. "WRF" line is the result of coupled hydrometeorological model. "SDP" line is the result of hydrological model using SDP observation data (chapter 6).

7.5 SNOW COVER

Snowfall occurs in the northern parts of Yodo River basin. The northern region of Lake Biwa usually experiences snowfall in the winter season. The snow cover at Yanagase observation station location just on the northern side of Lake Biwa is shown in Fig. 43. Appreciable quantities of snow cover are present in December, January, February and March of 2006. Snow cover started late in December of 2006 in Yanagase and the snow cover peak of nearly 150 mm in December is fairly simulated by the coupled hydrometeorological model in comparison to the hydrological model using SDP observation data. Snow cover in January and February is generally predicted adequately by both models, but with some underpredictions in peak values. In March 2006, the snow cover was largely underpredicted by both coupled hydrometeorological model and hydrological model using SDP observation data. On the whole, snow cover days are adequately predicted by the coupled hydrometeorological model.

7.6 CONCLUSION

In this chapter, the hydrological modeling approach of chapter 6 was improved upon by introducing a one-way model coupling technique, in which WRF mesoscale model was coupled with distributed hydrological model. The coupled hydrometeorological model has two-fold advantage over the original hydrological model, which uses observation data as atmospheric forcings.

Firstly, the original hydrological model uses SDP observation station data that is constructed by Thiessen polygon method from 10 observation stations. Regional and mesoscale phenomena occurring in the basin cannot be realistically represented by these limited observed data. In comparison, mesoscale meteorological models are capable of simulating mesoscale and regional physical phenomena at higher spatio-temporal resolutions and we do not have to rely on only the statistical downscaling of meteorological variables to the very fine spatial resolution required by hydrological models. Thus, dynamic downscaling of meteorological variables into atmospheric forcing for hydrological model is made possible by coupling the nested mesoscale meteorological model with the distributed hydrological model.
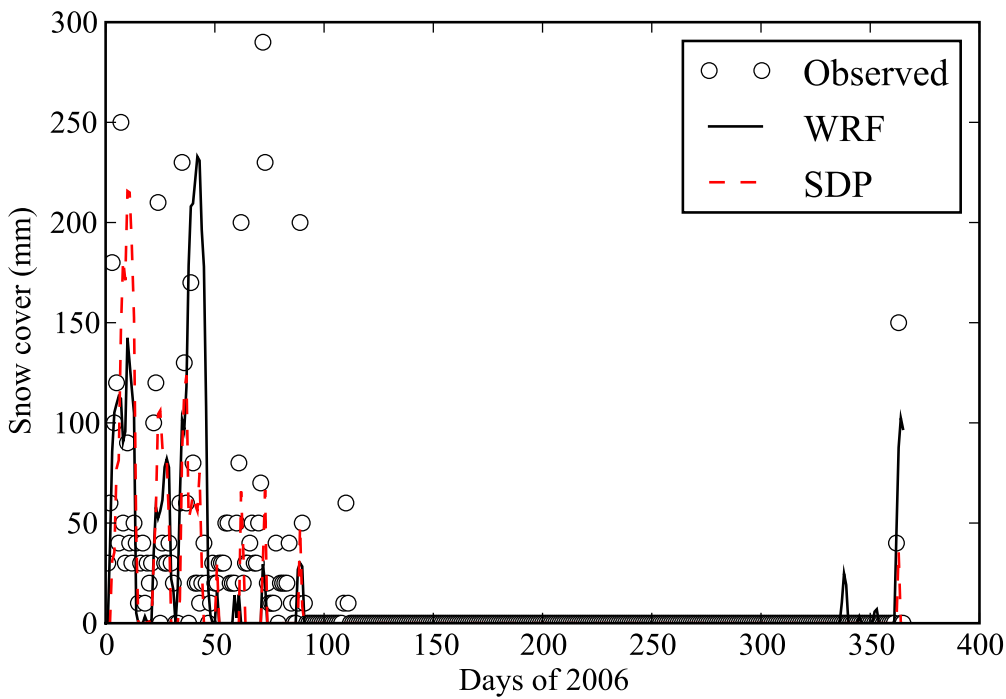
Figure 43: Snow cover for Yanagase observation station. "WRF" line is the result of coupled hydrometeorological model. "SDP" line is the result of hydrological model using SDP observation data (chapter 6).

Secondly, the prediction and projection of the water resources at basin-scale is made possible by coupling mesoscale meteorological model with the distributed hydrological model. The atmospheric forcings in future climate change scenarios can be passed to the distributed hydrological model by using the coupled hydrometeorological model.

Using the limited observation data available for river discharge and dam outflows, the accuracy and performance of coupled hydrometeorological model was sufficiently validated against the observed data containing river discharge and snow cover. From the results, it can be concluded that outflows from regulated reservoirs and river discharge at observation stations are reasonably predicted by the coupled hydrometeorological model with adequate representation of the peak flows in the hydrographs. The application of the coupled hydrometeorological model to study the effects of climate change on water resources of Yodo River basin will be presented in chapter 8.

EFFECT OF FUTURE CLIMATE CHANGE ON HYDROMETEOROLOGY OF YODO RIVER BASIN

8.1 INTRODUCTION

The coupled hydrometeorological model developed and validated in chapter 7 is applied in the study of the future climate change scenario related to water resources in Yodo River basin.

Present and future environmental scenario of Yodo River basin is formulated based on Intergovernmental Panel on Climate Change (IPCC) climate change scenarios. The future scenario is simulated by dynamically downscaling the global climate model output using a regional or mesoscale model. In this chapter, Community Climate System Model (CCSM) global results for IPCC future scenario are used as initial and boundary conditions for WRF mesoscale model used in the coupled hydrometeorological modeling of Yodo River basin.

The current water resource scenario of Yodo River basin is compared with the future water resource scenario that could occur in the future if the climate changes according to the emission scenarios developed by IPCC. Out of the several future emission scenarios proposed by Nakicenovic and Swart (2000), the average climate scenario of A1B SRES is studied at Yodo River basin. Then, assessment of water resource and its future scenario in Yodo River basin is carried out with specific discussions on the change in air temperature, basin precipitation, evapotranspiration, snow cover, and snow melting. Similarly, the change in the frequency of occurrence of heavy precipitation in the future, change in the intensity of precipitation that increase the risk of flooding, and the change in spells of dry periods that increase the risks of drought are also discussed. Finally, the changes in river discharge and reservoir outflows in the future climate change scenario in comparison to present observed water flows are discussed.

8.2   PRESENT AND FUTURE SCENARIOS OF YODO RIVER BASIN

8.2.1   *Present scenario*

Generally, a multi-year long-term simulation is carried out to estimate the effect of climate change on the atmospheric and terrestrial environment. The large-scale variabilities in atmosphere and ocean are necessary to be captured by the atmospheric and ocean models using decadal time scales. Such long-term simulations had been largely confined to supercomputers in past decades. But recently, development of cluster of workstations containing several computing processors capable of parallel computations has provided a practical solution to shorten the simulation time using more accessible and cheaper computational resources. With the increase in the speed of computing, the scope for high-resolution regional simulation has also increased. In this study, a small Linux cluster containing 27 Pentium-IV processors was used and the limited computational power meant that the actual simulation period had to be compromised to a short and manageable period. For assessing and comparing the present water resource of Yodo River basin with the future scenario, present scenario was chosen as the year 2006. The availability of historical records of hydrometeorological data in Yodo River basin is useful in deciding the year for simulating the present scenario. Two very important hydrometeorological variables, near-surface air temperature (Fig. 44) and precipitation (Fig. 45) were analyzed for the period of 1975−2008 at three different observation stations in Yodo River basin. Both temperature and precipitation historical trend shows that the year 2006 is not very far from the trendline with approximately 0.3 K far from the temperature trendlines and approximately 200 mm far from the precipitation trendlines. Thus, year 2006 can safely be considered as a normal year without any unusual deviations from the past trend of air temperature and precipitation. Henceforth, year 2006 will be considered as representative of the present-day environmental scenario.

8.2.2   *Future scenario*

IPCC has prepared a report called "Special Report on Emissions Scenarios (SRES)" containing various future emissions scenarios in order to project the
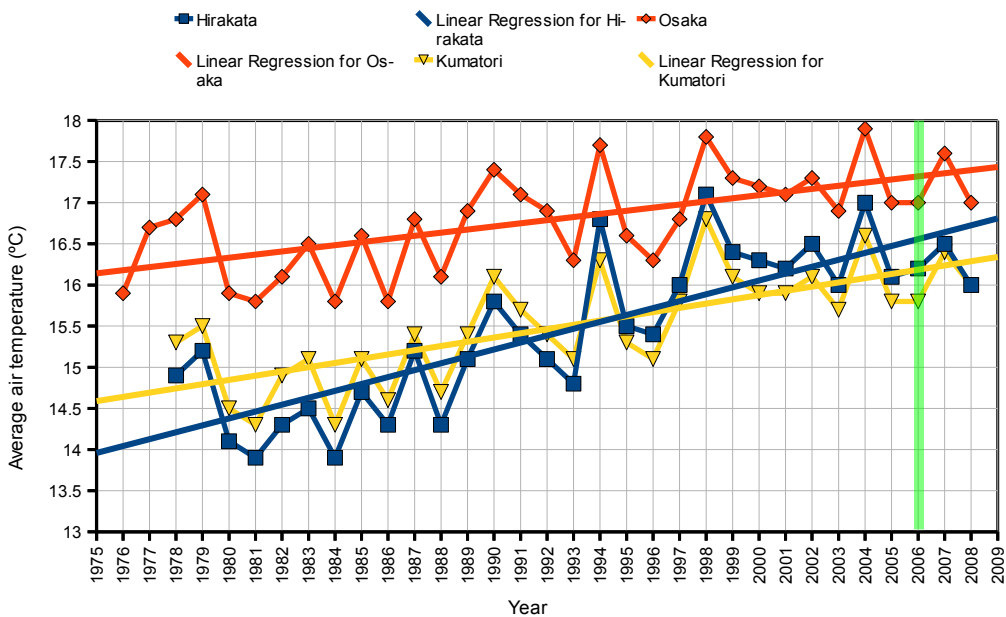
Figure 44: Past trend of average near-surface air temperature in Hirakata, Osaka and Kumatori.
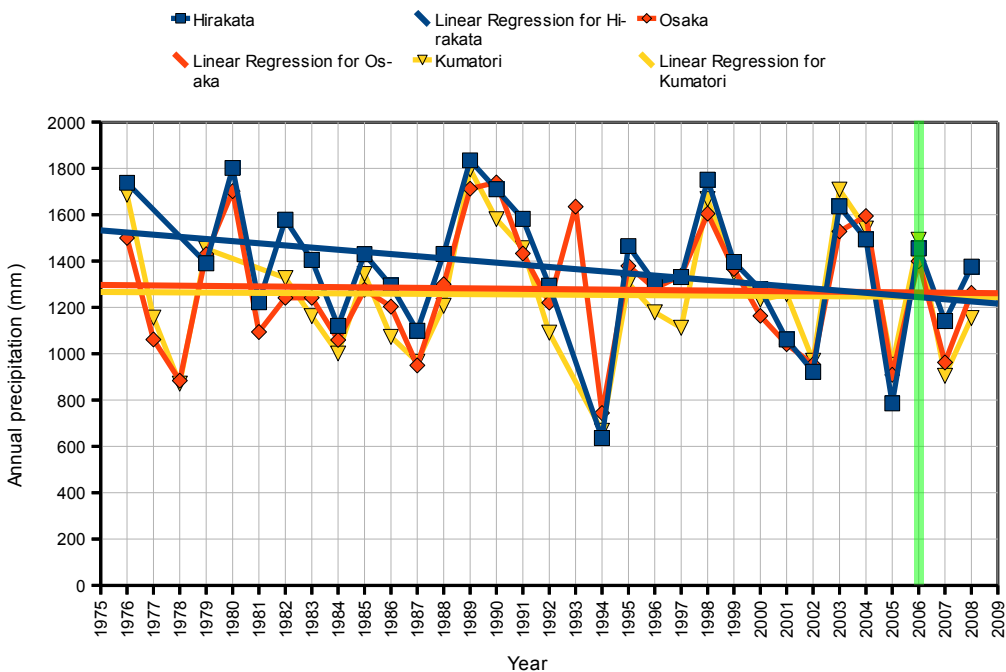

Figure 45: Past trend of annual precipitation in Hirakata, Osaka and Kumatori.

future climate and investigate the future climate change by global circulation models (Nakicenovic and Swart, 2000). Different assumptions have been made regarding future greenhouse gas emissions, future technological development, future economic development and fuel consumption pattern. Four main clusters of qualitative storylines based on the future trends in population, wealth, technology, and energy use are known as A1, A2, B1 and B2 SRES scenarios. These scenarios are assumed to be equally valid without any probability allocated for their occurrences. A1 storyline proposes a future of the 21st century with rapid economic growth, population increasing till 2050 and then declining, and rapid increase in the use of efficient technologies. There are three groups in A1 storyline, called A1FI, A1T and A1B, which put technological emphasis on fossil fuel energy sources, non-fossil energy sources and overall balanced energy sources respectively. A2 storyline describes a heterogeneous world with regionally oriented economic growth and slow technological changes. B1 storyline proposes a more convergent world, which is oriented towards service and information economic changes. B2 storyline describes the future oriented towards more local and regional approach in tackling economic, social and environmental problems. Out of these IPCC SRES storyline scenarios, only A1B scenario is studied in this chapter. A1B is chosen because it is an average climate scenario with balanced development of energy technologies. Five-year period in the future (2050−2054) is chosen as simulation period for the future scenario. Though a much longer time period is desirable than 5-year period, the high computational cost of mesoscale meteorological modeling has limited the time period for the current study. Though the simulation of 5-year period may not fully capture long-term variabilities in climate variables, the results from this study will prove to be a useful guide to the full implementation of coupled hydrometeorological modeling approach to assess the water resources of Yodo River basin.

8.3   INPUT DATA

US NCEP (National Centers for Environmental Prediction) FNL (Final) Operational Global Analysis data was used to generate initial and boundary conditions for WRF in the coupled hydrometeorological modeling of present scenario.

To study the effect of climate change in future scenario, we need to model the future atmospheric conditions by projecting environmental, social, economic and technological scenarios in the future. At the global scale, such climatic projections are developed by using General Circulation Models (GCMs), which are driven by climate conditions based on future scenarios. Many GCMs are currently available, such as Hadley Center Climate Model (HadCM3), ECHAM5, Geophysical Fluid Dynamics Laboratory Coupled Model (GFDL CM2.X), Parallel Climate Model (PCM), Community Climate System Model and so on.

CCSM3 is one of the complex AOGCMs (Atmosphere-Ocean GCMs), in which atmospheric model, land surface model, ocean model and sea-ice model are coupled by a coupler program to simulate the climate of earth (Vertenstein et al., 2004). It contains NCAR Community Atmosphere Model version 3 (CAM3) as the atmospheric general circulation model, Community Land Model version 3 (CLM3) as the land surface model, and modified Parallel Ocean Program (POP) as ocean model. The past, present and future scenarios of the earth's climate can be simulated by CCSM coupling all these sub-models that can also be run standalone.

CCSM3 supports many spatial resolutions, among which the atmosphere and land models can have T85 (256 longitudes, 128 latitudes), T42 (128 longitudes, 64 latitudes), T31 (96 longitudes, 48 latitudes) and T62 (192 longitudes, 94 latitudes) Gaussian grids, and 2x2.5 type C grid (144 longitudes, 91 latitudes); and, ocean and ice models can have gx1v3 (320 longitudes, 384 latitudes) and gx3v5 (100 longitudes, 116 latitudes).

Output data from CCSM3 are available at http://www.earthsystemgrid. org/ for multi-century simulations that were created by Climate and Global Dynamics Division, National Center for Atmospheric Research, University Corporation for Atmospheric Research, and submitted to IPCC AR4 report. A1B scenario output from CCSM was used to provide future initial and boundary conditions of the WRF mesoscale meteorological model.

8.4 DOWNSCALING CCSM DATA USING WRF MODEL

CCSM3 output data, published by NCAR, was collected via the Earth System Grid (ESG, http://www.earthsystemgrid.org/) data repository. Output data

generated by CCSM3 consists of atmosphere, ocean, ice and land components. CCSM3 atmosphere and land models share the identical horizontal grid called T85, which is a 256 by 128 regular longitude/latitude global horizontal grid (approximately 1.4 degree resolution). CCSM3 SRES A1B fully coupled run consists of 100 years (2000 − 2099) of output data. The atmosphere model in CCSM3 has 26 vertical hybrid sigma pressure levels and 6-hourly atmospheric output data was available for the entire time period.

The atmospheric model data (CAM model data) in hybrid sigma coordinate system were interpolated to the WRF Preprocessing System (WPS) pressure levels of 10, 20, 30, 50, 70, 100, 150, 200, 250, 300, 350, 400, 450, 500, 550, 600, 650, 700, 750, 800, 850, 900, 925, 950, 975 and 1000 hPa using Fortran programs. The NetCDF binary format data of CCSM3 were directly converted to the WPS intermediate binary files. The 3D and 2D variables shown in Table 15 are necessary to be converted from CCSM NetCDF format to the WPS intermediate format variables.

Relative humidity

Relative humidity was not directly available in the A1B scenario output from CCSM. To derive relative humidity from the existing output variables in CCSM, specific humidity from CCSM, Q, was converted to relative humidity by first converting specific heat to water vapor mixing ratio, q, using the relation

$$q = \frac{Q}{1-Q} \tag{8.1}$$

Then, using water vapor mixing ratio and surface pressure in eq. 7.1, water vapor pressure was calculated. Finally, relative humidity was calculated using eq. 8.2.

$$RH = 100 \frac{e\,(P - e_s)}{e_s\,(P - e)} \tag{8.2}$$

Table 15: WRF WPS input variables and corresponding CCSM output variables.

CCSM VARIABLES		WPS VARIABLES	
T	Temperature	TT	Temperature
Q	Specific humidity	RH	Relative humidity
U	U-component of hor. wind	UU	U-component of hor. wind
V	V-component of hor. wind	VV	V-component of hor. wind
Z_3	Geopotential height	GHT	Geopotential height
PS	Surface pressure	PSFC	Surface pressure
PSL	Mean sea level pressure	PMSL	Mean sea level pressure
LANDFRAC	Fraction of surface area covered by land	LANDSEA	Land/sea flag
TS	Surface temperature	SKINTEMP/ SST	Skin temperature/sea surface temperature
H_2OSOI	Soil moisture		Soil moisture
TSOI	Soil temperature		Soil temperature
SNOWHLND	Water equivalent of accumulated snow depth	SNOW	Water equivalent of accumulated snow depth

RH Relative humidity

e Water vapor pressure (calculated from eq. 7.1)

e_s Saturated water vapor pressure

P Pressure

q Water vapor mixing ratio

Saturated water vapor pressure was calculated according to Bolton (1980) using eq. 8.3.

$$e_s = 6.112 \exp\left(17.67\, \frac{T - 273.15}{T - 29.65}\right) \tag{8.3}$$

where, T is air temperature.

Soil data for Noah Land surface model in WRF

The land surface model of CCSM contains 10 layers of soil having 0.7100635, 2.7925, 6.225858, 11.88651, 21.21934, 36.60658, 61.97585, 103.8027, 172.7635, and 286.4607 centimeter depths respectively. These were converted to 4 soil layers of Noah LSM in WRF (0-10 cm, 10-40 cm, 40-100 cm, and 100-200 cm soil layers) using NCL (NCAR command language, `http://www.ncl.ucar.edu/`). The monthly average soil data from CLM3 were interpolated to 6-hourly data required by WRF.

8.5   COUPLED HYDROMETEOROLOGICAL MODELING FOR PRESENT AND FUTURE SCENARIOS

US NCEP FNL analysis data was used as initial and boundary conditions of WRF in the coupled hydrometeorological modeling of present scenario. Similarly, CCSM3 A1B SRES global output data were used as initial and boundary conditions of WRF for coupled modeling of future scenario of Yodo River basin. The coupled hydrometeorological modeling approach described in chapter 7 is applied for both the present and future scenarios of Yodo River basin. The present scenario was simulated for the year 2006 and the future scenario was simulated for the period of 2050−2054. In both of the scenarios,

the WRF model is initialized only once in the beginning of the simulation. The alternate method of periodically initializing the mesoscale model with the GCM data was not used because of short simulation time period. The 5-year simulation of future scenario was done in a batch of five simulations, in which the simulation was restarted after every 1-year simulation.

8.6 FUTURE WATER RESOURCE ASSESSMENT OF YODO RIVER BASIN

8.6.1 *Change in near-surface air temperature*

The near-surface air temperature results from the coupled hydrometeorological simulation of present and future scenarios of Yodo River basin show an overall rise in air temperature in the future (Fig. 46). Winter, Spring, Summer and Autumn seasons in the future scenario show rise in air temperatures by approximately 1.7 K, 1.3 K, 0.9 K and 0.4 K respectively. The increase in the air temperature is mostly attributed as the effect of global warming and climate change (IPCC, 2007b). Table 16 shows the monthly average air temperature for present and future scenarios. The annual average of the increase in temperature in future is found to be approximately 1 K with largest increase in the winter season. The general trend of warming can also be observed from the monthly average temperature of Yodo River basin with some decrease in air temperature in some months. Though a longer time period than the currently used future scenario period is needed to observe the long-term trend in future air temperature, the results shown here do indicate the agreement between the simulated air temperature and the rising temperature trend generally observed in projected temperatures of Japan (Fig. 4).

8.6.2 *Change in evapotranspiration*

The rate of evapotranspiration in the Yodo River basin can be expected to rise slightly during the winter and spring seasons (Fig. 47). Though many factors can contribute to the increase in evapotranspiration like effect of increase in CO_2 on plants, surface wind and energy, the major contribution comes from the increase in precipitation in land (Bates et al., 2008). It has been

Table 16: Monthly average air temperature for present and future scenarios in Yodo River basin.

|	2006	2050	2051	2052	2053	2054	AVERAGE OF 2050-54
Jan	276.4	280.4	279.4	280.1	277.7	279.7	279.45
Feb	277.9	280.2	279.5	278.0	279.3	278.3	279.1
Mar	280.0	281.1	280.5	281.3	281.2	281.9	281.2
Apr	284.7	285.8	285.5	287.1	286.9	285.1	286.1
May	290.1	292.3	291.1	290.9	291.8	290.9	291.4
Jun	293.8	296.8	294.9	297.1	295.0	296.8	296.1
Jul	297.7	297.9	298.6	298.3	298.2	298.8	298.4
Aug	299.3	299.6	299.5	298.8	298.2	299.5	299.1
Sep	295.1	296.1	297.1	297.4	297.2	297.7	297.1
Oct	290.8	290.1	288.7	291.6	291.6	291.0	290.6
Nov	285.6	284.3	285.1	284.6	286.0	284.8	284.9
Dec	280.3	281.6	280.2	280.4	281.5	281.8	281.1
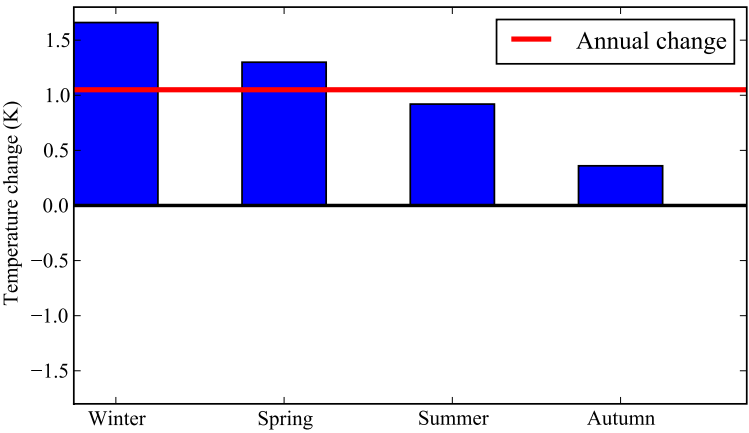
Figure 46: Change in seasonal and annual average air temperature in A1B future scenario compared to present scenario in Yodo River basin. Present scenario temperature is for 2006 and future scenario temperature is average of 2050 to 2054.
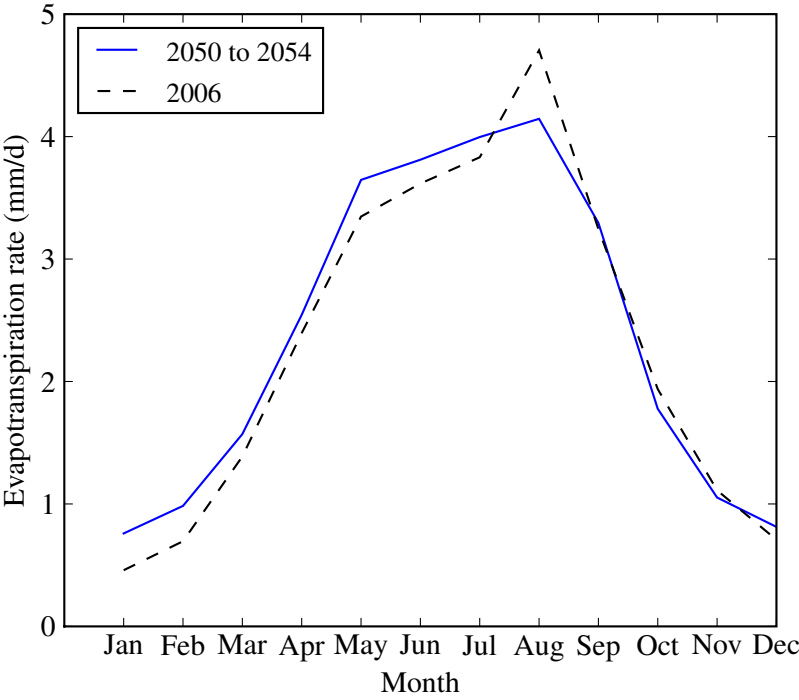
Figure 47: Comparison of monthly evapotranspiration rate between present and future scenarios in Yodo River basin.

postulated that the increasing precipitation on the land surface increases the land surface moisture availability and thus the rate of evapotranspiration is likely to increase. In Yodo River basin also, the overall increase in land precipitation during the period of January to June in future scenario compared to the present scenario (Fig. 52b) could have contributed towards the increase in evapotranspiration. Moreover, temperature rise in future scenario (Fig. 46) could have increased moisture demand in the atmosphere and subsequently evapotranspiration rate might have increased compared to the current scenario. A decrease in evapotranspiration in the future scenario is evident in August, October and November, which might have been mainly caused by some decrease in the average air temperature in these three months (Table 16).

8.6.3 *Change in snow cover and snow melting*

Snow cover is globally affected by combined effect of change in air temperature and precipitation, and snow depth is inversely proportional to air temperature

at places having seasonal snow cover (Bates et al., 2008). Due to global warming and the ensuing increase in air temperature, snow cover is expected to decrease in most parts of the world. This decrease in snow depth is evident from the decreasing trend of snow depth in the 21st century obtained from CCSM3 results provided for IPCC AR4 report (Fig. 48). In the future scenario simulation period of 2050 to 2054 in the current study, the global (60-90N) snow depth is projected to decrease from approximately 9.5 cm in 2050 to 9.2 cm in 2052 and it is again projected to rise to around 9.5 cm by 2055. Thus, significant variations in snow depth occur in a 5-year time even when the long-term trend is decreasing. Fig. 49 compares the snow depth in Yodo River basin between the current and future scenarios. Snow cover is seasonally available mostly in the northern part of Yodo River basin. So the wintertime snow depth in Yodo River basin is expected to change in the future (Fig. 49). Fig. 49a shows that the monthly average snow depth of 2050−2052 will decrease by nearly 2 cm in January and February. This decrease is most probably due to expected increase in winter air temperature during this period (Table 16). Some increase in snow depth in March and April has been projected, which may be partially attributed to some increase in precipitation in March and April of 2051 and 2052 compared to 2006. Year 2053 and 2054 have not been included in Fig. 49a because snow depth in 2053 and 2054 were relatively higher than other years (Fig. 49b). Especially the snow depth of the year 2053 seems to be very high with maximum snow depth of approximately 25 cm in February, and this increase may be partially attributed to substantial increase in precipitation in January, February and March of 2053. Though the scenario simulation period is only 5 years, the global trend of decrease of snow cover from 2050 to 2052 and then increase from 2052 to 2055 is found to be broadly applicable to Yodo River basin in 2050−2054 period.

Knowing that snow cover decreases in January and February of 2050−2052 period (Fig. 49a), the runoff from snow melting also is expected to decrease in the period of January to March due to this decrease in snow cover (Fig. 50). Consequently, the water supply from snow melting runoff may possibly be affected during wintertime in Yodo River basin.
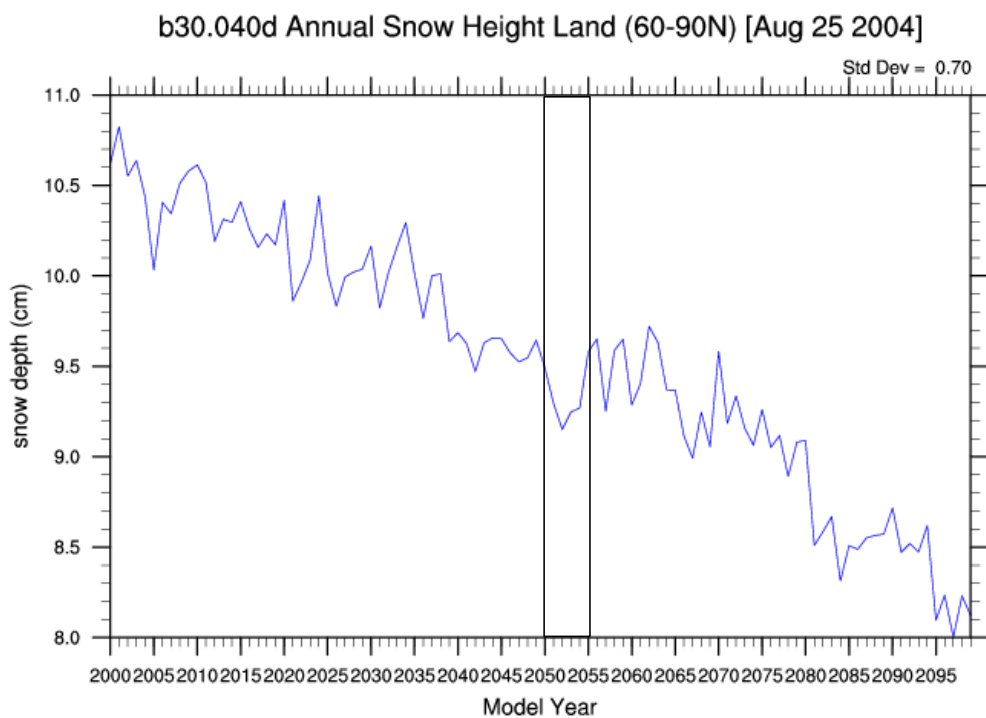
Figure 48: Snow depth in A1B scenario from CCSM3 results provided for IPCC AR4
        report.
(Source: NCAR, http://www.cgd.ucar.edu/cms/stevens/ccsm3/b30.040d/
b30.040d.nh.snowhlnd.png)
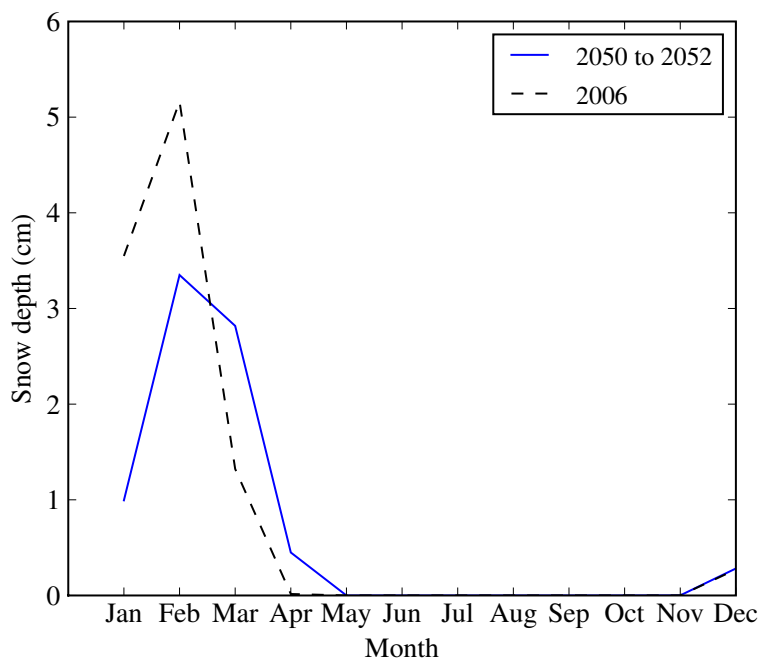
(a) Monthly average snow depth.
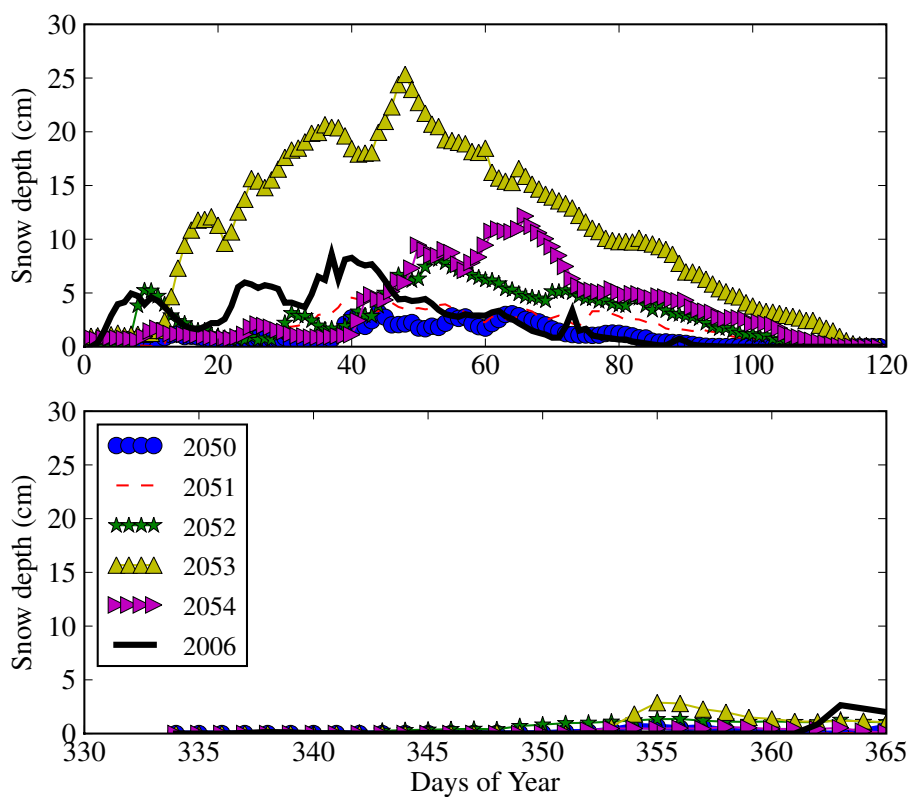
(b) Daily snow depth.

Figure 49: Comparison of snow depth between present and future scenarios in Yodo River basin.
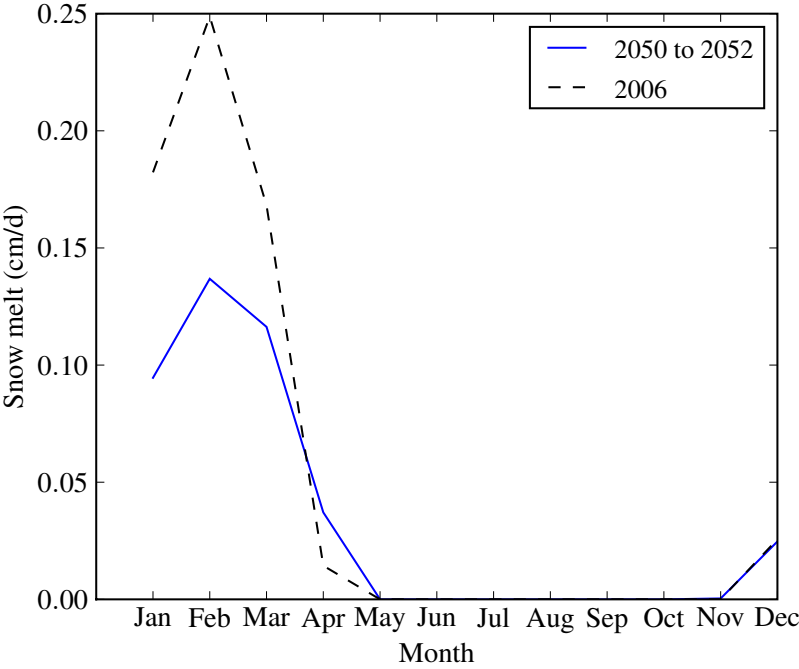
Figure 50: Comparison of monthly snow melting runoff between present and future
scenarios in Yodo River basin.

8.6.4 *Change in basin precipitation*

Comparing the precipitation from CCSM (a single mesh covering Yodo River
basin) and WRF with the observed Radar GPV precipitation in Yodo River
basin, CCSM seems to severely underpredict the high precipitations in the
rainy month of July 2006 (Fig. 51). Similarly, CCSM substantially under-
predicts precipitation in several other months. It clearly indicates that GCM
precipitation is unreliable in predicting the basin-scale precipitation, and hence,
regional and mesoscale prediction of precipitation using models such as WRF
is undeniably essential for basin-scale hydrometeorological modeling.

Annual precipitation in Yodo River basin is projected to be nearly same or
slightly less in 2050−2054 period compared to the present scenario (Fig. 52b),
which largely agrees with the historical trend of precipitation in Japan (Fig. 2).
In 2050−2054 period, only the year 2052 shows a substantial decrease in annual
precipitation, and this decrease is mainly caused by very low precipitation
during rainy season of June and July (Fig. 52b). The low-precipitation period
of 2052 during rainy season is also indicated by the CCSM precipitation results
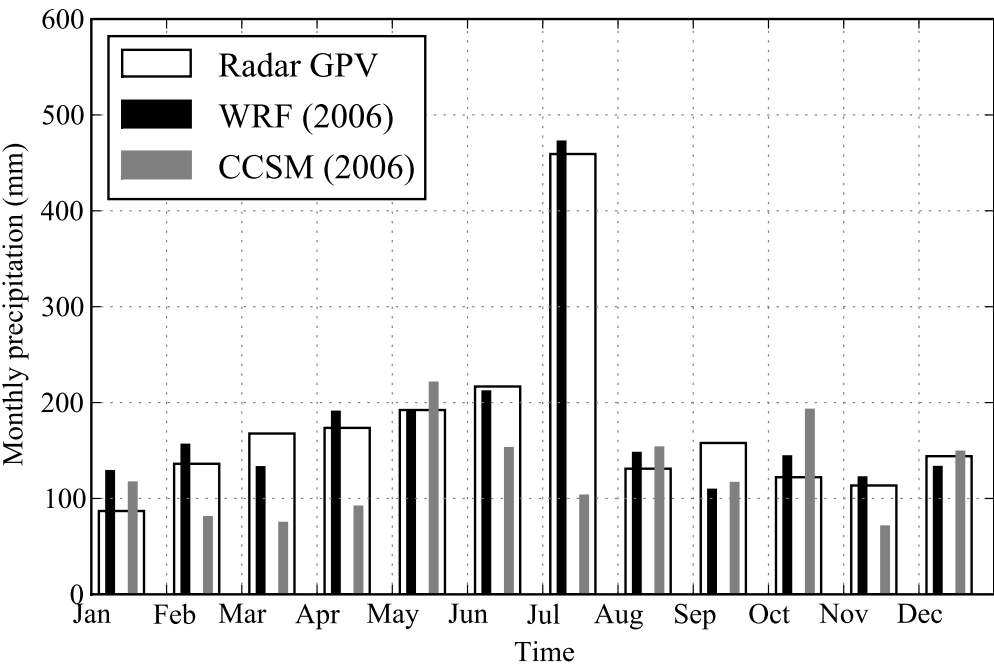
Figure 51: Comparison of CCSM and WRF precipitation with Radar GPV observation data in 2006 for Yodo River basin. CCSM data is from a single mesh that covers Yodo River basin.

(Fig. 52a). The fact that low precipitation in rainy season of 2052 is shown by both CCSM and WRF model suggests a large-scale climate variability affecting the precipitation events in 2052. The regional climate may vary in magnitude and phase due to variability of large-scale atmospheric circulations and teleconnections such as El Niño−Southern Oscillation (ENSO) and Pacific Decadal Oscillation (PDO) that vary on decadal scale (Bates et al., 2008). Broadly speaking, precipitation amount in Yodo River basin will change in the future and the large-scale variabilities as well as regional and local climate can likely contribute to this change.

8.6.5   *Change in precipitation intensity*

Extreme precipitation events are expected to rise with global warming due to increasing greenhouse gases and consequently the risk of flooding and drought are also expected to increase (Bates et al., 2008). The intense precipitations may be concentrated in short time periods and long dry periods may be observed in
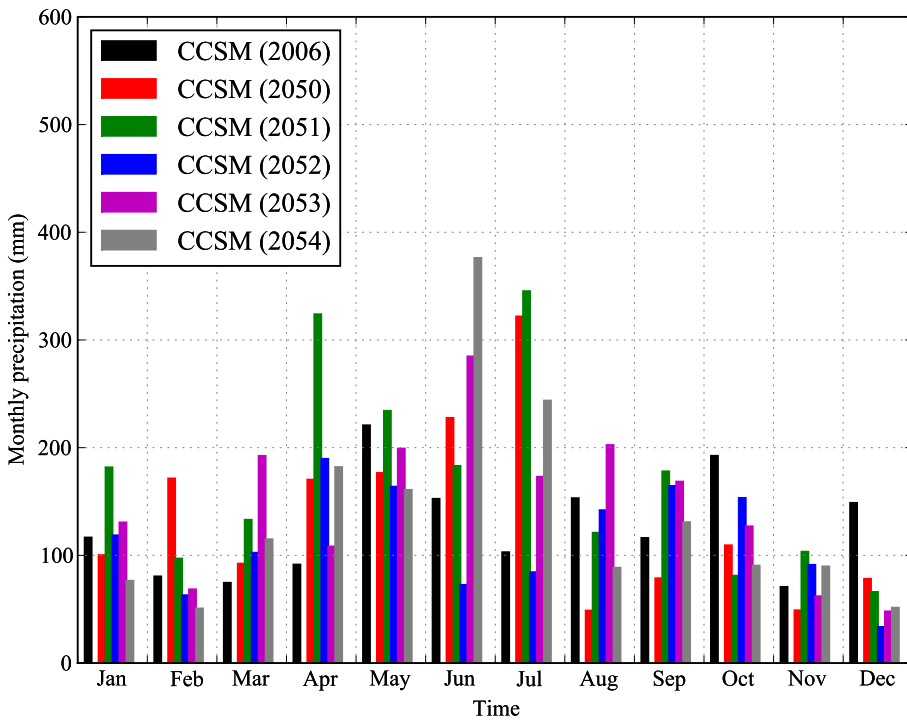
(a) Monthly precipitation at a single grid of CCSM covering Yodo River basin.
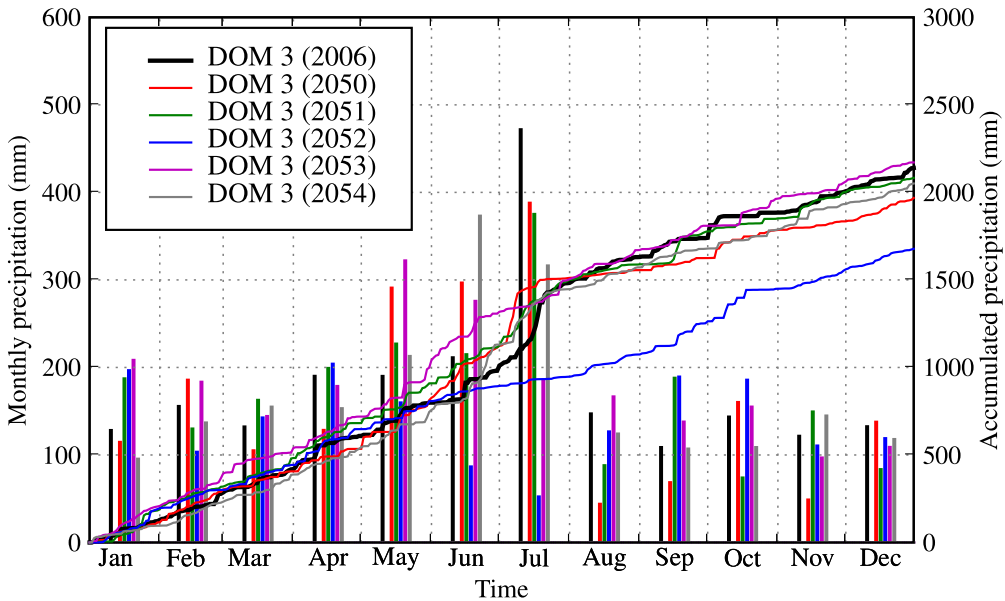
(b) Accumulated and monthly precipitation from WRF for total Yodo River basin.

Figure 52: Comparison of accumulated and monthly precipitation between present and future scenarios in Yodo River basin.
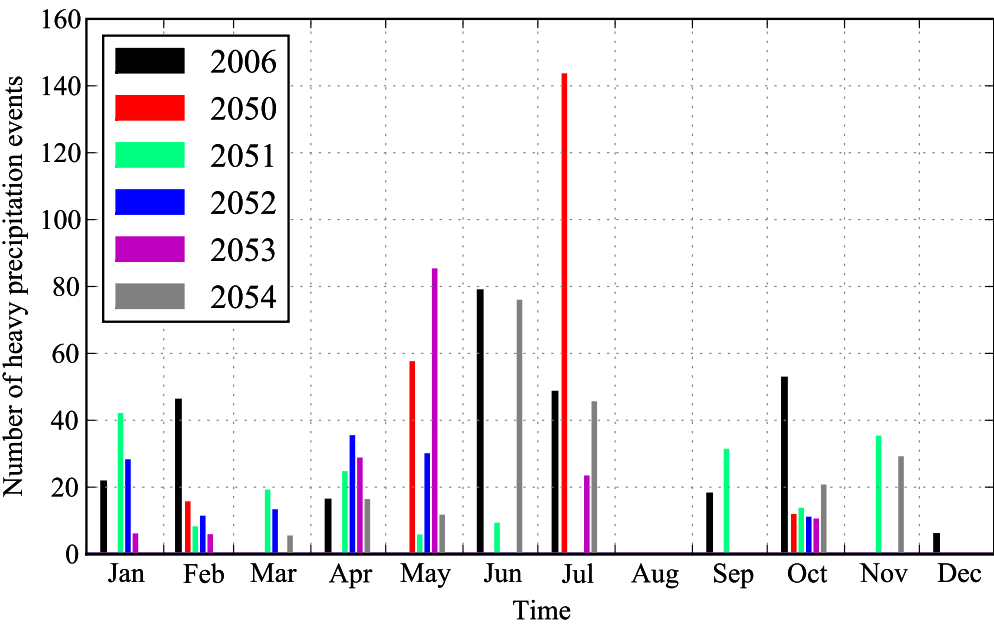
Figure 53: Comparison of heavy precipitation events over total grid mesh between present and future scenarios in Yodo River basin. Heavy precipitation events are calculated as days having precipitation greater than 5 mm.

between. In Yodo River basin, the number of occurrence of heavy precipitation events (calculated as days having precipitation greater than 5 mm) are shown in Fig. 53. Largest peak of heavy precipitation occurs in July 2050. Thus, the risk of flooding is likely to persist if not decrease in the future rainy season. In May, all the years in the future scenario show heavy precipitation events in contrast to none such events in present scenario of 2006. Thus the flooding risk might possibly shift more towards earlier time period than the present-day rainy season.

To check the spatial distribution of extreme precipitation, precipitation intensity was calculated as annual total precipitation divided by the number of wet days, where days having more than 10 mm are considered as wet days (Bates et al., 2008). Fig. 54 shows the spatial map of the difference of precipitation intensities between the present and future scenarios. Though the overall spatial distribution of precipitation intensity shows variations throughout the five years of future scenario, some generally high-intensity areas can be identified in the south-eastern and western region of Yodo River basin.

Figure 54: Difference of precipitation intensity between future (2050-2054) and present (2006) in Yodo River basin. The thick basin boundaries are same as in Fig. 20.

8.6.6   *Change in dry days*

Similar to the precipitation intensity map in the previous subsection, dry day patterns in Yodo River basin were calculated as annual maximum number of consecutive dry days, where days having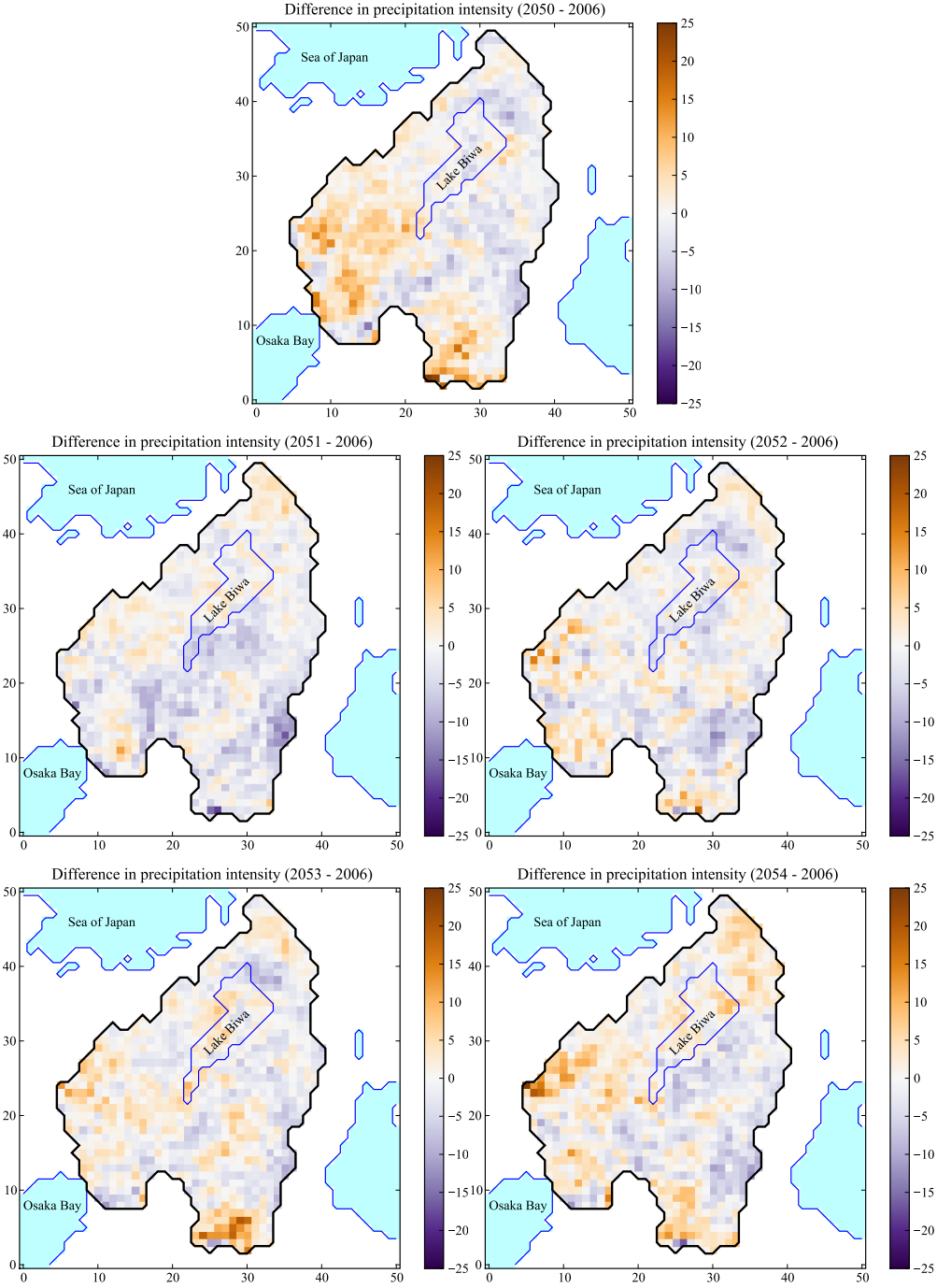 precipitation less than 0.5 mm are considered as dry days (Bates et al., 2008). Fig. 55 shows the difference of dry days spatial pattern in the Yodo River basin between the present and future scenarios. The south-eastern area of Yodo River basin is generally having more dry day periods in all the future scenario years. One important conclusion from the study of extreme precipitation events in Yodo River basin can be the increase in heavy precipitation event as well as dry periods in the lowermost eastern regions of Yodo River basin. The implication of such extreme precipitation events may be increase in risk of floods and droughts in the south-eastern Yodo River basin.

8.6.7   *Change in river discharge*

River discharge are mainly affected by magnitude and temporal distribution of precipitation in the future climate change scenarios (Bates et al., 2008). Water flows in rivers and lakes in Yodo River basin are affected by the network of reservoirs to control and distribute water resources in the basin area. Fig. 56 shows the change in water flow due to climate change in the future. River discharge in 2006 has been used as the present-day scenario for assessment of change in discharge from rivers. In all the discharge data at dam and observation stations presented in Fig. 56, maximum peak discharge has decreased in the future scenario when compared to the modeled present-day scenario. Moreover, the peak discharge seems to have shifted to earlier time periods than the current peak discharges. At Amagase dam, the outflow rate has increased just before the usual rainy season of June and July in the future A1B scenario. Consequently, river discharges during January-June period has also increased at Hirakata and Takahama observation stations. It also implies that the downstream region of Osaka might be overwhelmingly affected by the discharge from Amagase, which in turn receives water flow from the Lake Biwa sub-basin. The annual discharges for all the sites were found to decrease in the future except at Amagase (Table 17). All in all, river discharges
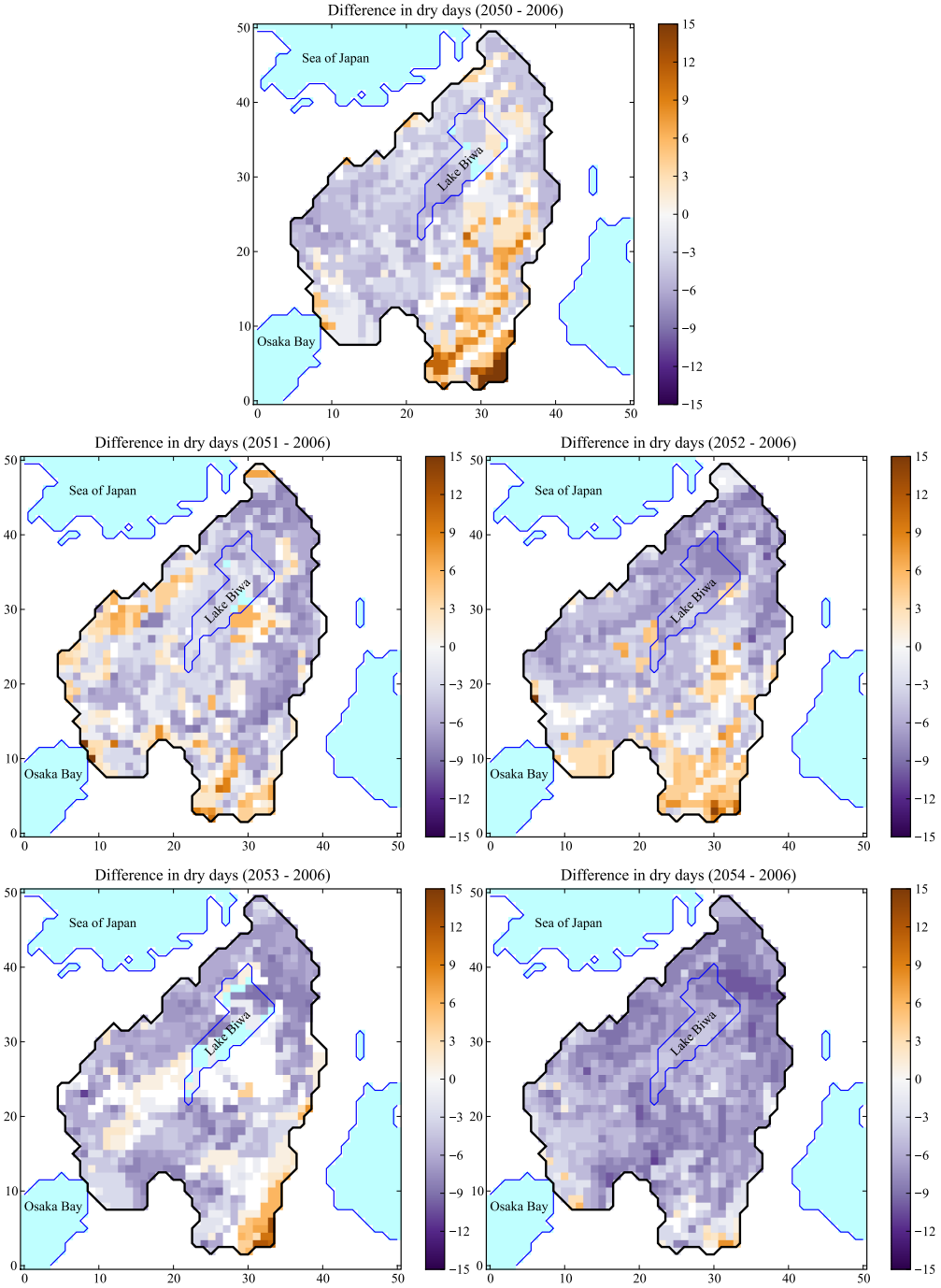
Figure 55: Difference of dry days between future (2050-2054) and present (2006) in Yodo River basin. The thick basin boundaries are same as in Fig. 20.

Table 17: Annual outflow from dams at present (2006) and future (2050-2054) in Yodo River basin.

DAM	OUTFLOW	$(m^3 * 10^6)$
	AVERAGE OF 2006	AVERAGE OF 2050 TO 2054
Amagase	4348.2	5502.1
Hiyoshi	442.7	400.8
Takayama	302.8	247.4
Nunome	41.7	34.3

in Yodo River basin are more likely than not to decrease in the future. The decrease in river discharge may be more evident in peak discharges and the peak discharges may even come earlier during the year. The decreasing river discharges and changing peak discharge time period may have several consequences related to irrigation problems, flood control strategies, dam construction and operation, and so on.

8.7 CONCLUSION

With an objective of developing a prediction tool for water resources in Yodo River basin, the use of one-year simulation period for the present scenario has allowed us to validate the utility and usefulness of the water resource prediction and assessment by using the coupled hydrometeorological model developed in chapter 7.

Using the coupled hydrometeorological modeling approach, the effect of climate change on the water resources of Yodo River basin was assessed by describing changes in several hydrologically relevant processes and phenomena such as near-surface air temperature, evapotranspiration, precipitation, snow cover and snow melting runoff, heavy precipitation, dry periods (drought), and river discharges. Several likely important conclusions regarding the water resources of Yodo River basin in the future scenario were drawn, which may potentially be relevant in the integrated water management of Yodo River
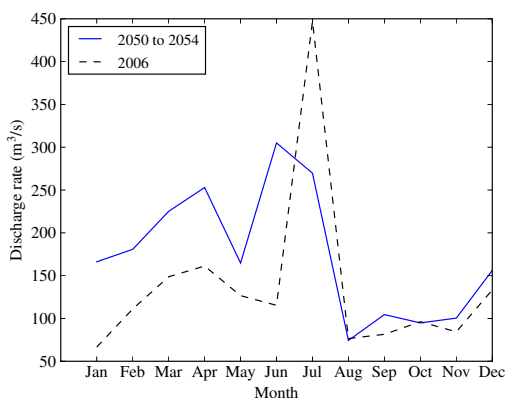
(a) Amagase dam.
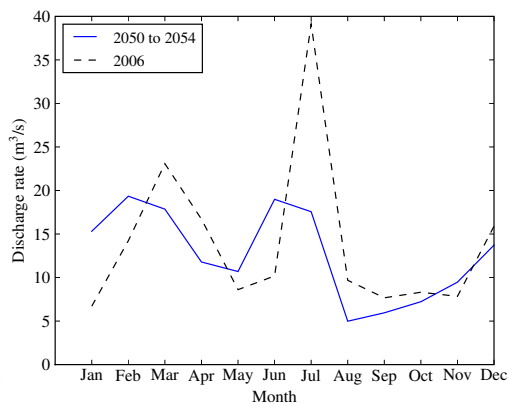
(b) Hiyoshi dam.
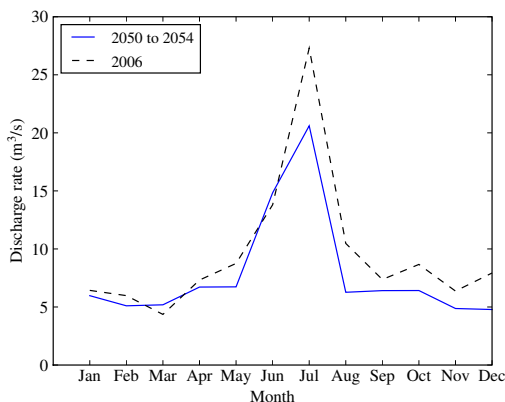
(c) Takayama dam.
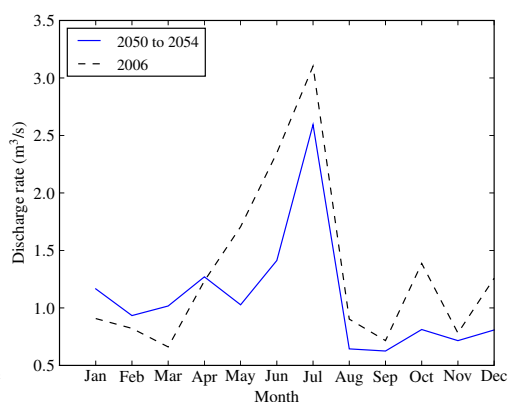
(d) Nunome dam.
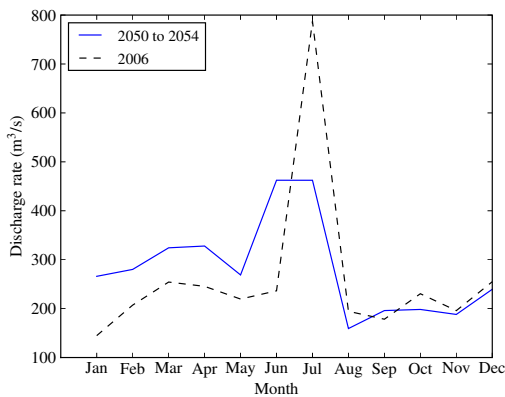
(e) Hirakata observation station.
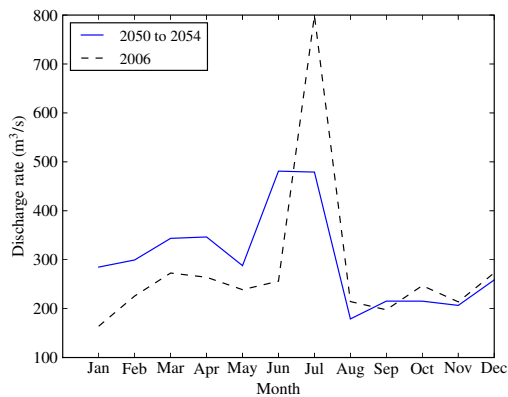
(f) Takahama observation station.

Figure 56: Comparison of monthly average discharge between present and future scenarios in Yodo River basin.

basin. It is important to note that this chapter has presented a short typical example of the effect of future climate change on basin hydrology of Yodo River basin. It would be worthwhile to extend the study to longer time periods to build more confidence in the utility of the presented coupled hydrometeorological modeling system. All in all, the coupled hydrometeorological approach used in this study was found to be suitable for the mesoscale prediction and basin-scale assessments of water resources in Yodo River basin.

9

CONCLUSIONS

As highlighted in chapter 1, Yodo River basin faces the challenge of integrated water resource management and the potential risk from climate change. To identify the existing and future water resource problems in the river basin, we need a reliable system to assess and disseminate the hydrometeorological information related to the water cycle at basin-scale. Water cycle in a river basin is a circulatory system in which the movement of water involves different media like atmosphere, land, soil sub-surfaces and so on. Water cycle in Yodo River basin is also affected by the economic and urban growth. Thus, it strongly corroborates the need of integrated study of the behavior of basin water cycle including the atmospheric, hydrological and land surface systems involved in the movement of water. With better modeling tools and increase in computational resources, regional and local scale studies are now more manageable to accurately assess the water resources of a river basin.

Chapter 2 provides a review of the past research work related to water resource assessment in Japan, and different atmospheric and hydrological modeling approaches taken for integrated study of basin hydrometeorology.

The need for comprehensive integrated water resource management in Yodo River basin, along with the knowledge of existing assessment tools and techniques, demonstrates that we require a more efficient and generalized approach for prediction and projection of basin water cycle. As a solution to this need, a coupled mesoscale hydrometeorological modeling approach is proposed for the integrated water resource assessment of Yodo River basin.

In this methodology, high-resolution mesoscale meteorological modeling and hydrological modeling are carried out to simulate the water cycle and its relevant processes in a coupled manner. Chapter 3 describes different physically based models used for developing a coupled hydrometeorological modeling system to study the water resources of Yodo River basin.

In chapter 4, mesoscale meteorological modeling technique was used to dynamically downscale the regional and global analysis datasets to the very high-resolution of Yodo River basin and Osaka Prefecture region. Two mesoscale

meteorological models known as MM5 and WRF were able to reasonably simulate the important hydrometeorological variables like precipitation, air temperature, wind speed and solar radiation. The observed meteorological fields available in various observation stations of Yodo River basin were used to validate the simulation results of the mesoscale meteorological models. Near-surface air temperature was generally predicted with good accuracy and high correlation with the observed values and faithful reproduction of diurnal variation. Horizontal wind was also simulated within acceptable levels of accuracy.

High-resolution MSM GPV meteorological data and US NCEP analysis data were used as initial and boundary conditions for mesoscale meteorological models. After validation with a large set of meteorological observation data of Osaka Prefecture, both of these data were found to be suitable for providing meteorological initial and boundary conditions for basin-scale meteorological simulations with very fine horizontal resolution of 1 x 1 km^2.

Meteorological variables are influenced by different types of physical processes occurring at different time scales. The analysis of the contribution of different time scales to meteorological variables is helpful in validating the capability of mesoscale meteorological models to reproduce the effect of physical processes occurring at different time scales. Time scale analysis of air temperature and wind speed simulated by MM5 was carried out to investigate the contribution of different time scale components to the overall long-term time series of the meteorological variables in Osaka region. We could conclude that the diurnal component of time scale was simulated with high correlation with the observed data. Also, the representation of processes occurring at very short time scales have scope for improvement in mesoscale modeling.

Precipitation is an important hydrometeorological variable influencing the water resources of a river basin. In Yodo River basin, WRF mesoscale meteorological model was used to predict meteorological variables with grid size of 3 km. Distributed hydrological modeling of a river basin requires input data at very high spatial resolution and the hydrological model used in this study had grid size of 1 km. Since mesoscale meteorological models are computationally demanding, the horizontal spatial resolution was set at 3 x 3 km^2. WRF output data were then downscaled to subgrids having 1 x 1 km^2 spatial resolution by using terrain height correction method. The precipitation data from WRF was extensively validated with SDP observation data and Radar GPV data

of Yodo River basin for the year 2006. Mesoscale precipitation was generally well simulated by WRF for Yodo River basin. Total accumulated precipitation and the temporal variation in precipitation was reasonably reproduced by WRF. It was found that the use of high-resolution grid domain was better in producing the overall precipitation in the river basin than coarse grid domain. The orographic precipitation in the highly mountainous region in Yodo River basin is also reasonably well predicted by WRF. The fine horizontal scale of WRF domain could have improved the orographic features and subsequently the representation of precipitation variability in mountainous regions could have improved. All in all, mesoscale precipitation simulated by WRF is recommendable for modeling and forecasting the hydroclimate of Yodo River basin.

Yodo River basin has several urban regions such as the Osaka region, which can significantly affect the hydroclimate of the river basin. Due to the complex terrain and urban area in the Osaka region, diurnal pattern of air temperature in Osaka is closely associated with the urban canopy and the anthropogenic heat emitted from urban sources. In chapter 5, WRF mesoscale meteorological model was coupled with urban canopy model to improve the representation of urban canopy structure and also to include the effect of anthropogenic heat production in the cities.

The urban heat island effect of urban canopy was confirmed with an increase in nocturnal near-surface air temperature and a relatively small decrease at daytime. Moreover, with the addition of anthropogenic heat source, the nocturnal near-surface air temperature is further increased at regions with high-anthropogenic heat emission. The changes in precipitation due to the effect of urban heat island were also suitably demonstrated to suggest how the urban effect may influence the hydrological cycle in a river basin. Overall, changes in temperature and precipitation pattern are deemed as important consequences of urban heat island in Yodo River basin. Therefore, the water resource in Yodo River basin is likely to be affected by urban heat island phenomenon.

In chapter 6, response of Yodo River basin to atmospheric forcings was simulated for the year 2006 by using a distributed hydrological model containing an evapotranspiration model and a rainfall-runoff model. The hydrometeorological input such as precipitation and air temperature were obtained from the SDP observation data of Yodo River basin and they were gridded into the

mesh structure of the hydrological model using Thiessen polygon method. A simplified reservoir model was also used to simulate inflow, outflow and water level at major dam reservoirs in Yodo River basin. Outflow from the dams, basin discharge and river peak discharge in the observation stations were found to be fairly well-predicted by the hydrological model. Thus the distributed hydrological model presented in chapter 6 could conclusively fulfill the objective of simulating the hydrological response of Yodo River basin to atmospheric forcings.

Chapter 7, the hydrological modeling approach of chapter 6 was modified and enhanced by coupling the output of WRF mesoscale model directly with distributed hydrological model. Instead of the traditional observation data used as atmospheric input data in the hydrological model, the high-resolution meteorological data from WRF model was adapted to be used as the atmospheric forcings in the hydrological model. The coupled mesoscale meteorological - hydrological modeling system overcomes several problems associated with observation data from basin stations. Foremost, the sparse distribution of observation stations in the basin limits the level of regional and mesoscale features that can be ultimately reproduced by the hydrological model. Coupled hydrometeorological modeling system, consisting of WRF and distributed hydrological model, mostly overcomes this spatial problem by a producing high-resolution regular gridded meteorological data that is equivalent to a highly dense network of observation stations placed at very close proximity. The upshot of using the coupled hydrometeorological modeling system is that the local and regional variabilities inherently present in the meteorological data are better reproduced by virtue of high-resolution and physically-based modeling of the atmospheric processes. Even if we still need hydrometeorological data at finer resolution than the practically limited spatial resolution of mesoscale meteorological model, we can still resort to some statistical or regressional downscaling of the mesoscale output, which seems far better than directly downscaling the global climate data to local basin scales.

Second major advantage of coupled hydrometeorological modeling approach is the viability of regional water resource assessment of river basins in future climate change scenarios. The atmospheric forcings of future climate change scenarios, projected by global circulation models, can be dynamically

downscaled by the coupled hydrometeorological model for simulating the future trend of hydrological cycle and water resources.

In other words, dynamic downscaling of global analysis data into regional and mesoscale data by using mesoscale meteorological model augurs a bright prospect for improving the prediction and projection of hydrological cycle of a river basin like Yodo River basin. The comparison and validation of the coupled hydrometeorological model results against the observed river discharge and dam outflow data indeed reinforces the notion that regional modeling approach for water resource assessment is imperative for integrated management of river basins.

The application of the coupled hydrometeorological modeling system to investigate the effects of climate change on water resources of Yodo River basin was presented in chapter 8. Then, the effect of climate change on the water resources of Yodo River basin was assessed by evaluating the changes in water resources. Many outcomes of the assessment of water resources of Yodo River basin for the future scenario are likely to be worthwhile for the integrated water resource management. It should be noted that the presented example of the effect of climate change on water resources of Yodo River basin was carried out for only five years (2050-2054) time period in IPCC A1B future scenario due to limitation of the current computational resources. The simulation period doubtlessly needs to be extended to longer time periods to observe the long-term trend of change in water resources of Yodo River basin in the future scenarios. Nevertheless, the encouraging results of the presented water resource assessment of Yodo River basin certainly reasserts the need for integrated regional water resource assessment by using the coupled hydrometeorological modeling approach.

The overall conclusion that can be drawn from this thesis is that the investigation of present and future of water resources in Yodo River basin clearly benefits from the mesoscale, atmosphere-hydrology coupled, distributed hydrological modeling approach implemented in this thesis.

Some key findings of this thesis are enumerated below:

- Important atmospheric forcings, like air temperature and land precipitation, can be predicted with sufficient representation of their spatial and temporal variations at Yodo River basin by mesoscale meteorological

modeling approach. The basin-scale meteorological modeling markedly improves the results from global-scale models.

- Anthropogenic and urban forcings could likely affect air temperature and precipitation at basin scales. The effects of urbanization might interact with climate change and impact the water resources of Yodo River basin.

- Hydrologically relevant processes like precipitation, evapotranspiration, infiltration, surface runoff, river discharge, reservoir operations, and water intake and withdrawal could be successfully incorporated in the distributed hydrological model for Yodo River basin. The coupling of mesoscale meteorological model with the distributed hydrological model could comprehensibly predict the hydrological cycle of Yodo River basin.

- Assessment of basin-scale impacts of climate change on hydrological cycle of Yodo River basin could be accomplished by using the high-resolution coupled hydrometeorological modeling approach. It was shown that water resources of Yodo River basin are likely to be affected by climate change. Precipitation, extreme precipitation events, drought periods, evapotranspiration, snow cover, snow melting, river runoff were all found to be affected by the changing climate under IPCC A1B scenario.

All in all, the coupled hydrometeorological approach, developed for assessment of water resources in Yodo River basin, signals the suitability of regional basin-scale modeling for integrated water assessment of river basins, and motivates us to find early solutions to potential risks posed by climate change on our limited water resources.

Recommendations

Considering the conclusions summarized in this chapter, some specific recommendations for improving the water resource assessment of Yodo River basin have been set forth as shown below:

- The reliability and robustness of the coupled hydrometeorological modeling approach can be further verified by validating the modeling system

with other future climate change scenarios for longer time periods. In the future scenarios, the changes in land use and forest cover can be included to consider the impact of urban development in Yodo River basin.

- The effect of urbanization on air temperature and precipitation was demonstrated in chapter 5. The urban effect should be included in the coupled hydrometeorological model to improve the response of Yodo River basin to the impact of urbanization.

- The effect of Lake Biwa, the biggest lake in Japan, and interaction between dam reservoirs should be considered to improve the simulation of water release/intake and river flow in Yodo River basin.

- Incorporating the feedback from hydrological model to atmospheric model may possibly improve the effect of soil moisture and soil temperature on the hydrological cycle of river basin.

- Impact of climate change on water quality in the multimedia environment of Yodo River basin can be investigated by using the water flow information provided by the coupled hydrometeorological modeling system.

- Water risk assessment can be implemented in Yodo River basin by using the high-resolution spatio-temporally varying data of water resources from the coupled hydrometeorological system.

- The results of water resource assessment of Yodo River basin, such as the magnitude and frequency of extreme climatic events, and impact of climate change on water availability and river discharge, should be implemented in early adaptive water resource management to confront and counteract the potential risks posed by present and future climate change.

A

No.	Latitude	Longitude	Place Name
104	34.7300	135.5611	Moriguchifuminkenkoupuraza
107	34.6797	135.5353	Kokusetsuoosaka
109	34.8167	135.5686	Ibarakishiyakusho
110	34.7661	135.6281	Neyagawashiyakusho
112	34.5256	135.4467	Takaishichuugakkou
115	34.8250	135.4475	Ikedashiritsuminamihatakaikan
116	34.7119	135.6236	Daitoushiyakusho
117	34.5717	135.6419	Furitsushuutokugakuin
118	34.4358	135.3661	Kaidukashishoubousho
120	34.8839	135.6631	Shimamotochouyakuba
121	34.4994	135.5972	Tondabayashishiyakusho
124	34.4456	135.4581	Midorigaokashougakkou
125	34.4389	135.5650	Mikkaichikouminkan
127	34.5750	135.5975	Fujiiderashiyakusho
129	34.4692	135.3792	Kishiwadachuuoukouen
130	34.4039	135.2989	Sanochuugakkou
152	34.7400	135.5600	Yodogawakougyoukoukou
155	34.5789	135.5511	Matsubarakitashougakkou
164	34.3983	135.3094	Suehirokouen
165	34.4836	135.3811	Amanogawagesuiponpujou
166	34.4553	135.5636	Kawachinaganofuminkenkoupuraza
167	34.5192	135.4439	KamodoruMBS
168	34.7378	135.6319	Kokusetsushijounawate
201	34.7075	135.5044	Seibishougakkou

No.	Latitude	Longitude	Place Name
202	34.6828	135.4522	Konohanakuyakusho
203	34.6408	135.4742	Hiraoshougakkou
204	34.7056	135.4408	Yodochuugakkou
205	34.7189	135.4842	Yodogawakuyakusho
206	34.6564	135.5342	Katsuyamashougakkou
207	34.7272	135.5414	Oomiyachuugakkou
208	34.6975	135.5428	Seikenshougakkou
209	34.6092	135.4794	Kiyoeshougakkou
210	34.6200	135.5453	Setsuyouchuugakkou
211	34.6486	135.4986	Imamiyachuugakkou
212	34.6747	135.4900	Horieshougakkou
213	34.6308	135.4328	Nankouchuuoukouen
215	34.7092	135.5858	Matsutakitashougakkou
216	34.6622	135.4908	Nanbachuugakkou
251	34.6975	135.5014	Umedashinmichi
252	34.7042	135.4369	Dekijimashougakkou
253	34.6228	135.4903	Kitakohamashougakkou
254	34.6367	135.5386	Kumatachoukousaten
255	34.7153	135.5619	Shinmorishoujishougakkou
256	34.6975	135.4703	Ebienishishougakkou
257	34.6689	135.5428	Imazatokousaten
258	34.7036	135.5778	Matsutachuugakkou
259	34.6092	135.4731	Suminoekousaten
260	34.7486	135.5281	Kamishinjoukousaten
261	34.6047	135.5122	Abikochuugakkou
301	34.5711	135.4719	Shourinji
302	34.5442	135.4583	Hamadera
303	34.5594	135.5153	Kanaoka
304	34.5939	135.4725	Sanpou

No.	Latitude	Longitude	Place Name
305	34.4867	135.5122	Wakamatsudai
307	34.5600	135.4558	Ishidu
309	34.5264	135.5289	Tomioka
310	34.4892	135.4878	Momoyamadai
311	34.5394	135.5011	Fukai
351	34.5742	135.4836	Sakaishiyakusho
352	34.5692	135.4719	Dai2hanwa
355	34.5661	135.5006	Choukan
356	34.5583	135.4478	Wangan
357	34.5689	135.5158	Tokiwahamadera
358	34.5283	135.5072	Hanwafukaihatayama
359	34.5006	135.4875	Hanwasenboku
401	34.5267	135.4325	Takaishishikougaikanshisenta
601	34.7533	135.4731	Noda
602	34.7375	135.4742	Sennari
651	34.8072	135.4906	Senri
652	34.7808	135.4697	Toyonakashiyakusho
701	34.7600	135.5028	Suitashinishishoubousho
703	34.8117	135.5169	Suitashikitashoubousho
704	34.7600	135.5317	Kawazono
753	34.7564	135.5214	Suitakanisaibansho
801	34.6650	135.5756	Higashioosakashinishihokensenta
802	34.6675	135.6394	Higashioosakashiasahimachichousha
851	34.6681	135.5975	Higashioosakashikougaikanshisenta
901	34.8597	135.6819	Kuzuha
902	34.8144	135.6508	Hirakatashiyakusho
903	34.8181	135.7058	Wanikouen
904	34.7906	135.6489	Kouri
951	34.8297	135.6875	Shoudai

No.	Latitude	Longitude	Place Name
952	34.7958	135.6267	Nakaburi
953	34.8222	135.7250	Nagao
1001	34.7878	135.6800	Katanoshiyakusho
1102	34.7525	135.5892	Dai1sokuteikyoku(Kinda)
1103	34.7553	135.5811	Dai2sokuteikyoku(Dainichi)
1104	34.7253	135.5786	Dai3sokuteikyoku(Nishiki)
1201	34.7394	135.5878	Kadomashiyakusho
1202	34.7225	135.5881	Kadomashiminami
1301	34.5794	135.6289	Kashiwarashiyakusho
1351	34.5558	135.6383	Nishimeihankashiwaraasahigaoka
1402	34.5725	135.6225	Doumyoujihigashishougakkou
1501	34.5894	135.5706	Ooborikyuushokusenta
1502	34.5939	135.5650	Ootsukakoukou
1851	34.4608	135.3708	Kishiwadashiyakusho
2001	34.4017	135.3561	Kumatorichouyakuba
2101	34.8317	135.6064	Takatsukiminami
2102	34.8631	135.5986	Takatsukikita
2151	34.8511	135.6100	Takatsukishiyakusho
2152	34.8622	135.6067	Midorigaoka
2202	34.6256	135.6022	Yaofuminkenkoupuraza
2203	34.6353	135.5556	Mizukoshi
2301	34.7772	135.6408	Narita

B

PUBLICATIONS

Some portions of this thesis have been taken from the following publications:

PEER-REVIEWED JOURNAL PAPERS

1. Kundan Lal Shrestha, Akira Kondo, Akikazu Kaga, and Yoshio Inoue. Validation of spatially downscaled mesoscale precipitation for hydrometeorological modeling of Yodo River Basin. *Journal of Japan Society for Atmospheric Environment*, 2010. (in press)

2. Kundan Lal Shrestha, Akira Kondo, Akikazu Kaga, and Yoshio Inoue. High-resolution modeling and evaluation of ozone air quality of Osaka using MM5-CMAQ system. *Journal of Environmental Sciences*, 21(6):782–789, 2009.

3. Kundan Lal Shrestha, Akira Kondo, Chikara Maeda, Akikazu Kaga, and Yoshio Inoue. Investigating the contribution of urban canopy model and anthropogenic heat emission to urban heat island effect using WRF model. *Transactions of the Japan Society of Refrigerating and Air Conditioning Engineers*, 26(1):45– 55, March 2009.

PEER-REVIEWED INTERNATIONAL CONFERENCE PAPER

1. Kundan Lal Shrestha, Akira Kondo, Akikazu Kaga, and Yoshio Inoue. High-resolution air quality modelling and time scale analysis of ozone and NOx in Osaka, Japan. In *WIT Transactions on Ecology and the Environment*, volume 116, pages 429–438, September 2008.

OTHER INTERNATIONAL CONFERENCE PAPER

1. Kundan Lal Shrestha, Akira Kondo, Chikara Maeda, Akikazu Kaga, and Yoshio Inoue. Numerical simulation of urban heat island using gridded urban configuration and anthropogenic heat data generated by a simplified method. In *The 7th International Conference on Urban Climate*, number A13-2, July 2009.

OTHER CONFERENCE PAPERS

1. Kundan Lal Shrestha, Akira Kondo, Chikara Maeda, Akikazu Kaga, and Yoshio Inoue. Investigating the contribution of anthropogenic heat emission to urban heat island effect using WRF-UCM model. In *Annual Conference of Japan Society of Refrigerating and Air Conditioning Engineers*, pages 423–426, 2008.

2. Kundan Lal Shrestha, Akira Kondo, Tazuko Morikawa, Hitoshi Kunimi, Seiji Nakatsuka, Akikazu Kaga, and Yoshio Inoue. Evaluating and comparing the predictions of meteorological models and their suitability for air quality modeling. In *The 47th Annual Meeting of Japan Society for Atmospheric Environment*, September 2006.

3. Kundan Lal Shrestha, Akikazu Kaga, Akira Kondo, and Yoshio Inoue. Validation and development of an integration technique of JMA/GPV-MSM data into the MM5-MPP model. In *19th Symposium on Computational Fluid Dynamics*, number C5-6, December 2005.

MASTERS THESIS

1. Kundan Lal Shrestha. *Coupling and evaluating MM5 and RAMS meteorlogical models with CMAQ air quality model for better assessment of air pollutants*. Masters thesis, Graduate School of Engineering, Osaka University, 2007.

BIBLIOGRAPHY

A. Arnfield and C. Grimmond. An urban canyon energy budget model and its application to urban storage heat flux modeling. *Energy and Buildings*, 27 (1):61–68, 1998. (Cited on page 20.)

Y. Ashie, V. Ca, and T. Asaeda. Building canopy model for the analysis of urban climate. *Journal of Wind Engineering and Industrial Aerodynamics*, 81: 237–248, 1999. (Cited on pages 20 and 21.)

T. Barnett, R. Malone, W. Pennell, D. Stammer, B. Semtner, and W. Washington. The effects of climate change on water resources in the West: Introduction and overview. *Climatic Change*, 62(1):1–11, Jan. 2004. (Cited on page 33.)

B. Bates, Z. Kundzewicz, S. Wu, and J. Palutikof, editors. *Climate Change and Water. Technical Paper of the Intergovernmental Panel on Climate Change*. IPCC Secretariat, Geneva, 2008. (Cited on pages 147, 150, 154, 156, and 158.)

D. Bolton. The computation of equivalent potential temperature. *Monthly Weather Review*, 108(7):1046–1053, 1980. (Cited on page 146.)

V. Bonacquisti, G. Casale, S. Palmieri, and A. Siani. A canopy layer model and its application to Rome. *Science of The Total Environment*, 364(1-3):1–13, 2006. (Cited on pages 20 and 22.)

P. Caldwell, H.-N. Chin, D. Bader, and G. Bala. Evaluation of a WRF dynamical downscaling simulation over California. *Climatic change*, 95(3):499–521, 2009. (Cited on page 17.)

M. Chino and H. Nagai. Numerical research of regional environment on IT based laboratory. In *International Symposium of the Kanazawa University*, volume 1, pages 186–189. Kanazawa University, 2003. (Cited on page 28.)

P. J. Crutzen. New directions: The growing urban heat and pollution "island" effect–impact on chemistry and climate. *Atmospheric Environment*, 38(21): 3539–3540, July 2004. (Cited on page 20.)

C. Daly, R. P. Neilson, and D. L. Phillips. A statistical-topographic model for mapping climatological precipitation over mountainous terrain. *Journal of Applied Meteorology*, 33(2):140–158, 1994. (Cited on pages 26 and 108.)

J. Dolph, D. Marks, and G. King. *Watershed Management: Balancing Sustainability and Environmental Change*, chapter Sensitivity of the regional water balance in the Columbia River Basin to climate variability: Application of a spatially distributed water balance model, pages 233–265. Springer-Verlag, New York, 1992. (Cited on page 26.)

G. Drogue, J. Humbert, J. Deraisme, N. Mahr, and N. Freslon. A statistical-topographic model using an omnidirectional parameterization of the relief for mapping orographic rainfall. *International Journal of Climatology*, 22(5): 599–613, 2002. (Cited on page 108.)

J. Dudhia. A multi-layer soil temperature model for MM5. Preprints, The Sixth PSU/NCAR Mesoscale Model Users' Workshop, 1996. (Cited on page 54.)

J. Dudhia, D. Gill, K. Manning, W. Wang, and C. Bruyere. *PSU/NCAR Mesoscale Modeling System Tutorial class notes and users' guide: MM5 Modeling System Version 3*, 2005. (Cited on page 39.)

R. E. Eskridge, J. Y. Ku, S. T. Rao, P. S. Porter, and I. G. Zurbenko. Separating different scales of motion in time series of meteorological variables. *Bulletin of the American Meteorological Society*, 78(7):1473–1483, 1997. (Cited on page 67.)

H. Fan and D. J. Sailor. Modeling the impacts of anthropogenic heating on the urban climate of Philadelphia: a comparison of implementations in two PBL schemes. *Atmospheric Environment*, 39(1):73–84, Jan. 2005. ISSN 1352-2310. (Cited on page 83.)

R. C. Gilliam, C. Hogrefe, and S. Rao. New methods for evaluating meteorological models used in air quality applications. *Atmospheric Environment*, 40 (26):5073–5086, Aug. 2006. (Cited on page 69.)

R. Giridharan, S. Ganesan, and S. Lau. Daytime urban heat island effect in high-rise and high-density residential developments in Hong Kong. *Energy and Buildings*, 36(6):525–534, 2004. (Cited on page 20.)

R. Giridharan, S. Lau, and S. Ganesan. Nocturnal heat island effect in urban residential developments of Hong Kong. *Energy and Buildings*, 37(9):964–971, 2005. (Cited on page 20.)

Government of Japan. Japan's fourth national communication under the United Nations framework convention on climate change., Jan. 2006. URL http://unfccc.int/resource/docs/natc/japnc4.pdf. Copy number: JP-N/COM/4 E. (Cited on page 7.)

G. A. Grell, J. Dudhia, and D. R. Stauffer. A description of the fifth-generation Penn State/NCAR mesoscale model (MM5). NCAR Technical Note NCAR/TN-398+STR, 1994. (Cited on page 39.)

C. Grimmond. The suburban energy balance: methodological considerations and results for a mid-latitude west coast city under winter and spring conditions. *International Journal of Climatology*, 12(5):481–497, 1992. (Cited on page 20.)

S. Grimmond. Urbanization and global environmental change: local effects of urban warming. *Geographical Journal*, 173(1):83–88, 2007. (Cited on page 20.)

H. He, Q. Zhang, J. Zhou, J. Fei, and X. Xie. Coupling climate change with hydrological dynamic in Qinling mountains, China. *Climatic Change*, 94(3): 409–427, June 2009. (Cited on page 30.)

C. Hogrefe, S. Rao, P. Kasibhatla, W. Hao, G. Sistla, R. Mathur, and J. McHenry. Evaluating the performance of regional-scale photochemical modeling systems: Part II - Ozone predictions. *Atmospheric Environment*, 35(24):4175–4188, 2001a. ISSN 13522310 (ISSN). (Cited on pages 67 and 69.)

C. Hogrefe, S. Rao, P. Kasibhatla, G. Kallos, C. Tremback, W. Hao, D. Olerud, A. Xiu, J. McHenry, and K. Alapaty. Evaluating the performance of regional-scale photochemical modeling systems: Part I - Meteorological predictions. *Atmospheric Environment*, 35(24):4159–4174, 2001b. ISSN 13522310 (ISSN). (Cited on pages 65 and 67.)

U. Högström. Non-dimensional wind and temperature profiles in the atmospheric surface layer: A re-evaluation. *Boundary-Layer Meteorology*, 42(1): 55–78, Jan. 1988. (Cited on page 127.)

S.-Y. Hong and J.-W. Lee. Assessment of the WRF model in reproducing a flash-flood heavy rainfall event over Korea. *Atmospheric Research*, 93(4): 818–831, Aug. 2009. ISSN 0169-8095. (Cited on pages 16 and 27.)

S.-Y. Hong and H.-L. Pan. Nonlocal boundary layer vertical diffusion in a medium-range forecast model. *Monthly Weather Review*, 124(10):2322–2339, 1996. (Cited on page 54.)

S.-Y. Hong, Y. Noh, and J. Dudhia. A new vertical diffusion package with an explicit treatment of entrainment processes. *Monthly Weather Review*, 134(9): 2318–2341, 2006. (Cited on page 85.)

T. Ichinose, K. Shimodozono, and K. Hanaki. Impact of anthropogenic heat on urban climate in Tokyo. *Atmospheric Environment*, 33(24-25):3897–3909, 1999. ISSN 1352-2310. (Cited on pages 21 and 85.)

S. Ikebuchi, T. Kojiri, Y. Hagiwara, K. Tomosugi, Y. Takemon, K. Tanaka, and T. Hamaguchi. Water resources and environment assessment in river basin based on Hydro-BEAM. *Annuals of Disasaster Prevention and Research Institute, Kyoto University*, (49 C):113–118, 2006. (Cited on pages 25 and 34.)

IPCC. *Impacts, Adaptation and Vulnerability: Contribution of Working Group II to the Fourth Assessment Report of the Intergovernmental Panel on Climate Change*. Cambridge University Press, Cambridge, UK, 2007a. Contribution of Working Group II to the Fourth Assessment. (Cited on pages 2, 15, and 35.)

IPCC. *Climate change 2007: the physical science basis. Contribution of working group I to the fourth assessment report of the intergovernmental panel on climate change*. Cambridge University Press, Cambridge, 2007b. (Cited on pages 16 and 147.)

E. Jauregui. Heat island development in Mexico City. *Atmospheric Environment*, 31(22):3821–3831, 1997. (Cited on page 20.)

Y. Jia, G. Ni, Y. Kawahara, and T. Suetsugi. Simulation of hydrological cycle in an urbanized watershed and effect - evaluation of infiltration facilities with WEP model. *Journal of Hydroscience and Hydraulic Engineering*, 19(1):43–52, 2001. (Cited on page 25.)

Y. Jia, G. Ni, J. Yoshitani, Y. Kawahara, and T. Kinouchi. Coupling simulation of water and energy budgets and analysis of urban development impact. *Journal of Hydrologic Engineering*, 7(4):302–311, 2002. (Cited on page 25.)

Y. Jia, C. Niu, and H. Wang. Integrated modeling and assessment of water resources and water environment in the Yellow River Basin. *Journal of Hydro-Environment Research*, 1:12–19, 2007. (Cited on page 25.)

S. Kanada, C. Muroi, Y. Wakazuki, K. Yasunaga, A. Hashimoto, T. Kato, K. Kurihara, M. Yoshizaki, and A. Noda. Structure of mesoscale convective systems during the late Baiu season in the global warming climate simulated by a non-hydrostatic regional model. *SOLA*, 1:117–120, 2005. (Cited on page 35.)

S.-D. Kang and F. Kimura. Effect of tropical SST on the northwest Pacific subtropical anticyclone. Part I: Linear Rossby wave propagation. *Journal of the Meteorological Society of Japan*, 81(5):1225–1242, 2003. (Cited on page 72.)

S. Kim, Y. Tachikawa, K. Takara, and E. Nakata. Hydrologic prediction under global warming at Tone and Yod River basins using the output of global 20-km mesh GCM. *Annuals of Disasaster Prevention and Research Institute, Kyoto University*, (51 B):11–20, 2008. (Cited on page 34.)

Y.-H. Kim and J.-J. Baik. Maximum urban heat island intensity in Seoul. *Journal of Applied Meteorology*, 41(6):651–659, 2002. (Cited on page 20.)

Y.-H. Kim and J.-J. Baik. Daily maximum urban heat island intensity in large cities of Korea. *Theoretical and Applied Climatology*, 79(3-4):151–164, 2004. (Cited on page 20.)

Y.-H. Kim and J.-J. Baik. Spatial and temporal structure of the urban heat island in Seoul. *Journal of Applied Meteorology*, 44(5):591–605, 2005. (Cited on page 20.)

A. Kitoh, M. Hosaka, Y. Adachi, and K. Kamiguchi. Future projections of precipitation characteristics in east Asia simulated by the MRI CGCM2. *Advances in Atmospheric Sciences*, 22(4):467–478, July 2005. (Cited on page 35.)

T. Kojiri, Y. Kinai, and J. Park. Integrated river basin environment assessment on water quantity and quality by considering utilization processes. In

Proceedings of the International Conference on Water Resources and Environment Research, pages 397–401, 2002. (Cited on pages 24 and 40.)

T. Kojiri, T. Hamaguchi, and M. Ode. Assessment of global warming impacts on water resources and ecology of a river basin in Japan. *Journal of Hydro-environment Research*, 1:164–175, 2008. (Cited on pages 24 and 34.)

M. Kolokotroni, I. Giannitsaris, and R. Watkins. The effect of the london urban heat island on building summer cooling demand and night ventilation strategies. *Solar Energy*, 80(4):383–392, 2006. (Cited on page 20.)

H. Kondo, T. Tokairin, and Y. Kikegawa. Calculation of wind in a Tokyo urban area with a mesoscale model including a multi-layer urban canopy model. *Journal of Wind Engineering and Industrial Aerodynamics*, 96(10-11):1655–1666, Oct. 2008. ISSN 0167-6105. (Cited on pages 20 and 21.)

J. Kondo. *Mizukankyounokishougaku*. Asakurashoten, Tokyo, 1994. (In Japanese). (Cited on page 75.)

M.-S. Koo and S.-Y. Hong. Diurnal cycle of the simulated precipitation in WRF: Physics sensitivity. In *9th WRF Users' Workshop*, NCAR Center Green Campus, June 2008. (Cited on page 72.)

V. Krysanova and A. Becker. Integrated modelling of hydrological processes and nutrient dynamics at the river basin scale. *Hydrobiologia*, 410(0):131–138, Sept. 1999. (Cited on page 107.)

S. V. Kumar, C. D. Peters-Lidard, J. L. Eastman, and W.-K. Tao. An integrated high-resolution hydrometeorological modeling testbed using LIS and WRF. *Environmental Modelling & Software*, 23(2):169–181, Feb. 2008. ISSN 1364-8152. (Cited on page 31.)

H. Kunstmann and G. Jung. Investigation of feedback mechanisms between soil moisture, land use and precipitation in West Africa. *IAHS-AISH Publication*, (280):149–159, 2003. ISSN 01447815 (ISSN). (Cited on page 31.)

H. Kunstmann and C. Stadler. High resolution distributed atmospheric-hydrological modelling for alpine catchments. *Journal of Hydrology*, 314(1-4):105–124, 2005. (Cited on page 30.)

H. Kusaka and H. Hayami. Numerical simulation of local weather for a high photochemical oxidant event using the WRF model. *JSME International Journal Series B Fluids and Thermal Engineering*, 49(1):72–77, 2006. (Cited on page 83.)

H. Kusaka and F. Kimura. Thermal effects of urban canyon structure on the nocturnal heat island: Numerical experiment using a mesoscale model coupled with an urban canopy model. *Journal of Applied Meteorology*, 43(12): 1899–1910, 2004a. (Cited on pages 20, 21, and 40.)

H. Kusaka and F. Kimura. Coupling a single-layer urban canopy model with a simple atmospheric model: Impact on urban heat island simulation for an idealized case. *Journal of the Meteorological Society of Japan*, 82(1):67–80, 2004b. (Cited on page 21.)

H. Kusaka, H. Kondo, Y. Kikegawa, and F. Kimura. A simple single-layer urban canopy model for atmospheric models: Comparison with multi-layer and slab models. *Boundary-Layer Meteorology*, 101(3):329–358, Dec. 2001. (Cited on pages 20 and 40.)

C. A. Lin, L. Wen, G. Lu, Z. Wu, J. Zhang, Y. Yang, Y. Zhu, and L. Tong. Atmospheric-hydrological modeling of severe precipitation and floods in the Huaihe River Basin, China. *Journal of Hydrology*, 330(1-2):249–259, Oct. 2006. (Cited on pages 27 and 29.)

C.-Y. Lin, F. Chen, J. Huang, W.-C. Chen, Y.-A. Liou, W.-N. Chen, and S.-C. Liu. Urban heat island effect and its impact on boundary layer development and land-sea circulation over northern Taiwan. *Atmospheric Environment*, 42 (22):5635–5649, July 2008. ISSN 1352-2310. (Cited on pages 21 and 83.)

Y.-L. Lin. *Mesoscale Dynamics*. Cambridge University Press, 2007. (Cited on page 37.)

W. P. Lowry. Urban effects on precipitation amount. *Progress in Physical Geography*, 22(4):477–520, 1998. (Cited on pages 20 and 103.)

R. W. Macdonald. Modelling the mean velocity profile in the urban canopy layer. *Boundary-Layer Meteorology*, 97(1):25–45, Oct. 2000. (Cited on page 90.)

N. Magee, J. Curtis, and G. Wendler. The urban heat island effect at Fairbanks, Alaska. *Theoretical and Applied Climatology*, 64(1-2):39–47, 1999. (Cited on page 20.)

V. Masson. A physically-based scheme for the urban energy budget in atmospheric models. *Boundary-Layer Meteorology*, 94(3):357–397, 2000. (Cited on page 20.)

V. Masson, C. Grimmond, and T. Oke. Evaluation of the town energy balance (TEB) scheme with direct measurements from dry districts in two cities. *Journal of Applied Meteorology*, 41(10):1011–1026, 2002. (Cited on page 20.)

S.-K. Min, S. Legutke, A. Hense, U. Cubasch, W.-T. Kwon, J.-H. Oh, and U. Schlese. East Asian climate change in the 21st century as simulated by the coupled climate model ECHO-G under IPCC SRES scenarios. *Journal of the Meteorological Society of Japan*, 84(1):1–26, 2006. (Cited on page 35.)

Ministry of Land, Infrastructure, Transport and Tourism. Water resources in Japan, 2008a. URL http://www.mlit.go.jp/tochimizushigen/mizsei/water_resources/index.html. (Cited on pages 3 and 5.)

Ministry of Land, Infrastructure, Transport and Tourism. Climate change adaptation strategies to cope with water-related disasters due to global warming (policy report), June 2008b. URL http://www.mlit.go.jp/river/basic_info/english/pdf/policy_report.pdf. (Provisional Translation). (Cited on page 2.)

Ministry of Land, Infrastructure, Transport and Tourism, Japan. Integrated water resource management addressing climate change and other risks. Technical report, Apr. 2008. (Interim Report). (Cited on page 7.)

A. Mochida, S. Murakami, T. Ojima, K. Sangjin, R. Ooka, and H. Sugiyama. CFD analysis of mesoscale climate in the greater Tokyo area. *Journal of Wind Engineering and Industrial Aerodynamics*, 67-68:459–477, 1997. (Cited on page 21.)

N. Mölders. *Coupled Models for the Hydrological Cycle: Integrating Atmosphere, Biosphere and Pedosphere*, chapter Feedbacks at the hydrometeorological interface, pages 192–208. Springer-Verlag, Berlin, 2005. (Cited on page 27.)

N. Mölders and A. Raabe. Testing the effect of a two-way-coupling of a meteorological and a hydrologic model on the predicted local weather. *Atmospheric Research*, 45(2):81–107, Oct. 1997. ISSN 0169-8095. (Cited on pages 27 and 32.)

N. Mölders and W. Rühaak. On the impact of explicitly predicted runoff on the simulated atmospheric response to small-scale land-use changes–an integrated modeling approach. *Atmospheric Research*, 63(1-2):3–38, July 2002. ISSN 0169-8095. (Cited on page 32.)

N. Mölders, A. Raabe, and G. Tetzlaff. A comparison of two strategies on land surface heterogeneity used in a mesoscale meteorological model. *Tellus*, 48: 733–749, 1996. (Cited on pages 31, 32, and 108.)

N. Nakicenovic and R. Swart, editors. *Special Report on Emissions Scenarios*. Cambridge University Press, Cambridge, 2000. (Cited on pages 139 and 142.)

D. Narumi, F. Otani, A. Kondo, Y. Shimoda, and M. Mizuno. Analysis of countermeasure for mitigating heat islands phenomena using a numerical model. Part 1 Effect of anthropogenic waste heat upon urban thermal environment. *Journal of Architecture, Planning and Environmental Engineering, AIJ*, 562:97–104, 2002. (In Japanese). (Cited on pages 21 and 91.)

A. Nawahda, T. Kojiri, and I. Kaihotu. Assessment of global warming impacts on water resources and ecology of a river basin in Japan. *Journal of Japan Society of Hydrology and Water Resources*, 18(3):293–305, 2005. (Cited on page 24.)

P. A. O'Gorman and T. Schneider. The physical basis for increases in precipitation extremes in simulations of 21st-century climate change. *Proceedings of the National Academy of Sciences*, 106(35):14773–14777, 2009. (Cited on page 18.)

T. Ohsawa, A. Hashimoto, S. Shimada, J. Yoshino, T. de Paus, D. Heinemann, and B. Lange. Evaluation of offshore wind simulations with MM5 in the Japanese and Danish coastal waters. Milan, 2007. Proceedings of European Wind Energy Conference EWEC. (Cited on page 69.)

T. Oke. The energetic basis of the urban heat island (symons memorial lecture, 20 may 1980). *Quarterly Journal, Royal Meteorological Society*, 108(455):1–24, 1982. (Cited on page 20.)

T. Oke. The urban energy balance. *Progress in Physical Geography*, 12(4):471–508, 1988. (Cited on page 20.)

R. Ooka. Recent development of assessment tools for urban climate and heat-island investigation especially based on experiences in Japan. *International Journal of Climatology*, 27(14):1919–1930, 2007. (Cited on page 20.)

R. Ooka, K. Harayama, S. Murakami, and H. Kondo. Study on urban heat islands in Tokyo metropolitan area using a meteorological mesoscale model incorporating an urban canopy model. *Fifth Symposium on the Urban Environment, 9.15*, pages –, 2004. (Cited on pages 20 and 21.)

Y. Qian, S. J. Ghan, and L. R. Leung. Downscaling hydroclimatic changes over the western US based on CAM subgrid scheme and WRF regional climate simulations. *International Journal of Climatology*, 2009. (in press). (Cited on page 16.)

V. Ramanathan and Y. Feng. Air pollution, greenhouse gases and climate change: Global and regional perspectives. *Atmospheric Environment*, 43(1): 37–50, Jan. 2009. ISSN 1352-2310. (Cited on page 26.)

S. T. Rao, I. G. Zurbenko, R. Neagu, P. S. Porter, J. Y. Ku, and R. F. Henry. Space and time scales in ambient ozone data. *Bulletin of the American Meteorological Society*, 78(10):2153–2166, 1997. (Cited on page 67.)

A. M. Rizwan, L. Y. Dennis, and C. Liu. A review on the generation, determination and mitigation of urban heat island. *Journal of Environmental Sciences*, 20(1):120–128, 2008. ISSN 1001-0742. (Cited on page 20.)

S. Running, R. Nemani, and R. Hungerford. Extrapolation of synoptic meteorological data in mountainous terrain and its use for simulating forest evapotranspiration and photosynthesis. *Canadian Journal of Forest Research*, 17(6):472–483, 1987. (Cited on page 108.)

D. J. Sailor and N. Dietsch. The urban heat island Mitigation Impact Screening Tool (MIST). *Environmental Modelling & Software*, 22(10):1529–1541, 2007. (Cited on page 20.)

T. Saitoh, T. Shimada, and H. Hoshi. Modeling and simulation of the Tokyo urban heat island. *Atmospheric Environment*, 30(20):3431–3442, 1996. (Cited on page 20.)

J. Sang, H. Liu, H. Liu, and Z. Zhang. Observational and numerical studies of wintertime urban boundary layer. *Journal of Wind Engineering and Industrial Aerodynamics*, 87(2-3):243–258, 2000. (Cited on page 20.)

H. Sasaki and K. Kurihara. Relationship between precipitation and elevation in the present climate reproduced by the non-hydrostatic regional climate model. *SOLA*, 4:109–112, 2008. (Cited on page 19.)

T. Sayama, Y. Tachikawa, and K. Takara. Assessment of dam flood control using a distributed rainfall-runoff prediction system. *Proceedings of Monitoring, Prediction and Mitigation of Water-related Disasters*, pages 59–64, 2005. (Cited on pages 23, 50, and 115.)

G. Seuffert, P. Gross, C. Simmer, and E. F. Wood. The influence of hydrologic modeling on the predicted local weather: Two-way coupling of a mesoscale weather prediction model and a land surface hydrologic model. *Journal of Hydrometeorology*, 3(5):505–523, 2002. (Cited on pages 27 and 32.)

J. Shepherd. Evidence of urban-induced precipitation variability in arid climate regimes. *Journal of Arid Environments*, 67(4):607–628, 2006. ISSN 0140-1963. (Cited on page 21.)

J. M. Shepherd. A review of current investigations of urban-induced rainfall and recommendations for the future. *Earth Interactions*, 9(12):1–27, 2005. (Cited on page 20.)

H. Shin and S.-Y. Hong. Quantitative precipitation forecast experiments of heavy rainfall over Jeju Island on 14-16 September 2007 using the WRF model. *Asia-Pacific Journal of Atmospheric Sciences*, 45(1):71–89, 2009. ISSN 19767633 (ISSN). (Cited on page 18.)

K. L. Shrestha, A. Kondo, A. Kaga, and Y. Inoue. High-resolution air quality modelling and time scale analysis of ozone and NOx in Osaka, Japan. In *WIT Transactions on Ecology and the Environment*, volume 116, pages 429–438, Sept. 2008. (Cited on page 100.)

R. K. Shrestha, T. Sayama, Y. Tachikawa, and K. Takara. Use of disaggregated rainfall data for distributed hydrological modeling in Yodo River basin. *Annuals of Disasaster Prevention and Research Institute, Kyoto University*, (48 B), 2005. (Cited on page 23.)

W. Skamarock, J. Klemp, J. Dudhia, D. Gill, D. Barker, W. Wang, and J. Powers. A description of the Advanced Research WRF version 2, NCAR technical note. Technical report, NCAR/TN-468+STR, 2005. (Cited on page 39.)

J. A. Smith, M. L. Baeck, J. E. Morrison, P. Sturdevant-Rees, D. F. Turner-Gillespie, and P. D. Bates. The regional hydrology of extreme floods in an urbanizing drainage basin. *Journal of Hydrometeorology*, 3(3):267–282, 2002. (Cited on page 25.)

S. Sugimoto and H. Hirakuchi. Simulation of precipitation caused by a Baiu front: an evaluation study with radar data. In *Weather Radar Information and Distributed Hydrological Modelling*, number 282, pages 51–58. International Association of Hydrological Sciences, 2003. (Cited on page 74.)

Y. Suzuki, E. Nakakita, and S. Ikebuchi. Numerical study of rainfall-topography relationships in mountainous regions of Japan using a mesoscale meteorological model. In *Weather Radar Information and Distributed Hydrological Modelling*, number 282, pages 43–50, Sapporo, Japan, 2003. International Association of Hydrological Sciences. (Cited on page 108.)

Y. Tachikawa, T. Sayama, H. Matsuura, T. Yamazaki, A. Yamaji, and Y. Michi-hiro. Development of a real-time runoff forecasting system using a physically-based distributed hydrologic model and its application to the Yodo River basin. *Journal of Natural Disaster Science*, 26(2):189–201, 2007. (In Japanese). (Cited on page 23.)

H. Taha. Urban climates and heat islands: albedo, evapotranspiration, and anthropogenic heat. *Energy and Buildings*, 25(2):99–103, 1997. ISSN 0378-7788. (Cited on page 20.)

I. Takayabu, H. Kato, K. Nishizawa, Y. N. Takayabu, Y. Sato, H. Sasaki, K. Kuri-hara, and A. Kitoh. Future projections in precipitation over Asia simulated by two RCMs nested into MRI-CGCM2.2. *Journal of the Meteorological Society of Japan*, 85(4):511–519, 2007. (Cited on page 17.)

A. H. Thiessen. Precipitation averages for large areas. *Monthly Weather Review*, 39(7):1082–1089, 1911. (Cited on page 108.)

H. Tong, A. Walton, J. Sang, and J. Chan. Numerical simulation of the urban boundary layer over the complex terrain of Hong Kong. *Atmospheric Environment*, 39(19):3549–3563, 2005. (Cited on page 20.)

K. E. Trenberth. Conceptual framework for changes of extremes of the hydrological cycle with climate change. *Climatic change*, 42(1):327–339, 1999. (Cited on page 18.)

G. Vaes, P. Willems, and J. Berlamont. Areal rainfall correction coefficients for small urban catchments. *Atmospheric Research*, 77(1-4):48–59, 2005. ISSN 0169-8095. (Cited on page 26.)

M. Verbunt, M. Zappa, J. Gurtz, and P. Kaufmann. Verification of a coupled hydrometeorological modelling approach for alpine tributaries in the Rhine basin. *Journal of Hydrology*, 324(1-4):224–238, June 2006. (Cited on pages 27 and 28.)

M. Vertenstein, T. Craig, T. Henderson, S. Murphy, G. R. C. Jr, and N. Norton. CCSM3.0 user's guide, 2004. URL http://www.ccsm.ucar.edu/models/ccsm3.0/ccsm/doc/UsersGuide/UsersGuide/UsersGuide.html. (Cited on page 143.)

S. Wagner, H. Kunstmann, A. Bárdossy, C. Conrad, and R. Colditz. Water balance estimation of a poorly gauged catchment in West Africa using dynamically downscaled meteorological fields and remote sensing information. *Physics and Chemistry of the Earth*, 34(4-5):225–235, 2009. (Cited on page 31.)

Water Resources Department, Ministry of Land, Infrastructure, Transport and Tourism. Achieving water security in Japan and worldwide, 2008. URL http://www.mlit.go.jp/tochimizushigen/mizsei/water_resources/index.html. (Cited on pages 16 and 33.)

K. J. Westrick and C. F. Mass. An evaluation of a high-resolution hydrometeorological modeling system for prediction of a cool-season flood event in a coastal mountainous watershed. *Journal of Hydrometeorology*, 2(2):161–180, 2001. (Cited on page 30.)

K. Yasunaga, M. Yoshizaki, Y. Wakazuki, C. Muroi, K. Kurihara, A. Hashimoto, S. Kanada, T. Kato, S. Kusunoki, K. Oouchi, H. Yoshimura, R. Mizuta, and A. Noda. Changes in the Baiu frontal activity in the future climate simulated by super-high-resolution global and cloud-resolving regional climate models. *Journal of the Meteorological Society of Japan. Ser. II*, 84(1):199–220, 2006. (Cited on page 35.)

Yodo River Office. The Yodo River, 2004. URL http://www.kkr.mlit.go.jp/yodogawa. (Cited on page 3.)

T. Yoshikane, X. Ma, F. Kimura, and M. Hara. Regional climatic simulation for hydrological model using WRF model around Yellow River basin. In *6th WRF / 15th MM5 Users' Workshop*, number 3.11. National Center for Atmospheric Research, June 2005. (Cited on page 28.)

J. Yoshitani, M. Kavvas, and Z.-Q. Chen. Coupled regional-scale hydrological-atmospheric model for the study of climate impact on Japan. In *Soil-Vegetation-Atmosphere Transfer Schemes and Large-Scale Hydrological Models*, number 270, pages 191–198, July 2001. (Cited on pages 27 and 33.)

M. Yoshizaki, C. Muroi, S. Kanada, Y. Wakazuki, K. Yasunaga, A. Hashimoto, T. Kato, K. Kurihara, A. Noda, and S. Kusunoki. Changes of Baiu (Mei-yu) frontal activity in the global warming climate simulated by a non-hydrostatic regional model. *SOLA*, 1:25–28, 2005. (Cited on page 35.)

S. Yu, B. Eder, R. Dennis, S.-H. Chu, and S. E. Schwartz. New unbiased symmetric metrics for evaluation of air quality models. *Atmospheric Science Letters*, 7(1):26–34, 2006. (Cited on pages 62 and 64.)

Z. Yu. Assessing the response of subgrid hydrologic processes to atmospheric forcing with a hydrologic model system. *Global and Planetary Change*, 25(1-2): 1–17, July 2000. ISSN 0921-8181. (Cited on page 29.)

Z. Yu, E. J. Barron, B. Yarnal, M. N. Lakhtakia, R. A. White, D. Pollard, and D. A. Miller. Evaluation of basin-scale hydrologic response to a multi-storm simulation. *Journal of Hydrology*, 257(1-4):212–225, Feb. 2002. ISSN 0022-1694. (Cited on page 29.)

C.-S. Zhan, J. Xia, Z. Chen, and Q.-T. Zuo. An integrated hydrological and meteorological approach for the simulation of terrestrial evapotranspiration. *Hydrological Sciences Journal*, 53(6):1151–1164, 2008. (Cited on page 33.)

Y. Zhang, P. Liu, B. Pun, and C. Seigneur. A comprehensive performance evaluation of MM5-CMAQ for the summer 1999 southern oxidants study episode, Part III: Diagnostic and mechanistic evaluations. *Atmospheric Environment*, 40(26):4856–4873, 2006. (Cited on pages 62 and 66.)

F. W. Zwiers and V. V. Kharin. Changes in the extremes of the climate simulated by CCC GCM2 under CO2 doubling. *Journal of Climate*, 11(9):2200–2222, 1998. (Cited on page 19.)

ACKNOWLEDGMENTS